Process Intensification by Heterogeneous Reactive Extraction

Doctoral Thesis
(Dissertation)

to be awarded the degree of

Doctor of Engineering (Dr.-Ing.)

submitted by

Dipl.-Ing. Bernhard Pfeuffer

from Wilhelmshaven

approved by the Faculty of

Mathematics/Computer Science and Mechanical Engineering,
Clausthal University of Technology.

Date of oral examination
September 23rd, 2011

Chairperson of the Board of Examiners

Prof. Dr. rer. nat. Alfons Weber

Chief Reviewer

Prof. Dr.-Ing. Ulrich Kunz

Reviewer

Prof. Dr.-Ing. Thomas Turek

Prof. Dr.-Ing. Ulrich Hoffmann

So eine Arbeit wird eigentlich nie fertig, man muß sie für fertig erklären, wenn man nach Zeit und Umständen das Möglichste getan hat.

J. W. von Goethe, Italienische Reise, 1787

Kurzfassung

Die sekundären Lösemittelalkohole 2-Propanol und 2-Butanol werden durch die säure-katalysierte Reaktion der entsprechenden Alkene Propen und den isomeren *n*-Butenen mit Wasser hergestellt, wobei in erster Hinsicht zwei Prozessvarianten unterschieden werden können. Der überwiegende Anteil der Weltproduktion wird durch das ältere indirekte Hydratisierungsverfahren, bei dem flüssige Schwefelsäure als Katalysator zum Einsatz kommt, hergestellt. Der kleinere Anteil wird durch heterogenkatalytische direkte Hydratisierungsverfahren produziert, die, je nach Katalysator, in einer Gasphase oder zwei nicht mischbaren Flüssigphasen durchgeführt werden.

Das indirekte Verfahren hat aufgrund der Verwendung flüssiger Schwefelsäure einige Nachteile gegenüber den direkten Verfahren. Nahezu alle Anlagenteile sind durch die Gegenwart von Schwefelsäure korrosiven Angriffen ausgesetzt und die Schwefelsäure muss nach einer prozessbedingten Verdünnung mit Wasser durch Destillation zurückgewonnen und dem Reaktor wieder zugeführt werden. Darüber hinaus ist die Selektivität zum gewünschten Alkohol relativ gering. Der offenbar einzige Vorteil dieses Verfahrens besteht in der Möglichkeit, Kohlenwasserstoff-Schnitte mit einem Alkengehalt von nur 40 % bis 60 % verarbeiten zu können.

Unter den direkten Verfahren ist der Flüssigphasenprozess besonders interessant, da hier die prinzipielle Möglichkeit zur Prozessintensivierung durch Integration von Reaktion und simultaner Abtrennung des Produktes besteht. Eine Reaktivextraktion scheint für das vorliegende Reaktionssystem besonders geeignet, da eine organische und eine wässrige Phase bereits vorhanden sind, die organische Phase den Katalysator nicht benetzt und das höhere Extraktionspotenzial für das Produkt aufweist. Durch simultane Extraktion des Alkohols wird die Folgereaktion zum Ether verlangsamt und die gewünschte Alkoholbildung beschleunigt.

Mit dieser Arbeit wurde ein konzeptioneller Entwurf für einen optimierten Herstellungsprozess zur heterogenkatalytischen Flüssigphasen-Hydratisierung linearer C_3- und C_4-Alkene an sauren Ionenaustauscherharzen auf Basis einer Reaktivextraktion entwickelt. Dazu wurden im Vorfeld experimentelle und theoretische Untersuchungen zur Thermodynamik, Reaktionskinetik, und Stofftransportkinetik unternommen. Die daraus gewonnen Erkenntnisse wurden in Simulationsprogrammen genutzt, um einen Reaktivextraktionsprozess zu entwerfen.

Für die experimentellen Untersuchungen wurde eine automatisierte Hochdruck-Labor-anlage konzipiert und aufgebaut, um Mikro- und Makrokinetik der Produkt- sowie wesentlicher Nebenproduktbildungen zu untersuchen. Die Anlage besteht im Wesentlichen aus einem kontinuierlich betriebenen Mehrphasen-Rührkesselreaktor und einer gaschromatographischen Online-Analytik. Die gewonnenen Versuchsergebnisse wurden zur Entwicklung geeigneter intrinsischer Reaktionsgeschwindigkeitsgesetze genutzt.

Schließlich wurde auf Basis der theoretischen und experimentellen Informationen ein eindimensionales Modell für einen Reaktivextraktor unter Berücksichtigung der nicht-idealen diffusiven Stofftransportvorgänge erstellt, um detaillierte Schlussfolgerungen für den weiteren Forschungsbedarf formulieren und eine mögliche großindustrielle Applikation skizzieren zu können. Zusätzlich wurde für die nach dem Reaktor folgenden thermischen Trennoperationen ein Computerprogramm zur Nichtgleichgewichtssimulation von Destillations- und Stripperkolonnen erstellt. Die Simulationsergebnisse zeigen, dass durch die Umstellung des Hydratisierungsprozesses von einem Rieselbettreaktor zu einer Reaktivextraktion mit strukturierter Packung, neben der erheblich verbesserten Reaktoreffizienz, Energieeinsparungen von ca. 40 % bezüglich der benötigten Verdampferwärme erzielbar sind. Diese außergewöhnliche Verbesserung unterstreicht, dass ein enormes Potenzial für Energiebedarfssenkungen in chemischen Produktionsprozessen besteht, welches mithilfe der Prozessintensivierung erschlossen werden kann.

Abstract

The secondary alcohols isopropyl alcohol (IPA) and *sec*-butyl alcohol (SBA) – an important class of solvents – are mainly manufactured by acid catalyzed hydration of their corresponding alkenes propene and the isomeric *n*-butenes with water, whereas, essentially, two process variants can be distinguished for the manufacture of secondary C_3- and C_4-alcohols. The major part of the world production is provided by the older indirect hydration process wherein sulfuric acid is employed as catalytically active component. The minor part is produced by the heterogeneously catalyzed direct hydration process which – depending on the used catalyst type – is conducted in the gas phase or in two immiscible liquid phases.

Due to the utilization of sulfuric acid the indirect process suffers from several drawbacks when compared to the direct process variants. Almost all plant equipment is subject to corrosive attacks by the sulfuric acid catalyst and, in addition, the sulfuric acid needs to be recovered by distillation due to dilution with water in the process. Furthermore, selectivity towards the desired product alcohol is relatively low. The only advantage which might be found for this process is the applicability of raffinate streams with an alkene content of only 40 % to 60 %.

Among the direct process variants the liquid phase process is notably interesting, as for this process, in principle an opportunity for process intensification by integration of reaction and simultaneous product separation is available. Due to the presence of two immiscible liquid phases, namely organic and aqueous phase, a reactive extraction process seems to be particularly qualified. Besides this, the aqueous phase wets the used acidic ion exchange resin catalyst exclusively and the organic phase extracts the product from the aqueous phase, thereby, also extracting the product from the catalyst which is saturated with water. By simultaneous removal of the main product alcohol the formation of the by-product is almost suppressed and the formation of the desired alcohol enhanced.

In this work a conceptual design of an improved process for the heterogeneously acid ion exchange catalyzed hydration of linear C_3- and C_4-alkenes based on reactive extraction is developed. For this purpose, experimental and theoretical investigations on thermodynamics, more specifically on fluid phase equilibria, micro- and macrokinetics of the reaction and multicomponent mass transfer have been undertaken. The obtained findings were used for a simulation

of the reactive extraction process, thereby, providing the basis for conceptual design.

An automated high-pressure laboratory plant has been designed and built for conducting kinetic experiments. Micro- and macrokinetics of main and side reactions were investigated in a continuously stirred multiphase tank reactor analyzing the change in phase composition by online gas chromatography. The experimental results were used for the development of appropriate intrinsic reaction rate models.

In conclusion, a one-dimensional model of a reactive extraction column was developed which considers besides the reaction kinetics nonideal diffusive mass transfer phenomena in order to allow for the conceptual design of a reactive extraction column. For the additional evaluation of post-reactive separation sequences a nonequilibrium distillation and stripping simulation program was written. The results show that besides the remarkably improved reactor performance the modified separation sequence leads to an energy saving of approx. 40 % with respect to the required evaporation heat for post-reactive distillation and stripping. This exceptional improvement emphasizes the potential of energy demand reductions in chemical manufacture processes which can be achieved by undertaking process intensification.

Acknowledgment

First of all, I would like to express my sincere gratitude to Prof. Ulrich Kunz, my supervisor, and to Prof. Thomas Turek for offering me this project and, thereby, giving me the opportunity to preparing this doctoral thesis. Furthermore, I would like to thank them for their great support and trust they always bestowed upon me. No minor thank is granted to Prof. (em.) Ulrich Hoffmann for his great interest in this work and for numerous and fruitful discussions which – in many cases – brought me to take a look on subjects from another point of view. I thank them all for having reviewed this thesis and I am hoping for further collaboration in the future.

Financial support by DFG (Deutsche Forschungsgemeinschaft) is gratefully acknowledged under the project term KU 853/4.

Many thanks are dedicated to the kind people of Sasol Solvents Germany, Dr. Detlef Hoell, Thomas Urban, Dr. Rafael Roggenbuck and Dr. Harald Kohnz for their constructive co-operation, support with data and funds. Without their initiative, the very interesting subject of this work might not have been considered, at least until today.

There are many more people, I have to thank. My colleagues at the Institute of Chemical Process Engineering who made my stay at the institute an enjoyable one. Very special thanks are dedicated to my predecessor Dr. Diana Petre for the good collaboration. My colleagues Vanessa Bacher, Dr. Raúl Cecilia (el Tablero orejón), Dr. Christian Eisenbeis with whom I could share the office in a comfortable way, Stefan Pinnow (Mr. LaTeX) and Dr. Christian Perbandt for their great support, friendship and many helpful discussions.

Furthermore, many objectives of this work would not have been included without the help of my bachelor and master students, Yasin Cengiz Celik, Fabian Nentwich, Carlos Andres Paz-Carvajal, Florian Schramm and Kristian Voelskow. The excellent reliability of the equipment is due to the professional employees of the workshop, Roland Schmidt and Henning Dunemann. As the reader may deduce from the few photographs showing tailor-made equipment they are doing a fantastic job.

Last but not least, I need to express my eternal gratitude to my family and friends, especially to my parents and my wife, Birgit, who always believed in me and who tolerated me spending so much time with this work with patience. You are wonderful!

Contents

List of Figures

List of Tables

1 Introduction

1.1 Production and Utilization of *sec*-Alcohols

Isopropyl alcohol.
The petrochemical which was produced for the first time on a commercial scale is isopropyl alcohol (IPA). In 1920, the Standard Oil Co. of New Jersey started the first plant worldwide for producing isopropyl alcohol from propene (P) and water (W) with a capacity of 75 metric tons per year. Today, the world production capacity for isopropyl alcohol comprises 1 800 000 metric tons per year.

Almost half of the world production capacity is located in the United States, one quarter in Western Europe, and approximately one quarter in Asia. Minor part of the worldwide isopropyl alcohol-production is provided in Central and South America (fig. 1.1).

Isopropyl alcohol is primarily used as solvent for paints, printing inks, in the production of silicon wafers, as reaction solvent in the manufacture of drugs, and as drying agent in fuels. Some isopropyl alcohol is employed as intermediate for the production of acetone and manufacture of base chemicals for cosmetics and pesticides. Isopropyl alcohol is also applied as antiseptic alcohol and as cleaning agent in industrial soldering of electrical circuits (Papa [1]).

***Sec*-butyl alcohol.**
According to isopropyl alcohol, *sec*-butyl alcohol is formed by the addition of water to the double-bond of *n*-butenes (B). Almost all *sec*-butyl alcohol produced is dehydrogenated to 2-butanone, also known as methyl ethyl ketone, which is an important solvent for coatings, resins, and adhesives due to its high ratio of dissolved matter/viscosity. Methyl ethyl ketone has properties similar to acetone, i. e. low boiling point, high evaporation rate, and is completely miscible with a broad range of hydrocarbons. In 2006, approximately 92 % of methyl ethyl ketone produced worldwide were obtained from dehydrogenation of *sec*-butyl alcohol (Hoell et al. [3]).

Approximately half of the world production capacity for *sec*-butyl alcohol-based methyl ethyl ketone resides in Asia, thirty percent in Western Europe, and twenty percent in the United States and in Central and South America (fig. 1.2). *Sec*-butyl alcohol is also employed as solvent, and, in a mixture with aromatic hydrocarbons, particularly suitable for alkyd resins and ethylcellulose

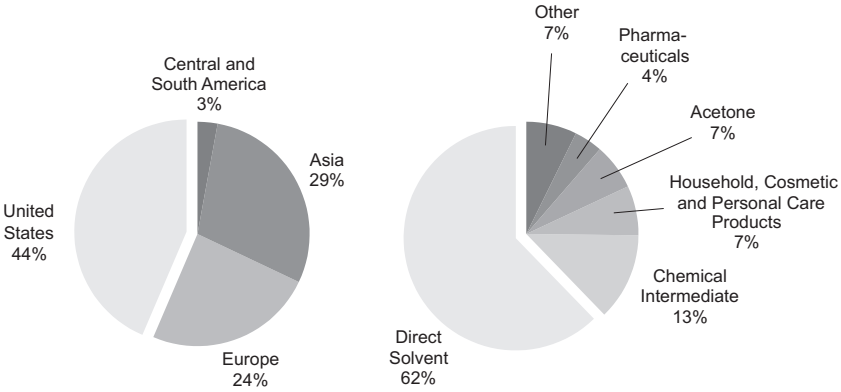

Figure 1.1: Location of IPA production sites and fields of application. World production total in 2008: 1 800 000 metric tons (Greiner and Inoguchi [2]).

lacquers. Moreover, *sec*-butyl alcohol is used for the production of amines and butyl acetate (Hahn et al. [4]).

The mentioned annual world production quantities of 1 800 000 metric tons isopropyl alcohol and 900 000 metric tons *sec*-butyl alcohol, respectively, emphasize the economical significance and the need for continuing retrieval of improved process alternatives.

1.2 Chemistry of *sec*-Alcohol Synthesis

Sec-Alcohols, i. e. isopropyl alcohol and *sec*-butyl alcohol, can be obtained either by hydration of the corresponding alkenes or by hydrogenation of corresponding ketones. *Sec*-butyl alcohol is a chiral molecule for which a racemic mixture of (2R)-butyl alcohol and (2S)-butyl alcohol is usually obtained by hydration. The commonly employed hydration catalysts – especially the acidic ion exchange resins considered in this work – are not enantio-selective. Therefore, stereochemical properties of *sec*-butyl alcohol, which, by the way, are usually also not of interest for most of the applications of *sec*-butyl alcohol, are generally not considered within this work.

The reaction path considered here is the hydration of alkenes, i. e. propene and *n*-butenes, for which the generalized overall equation can be written as:

$$C_nH_{2n} + H_2O \underset{H^+}{\overset{H^+}{\rightleftharpoons}} C_nH_{2n+1}OH\,. \tag{1.1}$$

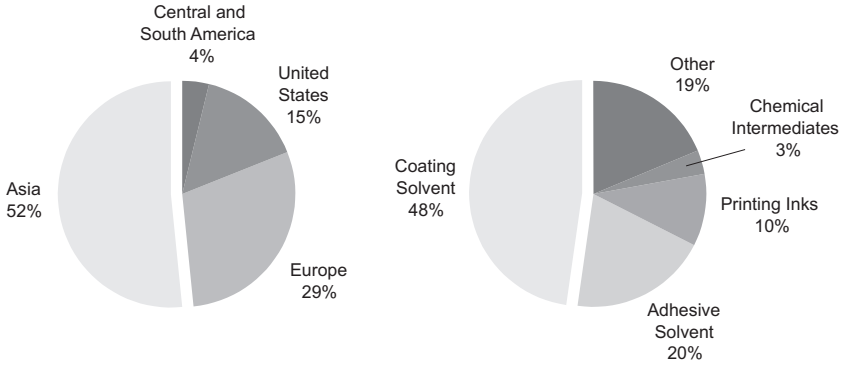

Figure 1.2: Location of SBA-based MEK production sites and fields of application. World production total for SBA-based MEK in 2008: 900 000 metric tons (Greiner and Funada [5]).

Due to Markovnikov's rule, from propene and *n*-butenes only secondary C_3- and C_4-alcohols can be obtained by the acid catalyzed hydration reaction. The hydration reaction is reversible and moderately exothermic. Heats of reaction for the ideal gases at 298.15 K and 101.3 kPa are compiled in table 1.1.

Possible side reactions are oligomerization of alkenes, polymerization of alkenes, and consecutive formation of secondary ethers which is the most important side reaction. The etherification reaction can proceed via two paths. Either two alcohol molecules condensate to give the secondary ether:

$$2\,C_nH_{2n+1}OH \underset{H^+}{\overset{H^+}{\rightleftharpoons}} C_{2n}H_{4n+1}O + H_2O\,, \tag{1.2}$$

or an alcohol molecule is linked to the double-bond of the corresponding alkene by an addition reaction:

$$C_nH_{2n+1}OH + C_nH_{2n} \underset{H^+}{\overset{H^+}{\rightleftharpoons}} C_{2n}H_{4n+1}O\,, \tag{1.3}$$

respectively. The consecutive etherifications of isopropyl alcohol and *sec*-butyl alcohol, which yield diisopropyl ether (DIPE) and DSBE, respectively, are reversible and exothermic to a similar extent compared to the related hydration reactions (table 1.1).

It is well accepted that the hydration reaction proceeds via a second order electrophilic addition mechanism (A_E2). In the first elementary reaction step a carbenium ion is formed from an alkene molecule by an acid proton which

Table 1.1: Heats of reaction of C_3- and C_4-hydration and -etherification reactions [6].

Product	Reaction type	Δh_r^0 kJ/mol
IPA	Addition	−51.4
sec-butyl alcohol (SBA)	Addition	−42.4
DIPE	Condensation	−16.0
DIPE	Addition	−67.4
DSBE	Condensation	−18.4
DSBE	Addition	−60.8

is attacked by the double-bond electrons of the alkene. In the second step a water molecule attaches to the carbenium ion under elimination of an acid proton (Nowlan and Tidwell [7]). The first reaction step is considered to be rate determining as the life cycle of the carbenium ion is extremely short. The dehydration of the alcohol as the reverse reaction forming the corresponding alkene proceeds via a first order elimination mechanism (E1).

From the hydration reaction, it can readily be deduced that both etherification reactions, i. e. addition and condensation, also proceed via a carbenium ion whereas the condensation is a first order nucleophilic substitution mechanism (S_N1). However, in all cases the formation of the carbenium ion can be considered as the rate determining step. As a consequence, when these reactions are homogeneously catalyzed the kinetics can probably be represented by a reaction rate expression which is elementary in nature.

1.3 Industrial Hydration Processes

Two possible routes exist for the formation of *sec*-alcohols from corresponding alkenes:

Indirect hydration wherein sulfuric acid is used to form mono- and dialkyl sulfates which are subsequently hydrolyzed by water forming the desired secondary alcohol, and

Direct hydration wherein heterogeneous acid catalysts are employed to convert the alkenes directly into the secondary alcohols.

Although worldwide approximately 50 % of isopropyl alcohol and *sec*-butyl alcohol are produced by indirect hydration processes, the underlying work focuses on the direct hydration. More specifically, it focuses on the liquid phase

direct hydration catalyzed by strong acidic ion exchange resins which provides only approximately 21 % and 16 % of worldwide manufacturing capacities for isopropyl alcohol and *sec*-butyl alcohol, respectively. The reason for favoring liquid phase direct hydration as research object is due to the generally higher potential for process intensification attempts compared to gas phase direct hydration processes, e. g. considering multi-functional reactors like reactive distillation, a liquid phase process can readily be extended by a second fluid phase as the catalyst employed here is already suitable for liquid phase operation. This is not the case for heterogeneous gas phase hydration catalysts which normally cannot withstand the hydrolytic nature of condensed phases.

1.3.1 Indirect Hydration

In a first step, the indirect hydration proceeds via the formation of mono- and dialkyl sulfates from alkenes with concentrated sulfuric acid as co-reactant:

$$\mathrm{C}_n\mathrm{H}_{2n} + \mathrm{H}_2\mathrm{SO}_4 \rightleftharpoons \mathrm{C}_n\mathrm{H}_{2n+1}\mathrm{OSO}_3\mathrm{H} \ , \tag{1.4}$$

$$2\,\mathrm{C}_n\mathrm{H}_{2n} + \mathrm{H}_2\mathrm{SO}_4 \rightleftharpoons (\mathrm{C}_n\mathrm{H}_{2n+1})_2\mathrm{OSO}_3 \ . \tag{1.5}$$

The first step is carried out as activated absorption which allows for feeding low alkene containing raffinate streams, i. e. the required alkene content amounts at least only to 10 wt% (cf. Burton and Wellman [8], Patterson [9]). However, most indirect hydration plants typically use raffinate streams containing 40 wt% to 60 wt% alkene as feedstock.

In the consecutive step water is added which hydrolyzes the mono- and dialkyl sulfates to form the secondary alcohol and dialkyl ether, respectively:

$$\mathrm{C}_n\mathrm{H}_{2n+1}\mathrm{OSO}_3\mathrm{H} + \mathrm{H}_2\mathrm{O} \rightleftharpoons \mathrm{C}_n\mathrm{H}_{2n+1}\mathrm{OH} + \mathrm{H}_2\mathrm{SO}_4 \ , \tag{1.6}$$

$$(\mathrm{C}_n\mathrm{H}_{2n+1})_2\mathrm{OSO}_3 + \mathrm{H}_2\mathrm{O} \rightleftharpoons (\mathrm{C}_n\mathrm{H}_{2n+1})_2\mathrm{O} + \mathrm{H}_2\mathrm{SO}_4 \ . \tag{1.7}$$

The dilution of sulfuric acid with water in the second step causes a significantly energy consuming reconcentration step of the acid solution by means of distillation to allow for recycling of acid in the process. Almost all units of the plant are subject to the highly corrosive sulfuric acid. Furthermore, the indirect hydration process causes serious environmental impact and suffers from low selectivity, i. e. the use of sulfuric acid as catalyst leads to large amounts of secondary dialkyl ethers, oligomers, and – with increasing temperature – also polymers. The possibility to use low alkene containing raffinate streams seems to be the only advantage of this process over direct hydration processes.

1.3.2 Direct Hydration

The first plant applied on a large scale for the direct hydration of propene with strong acidic ion exchange resins was started in 1972 by Deutsche Texaco AG in Meerbeck, Germany. The reactor was designed as co-currently operating trickle bed subdivided into multiple trays with intersectional injection of cooling water (fig. 1.3). The molar feed ratio of water to propene is about 12.5 : 1 to 15 : 1 and the conversion of propene is at least 75 % per pass (cf. Neier and Woellner [10]). Thus, the organic phase is almost consumed when the reaction mixture leaves the reactor and, as a consequence, the formed isopropyl alcohol has to be recovered from a dilute aqueous phase (approx. 5 mol % to 7 mol % of isopropyl alcohol). From the chemical engineer's point of view such unbalanced reactant streams do not represent an optimal reactor design with respect to very large recycle streams. Furthermore, the diluted aqueous phase needs to be concentrated to the near of the alcohol-water azeotrope by conventional distillation prior to an azeotropic distillation which recovers dry isopropyl alcohol.

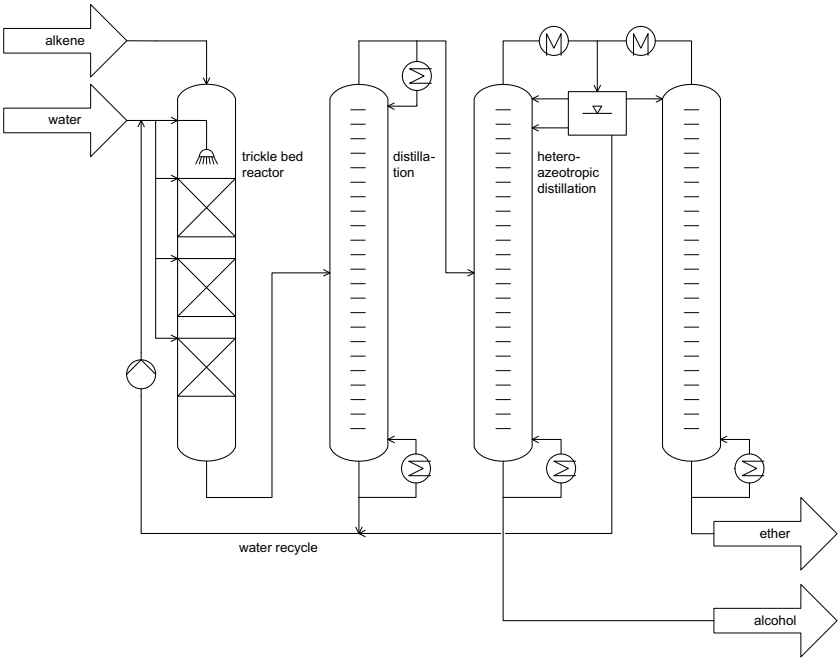

Figure 1.3: Trickle bed process for direct hydration of P.

In 1983 Deutsche Texaco AG started a production site for the ion exchange resin catalyzed liquid phase hydration of linear butene isomers. Here, Deutsche Texaco AG used a submerged fixed bed reactor with gas bubbling as described in Gianetto [11] or a flooded bed reactor as described in Al-Dahhan et al. [12], respectively. Due to the co-current up flow this reactor type has an improved wetting performance for which a significantly reduced molar feed ratio of water to *n*-butenes of about 1 : 2 is feasible. The *n*-butenes are not completely consumed and the product *sec*-butyl alcohol is enriched in the organic phase. Hence, *sec*-butyl alcohol can be recovered more easily from the organic phase, first by stripping of the unconverted *n*-butenes and, secondly by azeotropic distillation of the bottom product of the stripper. The reasoning for different catalytic multiphase reactor setups with respect to isopropyl alcohol and *sec*-butyl alcohol will be discussed more detailed in section 4.3.

More direct hydration processes are known either operated as gas phase or liquid phase processes whereas all processes employ heterogeneous catalysts. An overview of the most important direct hydration process variants and related operational conditions is provided in table 1.2

Table 1.2: Processes for direct hydration of linear C_3- and C_4-alkenes.

Prod.	Manufacturer	Phase / Catalyst	T °C	P MPa	Ref.
IPA	Veba Chemie (1966)	Gas / supported H_3PO_4	180 to 260	2.5 to 2.6	[13]
IPA	Tokuyama Soda (1973)	Liquid / $Na_3HSi(W_3O_{10})_4$	240 to 270	15 to 20	[14, 15]
IPA	Deutsche Texaco (1972)	Liquid / ion exchange resin	130 to 150	6 to 10	[10, 16]
SBA	Deutsche Texaco (1983)	Liquid / ion exchange resin	130 to 150	6 to 10	[17, 18]

1.4 Acidic Ion Exchange Resins as Catalysts

The most important type of today applied acidic ion exchange resins which are used as catalysts are crosslinked polystyrene polymers with divinylbenzene as crosslinking agent. After addition polymerization the resins are treated with concentrated sulfuric acid or chlorosulfonic acid to provide the catalytically used cation exchange function of the resin. The structure of the polystyrene-divinylbenzene copolymer is illustrated in fig. 1.4.

The macroscopic structure of acidic ion exchange resins can be divided into

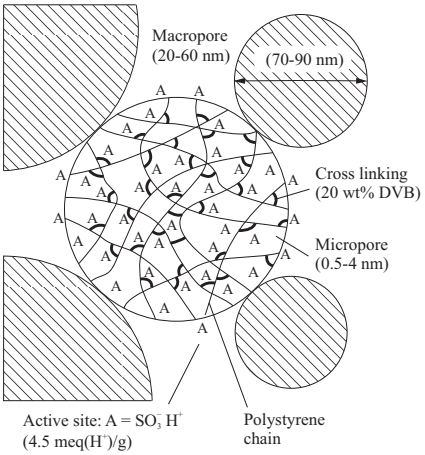

Figure 1.4: Schematic representation of the structure of sulfonic acid ion exchange resin. Adopted from [19, 20].

two types—gel and macroporous or macroreticular type resins. The matrix of dry gel type resins is completely collapsed, i. e. the resin is practically impermeable for the reactants and thus catalytically inactive. The acidic polymer matrix can increasingly swell in the presence of polar solvents with increasing polarity of the solvent and decreasing degree of crosslinking of the polymer matrix. The applicability of gel type resins is therefore limited to reactions carried out in polar solvents.

Macroporous type acidic ion exchange resins are agglomerates of gelphase spheres whereas the macroporous beads are of the same size as the gel type resins, typically ranging from 0.4 mm to 1.3 mm. Hence, the macroporous type resins expand the applicability of ion exchange resin catalysts to non-swelling reaction media and due to a generally improved accessability of the active sites these resins are today mostly used for catalytic purposes. Chakrabarti and Sharma [21] give a very comprehensive review on methods for ion exchange resin manufacture and catalytic application. In this work the macroporous sulfonic acid ion exchange resin Amberlyst DT of Rohm and Haas is used which is especially suitable for the common temperature range of the direct liquid phase hydration reaction (table 1.2).

1.5 Objectives of this Thesis

As can be deduced from the previous sections hydration of C_3- and C_4-alkenes has been employed on an industrial scale for quite a long time, either by the sulfuric acid catalyzed indirect process or by the direct process, catalyzed with acidic ion exchange resins. Although the direct hydration process has many advantages over the indirect process it is yet not superior over the indirect variant. Finding a reason for this situation is a major concern of the underlying work.

In order to resolve the main issues of the acidic ion exchange resin catalyzed hydration of C_3- and C_4-alkenes several reaction engineering aspects are investigated either by means of experimental work or simulation calculations, respectively:

Nonideal liquid phase thermodynamics comprising phase and chemical reaction equilibria are investigated by simulation,

Microkinetics are investigated in a continuously stirred multiphase tank reactor,

Multicomponent mass transfer across fluid-fluid interface, to outer catalyst surface, and within the polymer matrix of an ion exchange resin is simulated using the MAXWELL-STEFAN equations,

Macrokinetics are analyzed by comparison of experimental kinetic data influenced by mass transfer within the catalyst matrix and the developed microkinetic model supplemented with the dusty fluid model for multicomponent mass transfer in porous matter, and

Multicomponent Separation units are simulated with a nonequilibrium model.

Based on the results obtained from the above mentioned investigations an attempt towards process intensification of the acidic ion exchange resin catalyzed direct hydration is proposed.

A general overview on the topic of this work provides chapter 1, describing recent production capacities, utilization, and industrially applied processes for manufacturing of secondary C_3- and C_4-alcohols from related alkenes. Chapter 2 addresses work on modeling of physicochemical phenomena and mass transfer kinetics particularly important for nonideal liquid phase reaction systems. Chapter 3 starts with some preliminary considerations on a strategy for experimental investigations of the hydration reaction kinetics. Afterwards a detailed description of the designed experimental equipment and procedures which have been used during the course of this work will be given. A possibility for process intensification by applying heterogeneous reactive extraction—for the first time—to the ion exchange resin catalyzed liquid phase hydration of C_3- and C_4-alkenes is illustrated in chapter 4. The physicochemical models

described in chapter 2 are used in large scale simulations of a multifunctional hydration reactor and related separation units for product purification and recovery of unconverted reactants. The obtained results are presented and discussed in chapter 5.

References

[1] Papa, A. J. *Propanols*, in: M. Bohnet (Ed.). *Ullmann's Encyclopedia of Industrial Chemistry*, 7th Ed. Wiley-VCH, Weinheim, 2010.

[2] Greiner, E. O. C. and Y. Inoguchi. *Isopropyl Alcohol (IPA)*. CEH Product Review 668, SRI Consulting, 2009.

[3] Hoell, D., T. Mensing, R. Roggenbuck, M. Sakuth, E. Sperlich, T. Urban, W. Neier, and G. Strehlke. *2-Butanone*, in: M. Bohnet (Ed.). *Ullmann's Encyclopedia of Industrial Chemistry*, 7th Ed. Wiley-VCH, Weinheim, 2010.

[4] Hahn, H.-D., G. Dämbkes, N. Rupprich, and H. Bahl. *Butanols*, in: M. Bohnet (Ed.). *Ullmann's Encyclopedia of Industrial Chemistry*, 7th Ed. Wiley-VCH, Weinheim, 2010.

[5] Greiner, E. O. C. and C. Funada. *Methyl Ethyl Ketone (MEK)*. CEH Marketing Research Report 675, SRI Consulting, 2009.

[6] Cope, C. S. Equilibria in the Hydration of Propylene and of Butylenes. *J. Chem. Eng. Data* **11**, (1966), 379–383. DOI: 10.1021/je60030a027.

[7] Nowlan, V. J. and T. T. Tidwell. Structural Effects on Acid-Catalyzed Hydration of Alkenes. *Accounts Chem. Res.* **10**, (1977), 252–258.

[8] Burton, P. E. and W. E. Wellman. Process for Producing Isopropyl Alcohol and Di-Isopropyl Ether. U.S. Pat. 4,471,142. 1984.

[9] Patterson, J. A. Production of secondary butyl alcohol. U.S. Pat. 2,514,291. 1950.

[10] Neier, W. and J. Woellner. Use cation catalyst for IPA. *Hydrocarb. Process.* **51**, (1972), 113–116.

[11] Gianetto, A. *Multiphase Chemical Reactors*, in: A. Gianetto and P. L. Silveston (Eds.). *Multiphase Chemical Reactors*. Hemisphere Publishing, New York, 1986, pp 4–5.

[12] Al-Dahhan, M. H., F. Larachi, M. P. Dudukovic, and A. Laurent. High-Pressure Trickle-Bed Reactors: A Review. *Ind. Eng. Chem. Res.* **36**, (1997), 3292–3314. DOI: 10.1021/ie9700829.

[13] VEBA-Chemie AG. Process for Production of Alcohols by Catalytic Hydration of Olefins. G.B. Pat. 1,201,181. 1970.

[14] Onoue, Y., Y. Mitzutani, S. Akiyama, and Y. Izumi. Hydration with water. *Chemtech* **8**, (1978), 432–435.

[15] Izumi, Y., Y. Kawasaki, and M. Tani. Process for the Preparation of Alcohols. U.S. Pat. 3,758,615. 1973.

[16] Brandes, G., W. Neier, J. Wöllner, and W. Webers. Verfahren zur kontinuierlichen Herstellung von niederen Alkoholen, insbesondere Isopropanol. Ger. Pat. 2,147,740. 1973.

[17] Neier, W., W. Webers, R. Ruckhaber, G. Osterburg, and W. J. Ostwald. Process for the continuous production of secondary butyl alcohol. U.S. Pat. 4,476,333. 1984.

[18] Neier, W., W. Webers, M. Dettmer, and G. Osterburg. Process for the production of alcohols. U.S. Pat. 4,579,984. 1986.

[19] Pitochelli, A. R. *Ion Exchange Catalysis and Matrix Effects*. tech. rep., Rohm and Haas, Philadelphia, 1980.

[20] Sundmacher, K. Reaktivdestillation mit katalytischen Füllkörperpackungen : ein neuer Prozeß zur Herstellung der Kraftstoffkomponente MTBE. Ph.D. Thesis, Clausthal University of Technology, 1995.

[21] Chakrabarti, A. and M. M. Sharma. Cationic ion exchange resins as catalyst. *React. Polym.* **20**, (1993), 1–45. DOI: `10.1016/0923-1137(93)90064-M`.

2 Modeling and Simulation of Thermophysical Phenomena

The simultaneous phase and chemical equilibria of the C_3- and C_4-hydration systems are of particular importance as their reactants, i.e. water and alkenes, are only partially miscible in the liquid or liquid-like supercritical state, respectively. Therefore, the following subsections describe the modeling of liquid-liquid equilibria (LLE) involving supercritical alkenes, vapor-liquid equilibria (VLE) for separation simulation purposes, and chemical equilibria which are accompanied by the simultaneous phase split in the liquid state. Furthermore, the modeling of multicomponent mass transfer which is influenced by non-ideal fluid phase behavior is described.

2.1 Phase Equilibria

The thermodynamic condition for an equilibrium between multiple phases is the equality of temperature T, pressure P, and of the partial molar chemical potentials for each component μ_i in all coexisting phases $\alpha, \beta, \ldots, \zeta$

$$T^\alpha = T^\beta = \ldots = T^\zeta \,, \tag{2.1a}$$

$$P^\alpha = P^\beta = \ldots = P^\zeta \,, \tag{2.1b}$$

$$\mu_i^\alpha = \mu_i^\beta = \ldots = \mu_i^\zeta \,. \tag{2.1c}$$

The partial molar chemical potential can be obtained from:

$$\mu_i = \mu_i^0(T, P^0) + RT \ln \frac{\bar{f}_i}{f_i^0} \tag{2.2}$$

whereas the chemical potential $\mu_i^0(T, P^0)$ and fugacity f_i^0 of a component at reference state are independent of composition. As all phases must have the same temperature and pressure at equilibrium according to eqs. (2.1a) and (2.1b) also the chemical potential and fugacity at reference state will be equal within all coexisting phases. Hence, chemical potential and fugacity at reference state can be neglected. Inserting eq. (2.2) into eq. (2.1c) the phase

equilibrium condition reduces to the isofugacity criterion

$$\bar{f}_i\left(T,P,x^{\alpha}\right)=\bar{f}_i\left(T,P,x^{\beta}\right)=\ldots=\bar{f}_i\left(T,P,x^{\zeta}\right)\ . \tag{2.3}$$

The partial molar fugacity $\bar{f}_i$ can be expressed in two ways:

$$\bar{f}_i=x_i\gamma_i f_i^0\ , \tag{2.4a}$$

$$\bar{f}_i=x_i\bar{\varphi}_i P\ . \tag{2.4b}$$

In eq. (2.4a) f_i^0 is the standard fugacity of the pure liquid at system temperature and pressure which is independent of composition. This reference state is obligatory when the activity coefficient γ_i is computed with a common g^{E}-model (e.g. UNIQUAC, NRTL, etc.). However, depending on pressure and temperature the alkenes may be in liquid or supercritical state, respectively. This is particularly the case for relevant process conditions. Equation (2.4a) can not be applied to systems with supercritical components because this standard fugacity is only defined for the pure liquid which does not exist at supercritical conditions. In addition, the activity coefficient γ_i computed with a g^{E}-model is, strictly speaking, only valid for low pressures (<1 MPa). Hence, eq. (2.4b) is employed in this work for representing partial molar fugacities as this equation is generally valid regardless of the type of state (Walas [1], pp. 154-155).

2.1.1 Thermodynamic Model

The proper estimation of the thermodynamic behavior of partially miscible (unstable) liquids or liquid-like supercritical phases and of the components forming such phases is a prerequisite for detailed computer models on supercritical extraction processes. An unstable liquid exhibits the strongest case for thermodynamically non-ideal fluid phases. For the case of mixtures containing supercritical components, we are faced with the employment of an equation of state, including a mixing rule with the capability to express large molar excess free (Gibbs) energies. A lot of effort has been spent in the last 20 years in developing g^{E}-mixing rules for several equations of state (Valderrama [2]). One such model is the so-called volume translated Peng-Robinson equation of state (VTPR-EoS) of Ahlers and Gmehling [3–6] which will be presented briefly in the following paragraphs. They composed their model as a group contribution method by application of the universal functional activity coefficient (UNIFAC) model in order to provide g^{E}-data for the mixing rule of the cohesive energy parameter a. However, the prediction of LLE of hydrocarbon-alcohol-water systems with the UNIFAC model provides reliable results only at a qualitative level (Arce et al. [7]). Hence, in our application of the VTPR-EoS-model, the universal quasi-chemical (UNIQUAC) model is used for reproducing g^{E}-data.

Starting from the VTPR-EoS in the pressure explicit form

$$P = \frac{RT}{v + c - b} - \frac{a\alpha(T)}{(v + c)(v + c + b) + b(v + c - b)} \tag{2.5}$$

where b is the co-volume representing the most dense packing of molecules and a is the cohesive energy parameter representing attractive molecular interaction forces. Both parameters are determined from critical data for pure components. The temperature-dependent function, $a(T)$, improves the prediction of pure component vapor pressures. The volume correction, c, is defined by

$$c = v_{\text{exp}} - v_{\text{calc}} \qquad (T_{\text{r}} = 0.7) \tag{2.6}$$

and may be estimated from critical data to obtain the pure component correction, c_i

$$c_i = 0.252 \frac{RT_{\text{c},i}}{P_{\text{c},i}} (1.5448 z_{\text{c},i} - 0.4024) \tag{2.7}$$

if experimental molar volumes at a reduced temperature, $T_{\text{r}} = 0.7$, are not available.

Critical data and other pure component parameters for the components under consideration are given in table 2.1. For the computation of mixture and/or partial molar properties, the pure component parameters, $a_i(T) = a_i\alpha(T)$, b_i, and c_i have to be transformed by sufficient mixing rules into the mixture parameters, $a(T)$, b, and c.

Table 2.1: Thermophysical properties of the pure components [8].

Component	CAS-nr.	T_{c}	P_{c}	z_{c}	ω	r^{a}	q^{a}
		K	MPa	-	-	-	-
P	115-07-1	365.0	4.62	0.2756	0.148	2.25	2.02
1B	106-98-9	419.6	4.02	0.2767	0.187	2.92	2.56
*c*2B	590-18-1	435.6	4.21	0.2717	0.202	2.92	2.56
*t*2B	624-64-6	428.6	4.10	0.2741	0.214	2.92	2.56
IPA	67-63-0	508.3	4.76	0.2479	0.665	2.78	2.51
SBA	78-92-2	536.0	4.20	0.2523	0.576	3.45	3.05
DIPE	108-20-3	500.0	2.88	0.2672	0.340	4.74	4.09
W	7732-18-5	647.2	22.06	0.2294	0.344	0.92	1.40

[a] Gmehling and Onken [9]

For the mixing rule of the cohesive energy parameter, a, of the VTPR-EoS

according to Ahlers and Gmehling [4], we have

$$\frac{a(T)}{b} = \sum_i x_i \frac{a_i(T)}{b_i} - \frac{g^{\mathrm{E}}_{\mathrm{res}}}{0.53087} \tag{2.8}$$

where $g^{\mathrm{E}}_{\mathrm{res}}$ is the residual of the molar excess free (Gibbs) energy computed with the UNIFAC or UNIQUAC model, respectively (Fredenslund et al. [10], Abrams and Prausnitz [11]). The mixture parameters, b and c, are calculated from a quadratic mixing rule and a linear mixing rule, respectively.

This set of mixing rules allows computing composition-related thermodynamic data, e. g., partial molar fugacity coefficients, which are necessary for the simulation of LLE at high pressure or when supercritical components are present. However, the volume correction of the VTPR-EoS is only used for the calculation of densities. For all other purposes the volume correction is neglected. The reason for this approach is due to an inconsistence in the model which is discussed more detailed in Ahlers [12]. However, Péneloux et al. [13] found that the result of a phase equilibrium calculation does not depend on whether the volume correction is used or not.

The partial molar fugacity coefficients can be calculated from the following expression which is derived in appendix E.1.1:

$$\begin{aligned}\ln \bar{\varphi}_i = {} & \frac{\bar{b}_i}{b}\left(\frac{Pv}{RT} - 1\right) - \ln \frac{P(v-b)}{RT} \\ & - \frac{a}{2\sqrt{2}bRT}\left(\frac{\bar{a}_i}{a} + 1 - \frac{\bar{b}_i}{b}\right) \ln \frac{v + b\left(1+\sqrt{2}\right)}{v + b\left(1-\sqrt{2}\right)}\end{aligned} \tag{2.9a}$$

with the partial molar parameters, $\bar{a}_i$ and $\bar{b}_i$ (cf. Ahlers [12], pp. 66-68)

$$\bar{a}_i = b\left(\frac{a_i}{b_i} - \frac{RT\ln\gamma_i}{0.53087}\right) + \left(\sum_i x_i \frac{a_i}{b_i} - \frac{g^{\mathrm{E}}_{\mathrm{res}}}{0.53087}\right)\left(\bar{b}_i - b\right) \tag{2.9b}$$

$$\bar{b}_i = 2\sum_j x_j b_{i,j} - b \tag{2.9c}$$

whereas b and $b_{i,j}$ are calculated as

$$b = \sum_i \sum_j x_i x_j b_{i,j} \tag{2.9d}$$

and

$$b_{i,j}^{3/4} = \frac{b_i^{3/4} + b_j^{3/4}}{2} \ . \tag{2.9e}$$

2.1.2 Liquid-Liquid Equilibria

This section describes the simulation results obtained for the high pressure liquid-liquid equilibrium (HP-LLE) of the C_3- and C_4-hydration systems. The results presented here are obtained with the volume translated PENG-ROBINSON equation of state - universal quasi-chemical (VTPR-UNIQUAC) presented in section 2.1.1. The simulations are based on the RACHFORD-RICE flash algorithm which is described in, e. g. King [14], p. 75. Solving the RACHFORD-RICE equation

$$\sum_{i=1}^{n_c} \frac{z_i(K_i - 1)}{1 + \beta(K_i - 1)} = 0 \tag{2.10}$$

for β, where z_i is the mole fraction of component i in the feed mixture, K_i is the distribution coefficient of component i defined by

$$K_i = \frac{x_i'}{x_i''} = \frac{\bar{\varphi}_i''}{\bar{\varphi}_i'} \ , \tag{2.11}$$

and β is the ratio of amount light phase formed in the flash separation with respect to amount feed

$$\beta = \frac{n'}{n' + n''} \ , \tag{2.12}$$

the heavy phase mole fraction x_i'' can be obtained immediately from

$$x_i'' = \frac{z_i}{1 + \beta(K_i - 1)} \tag{2.13}$$

and the light phase mole fraction x_i' is calculated from eq. (2.11). Figure 2.1 shows a flow chart of the algorithm as being implemented in this work.

Results for the C_3-Hydration System

The pure component data needed by VTPR-UNIQUAC are given in table 2.1. However, mixture related data, i. e. UNIQUAC interaction parameters for the HP-LLE of this system, are not available from public literature resources. But, having access to experimental data (Horstmann et al. [15], Ihmels et al. [16, 17]), the missing parameters are fitted to these experimental data. The resulting UNIQUAC interaction parameters are compiled in table 2.2.

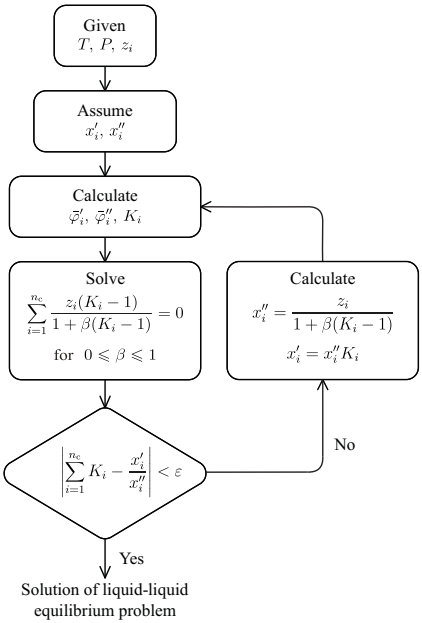

Figure 2.1: Flow chart of the Rachford-Rice algorithm.

Table 2.2: Binary UNIQUAC interaction parameters for the quaternary system P-W-IPA-DIPE for the high pressure LLE.

$i-j$	$a_{i,j}$ K	$a_{j,i}$ K
P-W	7122.2	1074.8
P-IPA	897.678	−581.276
P-DIPE	349.674	−201.326
W-IPA	426.493	246.864
W-DIPE	646.77	775.316
IPA-DIPE	−122.317	335.764

Figure 2.2 shows simulation results for the quaternary HP-LLE of the system propene-water-isopropyl alcohol-diisopropyl ether at 428 K and 9.5 MPa. The simulated binodal curve is represented by the grey-colored envelope which fits the experimental data points well. The ternary subsystems propene-isopropyl alcohol-water (frontal surface of tetrahedron) and diisopropyl ether-isopropyl alcohol-water (left hand surface of tetrahedron) show type I LLE, the subsystem propene-diisopropyl ether-water (bottom area of tetrahedron) has a type-II LLE, and the subsystem propene-diisopropyl ether-isopropyl alcohol (right hand surface of tetrahedron) is completely miscible throughout the entire concentration range.

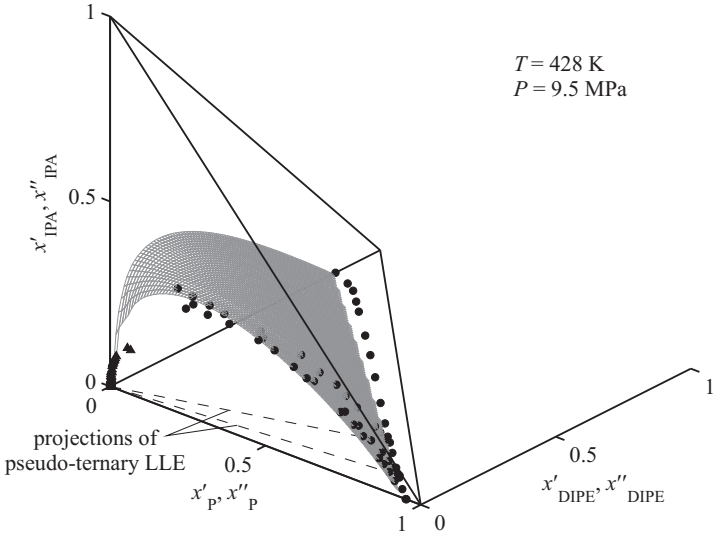

Figure 2.2: Isothermal, isobaric liquid-liquid equilibrium of the quaternary system P-DIPE-IPA-W; experimental data [15–17]: (▲) aqueous phase, (●) organic phase.

One ternary and two pseudo-ternary binodal curves with fixed molar feed ratios for propene and diisopropyl ether of 3.33 and 9.6, respectively, are depicted more detailed in figs. 2.3 to 2.5. For the pseudo-ternary mixtures with a propene to diisopropyl ether feed ratio of 9.6 (fig. 2.4), which resides between the ternary mixtures (fig. 2.3) and the pseudo-ternary mixtures with a feed ratio of 3.33 (fig. 2.5), the two data points close to the center of fig. 2.4 are somewhat far away from the calculated envelope. These data points show considerable lower isopropyl alcohol mole fractions in the organic phase than

the corresponding data points in the adjacent equilibrium charts. There is no theoretical proof for such a double-sided discontinuity. It obviously results from experimental uncertainties. All in all, simulation and experiments for the quaternary system agree well and, therefore, the thermodynamic model seems to be a promising tool for the description of HP-LLE of the reaction systems of interest.

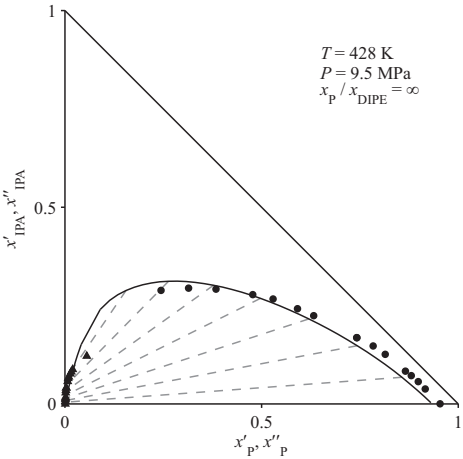

Figure 2.3: Isothermal, isobaric liquid-liquid equilibrium of the ternary system P-IPA-W; experimental data [15, 17]: (▲) aqueous phase, (●) organic phase.

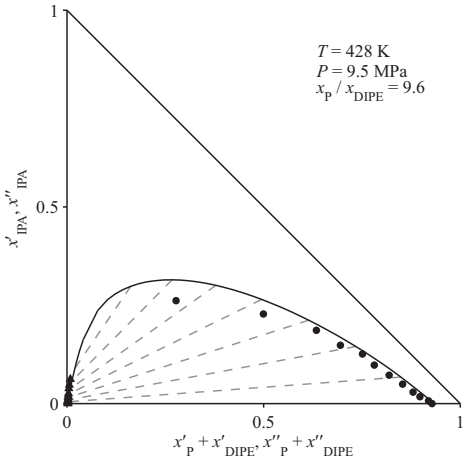

Figure 2.4: Isothermal, isobaric liquid-liquid equilibrium of the pseudo-ternary subsystem (P+DIPE)-IPA-W; experimental data [17]: (▲) aqueous phase, (●) organic phase.

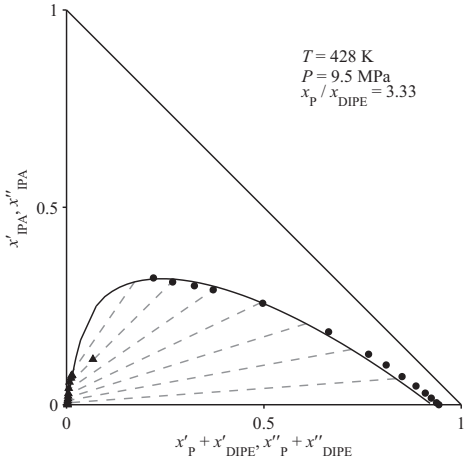

Figure 2.5: Isothermal, isobaric liquid-liquid equilibrium of the pseudo-ternary subsystem (P+DIPE)-IPA-W; experimental data [16]: (▲) aqueous phase, (●) organic phase.

Results for the C_4-Hydration System

Experimental data for the HP-LLE of the ternary system 1-butene-water-*sec*-butyl alcohol are accessible from the same source as for the C_3-hydration system (Horstmann et al. [18]), but, unfortunately, not from public literature resources. Interaction parameters for the UNIQUAC model are fitted to the experimental data at hand and are shown in table 2.3.

Table 2.3: Binary UNIQUAC interaction parameters for the ternary system 1B-W-SBA for the high pressure LLE.

$i-j$	$a_{i,j}$ K	$a_{j,i}$ K
1B-W	2503.1	982.79
1B-SBA	−805.59	1651.7
W-SBA	481.92	143.52

The potential by-product di-*sec*-butyl ether is not present in the experimental data and, hence, not included in the set of interaction parameters. However, the role of di-*sec*-butyl ether in the HP-LLE of the C_4-hydration system can safely be neglected. A proof for this statement is provided in section 3.4.2. The resulting simulation of the HP-LLE of the ternary system is illustrated in fig. 2.6. Also here, a sufficient representation of the experimental data is achieved with the VTPR-EoS.

2.1.3 Vapor-Liquid Equilibria

A reliable representation of the VLE of the quaternary system propene-water-isopropyl alcohol-diisopropyl ether in the pressure range 1 MPa to 2 MPa is needed for the simulation of distillation and stripping of a homogeneous organic liquid reactor outlet stream, respectively. Unconverted reactant propene – by far the lowest boiling component in the here considered system – can be recovered and recycled to the reactor feed by such a first distillation/stripping step. The pressure is arranged to a relatively high level, in order to save energy during recycling of propene. Due to the elevated pressure (1 MPa to 2 MPa), again, VTPR-UNIQUAC is employed here.

Fortunately, experimental VLE data for most of the subordinated binary systems are available from public literature resources. Only for the binary systems propene-diisopropyl ether and diisopropyl ether-water no data can be found in the literature. The VLE of these systems are, therefore, predicted by the VTPR-UNIFAC model and UNIQUAC interaction parameters are derived

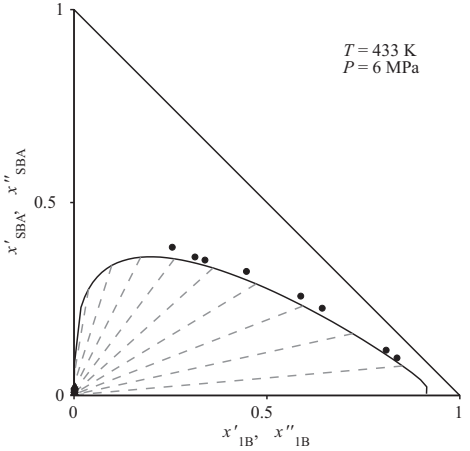

Figure 2.6: Isothermal, isobaric liquid-liquid equilibrium of the ternary system 1B-SBA-W; experimental data [18]: (▲) aqueous phase, (●) organic phase.

from their UNIFAC counterparts. The resulting interaction parameters are composed in table 2.4.

Table 2.4: Binary UNIQUAC interaction parameters for the quaternary system P-W-IPA-DIPE for VLE simulations with VTPR-UNIQUAC.

$i-j$	$a_{i,j}$ K	$a_{j,i}$ K	$b_{i,j}$	$b_{j,i}$	$c_{i,j}$ $10^{-3}\,\mathrm{K}^{-1}$	$c_{j,i}$ $10^{-3}\,\mathrm{K}^{-1}$
P-W	9493.7	465.8	39.9	−0.2707	1.0	3.5
P-IPA	276.007	−60.996	0.108	0.105	−0.286	−0.31
P-DIPE	72.752	208.782				
W-IPA	499.633	199.09	0.058	−0.226	−0.154	0.429
W-DIPE	282.102	389.523	−17.665	33.122	5.03	−9.31
IPA-DIPE	−126.108	342.43				

The fundamental principles for the separation sequence of a liquid phase alkene hydration process – discussed in section 5.1.2 for the C_3-hydration system – are also applicable to the C_4-hydration system and are, therefore, not considered in this work. This holds also for the analysis of VLE and vapor-liquid-liquid equilibria (VLLE), respectively.

The VLE simulations of the binary subsystems are conducted by bubble

point or dew point calculations, respectively. The first case corresponds to an isobaric calculation wherein pressure and mole fraction in the vapor are given and temperature and mole fraction in the liquid are determined iteratively by making use of eq. (2.3). In the latter case it is the other way around: temperature and mole fraction in the liquid are given whereas pressure and mole fraction in the vapor are calculated. The described combinations of either temperature with liquid phase mole fractions or pressure with vapor phase mole fractions are commonly used because pressure mainly affects the vapor phase and temperature has an essential impact on the liquid phase (Walas [1]).

Figure 2.7 illustrates the VLE of the binary system propene-diisopropyl ether at 298 K, 350 K and 400 K. propene is in the supercritical state at 400 K and corresponding pressures and, consequently, the two phase region is not existent throughout the entire mole fraction range.

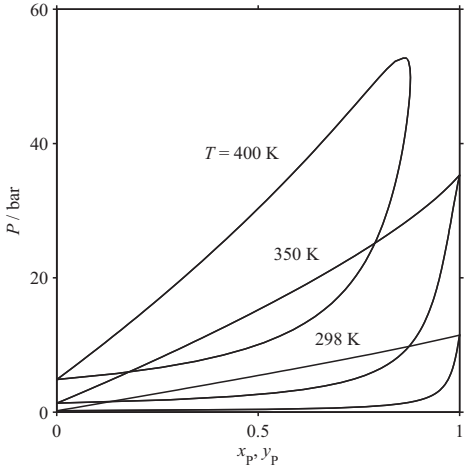

Figure 2.7: Isothermal vapor-liquid equilibria of the binary system P-DIPE; data points generated with the VTPR-UNIFAC model: (▼) vapor phase, (●) liquid phase.

This effect is also shown in fig. 2.8 for the binary system propene-isopropyl alcohol for 370 K which is slightly above the critical temperature of propene. The simulation fits the experimental data of Zabaloy et al. [19] well.

The system propene-water has a large miscibility gap, especially the solubility of propene in water is strongly limited to mole fractions below 0.2 mol % at 400 K and even decreases with temperature. Figure 2.9 shows a good correlation between simulation and experimental data of Li and McKetta [20].

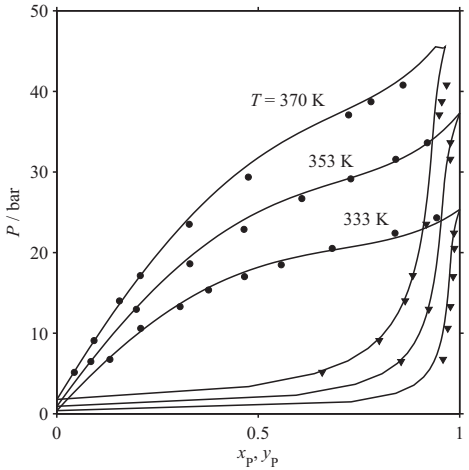

Figure 2.8: Isothermal vapor-liquid equilibria of the binary system P-IPA; experimental data [19]: (▼) vapor phase, (●) liquid phase.

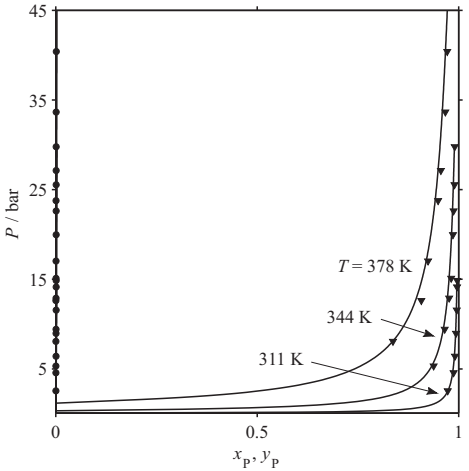

Figure 2.9: Isothermal vapor-liquid equilibria of the binary system P-W; experimental data [20]: (▼) vapor phase, (●) liquid phase.

Experimental data of Chamorro et al. [21] for the system diisopropyl ether-isopropyl alcohol at 313 K is also in good agreement with the simulation of the VTPR-UNIQUAC model (fig. 2.10). Especially the azeotropic behavior of this system is excellently reproduced.

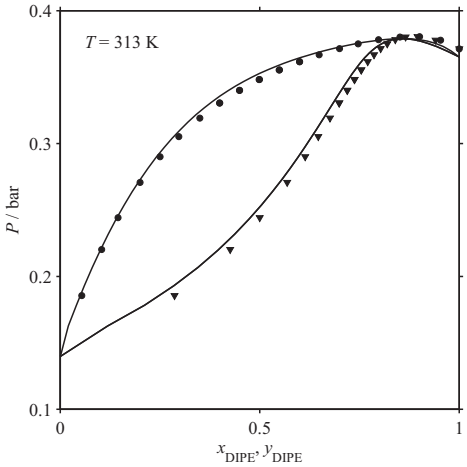

Figure 2.10: Isothermal vapor-liquid equilibrium of the binary system DIPE-IPA; experimental data [21]: (▼) vapor phase, (●) liquid phase.

This is also the case for the simulations of the azeotropic binary system isopropyl alcohol-water which is – in view of the large temperature range used in the study of Barr-David and Dodge [22] – in excellent agreement with their data for the subcritical state of isopropyl alcohol (fig. 2.11) as well as for the supercritical state (fig. 2.12).

2.1.4 Vapor-Liquid-Liquid Equilibria

The VLLE of the system diisopropyl ether-isopropyl alcohol-water arises in the heteroazeotropic separation of isopropyl alcohol and water with diisopropyl ether as entrainer. Other typically employed entrainers for the purification of isopropyl alcohol are cyclohexane and benzene (cf. Prokopakis and Seider [23]).

In experimental and simulation studies Seider and co-workers [24–26] exhaustively investigated the heteroazeotropic distillation of *sec*-butyl alcohol and water with di-*sec*-butyl ether as entrainer. Experimental VLLE data and the necessary thermophysical properties for the system di-*sec*-butyl ether-*sec*-butyl alcohol-water are provided by Kovach and Seider [27]. For the sake of

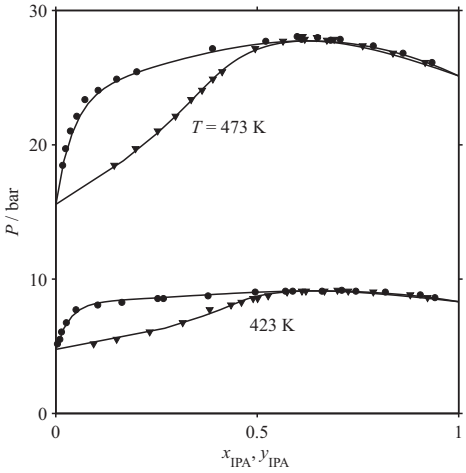

Figure 2.11: Isothermal vapor-liquid equilibria of the binary system IPA-W at subcritical conditions with respect to IPA; experimental data [22]: (▼) vapor phase, (●) liquid phase.

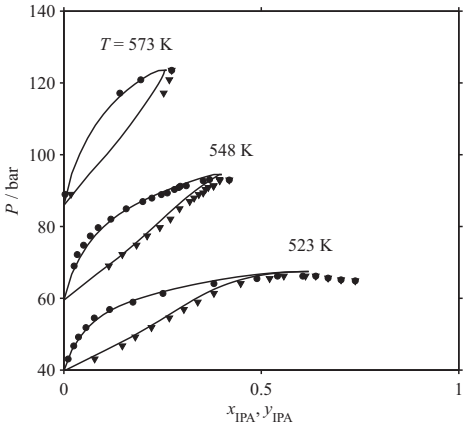

Figure 2.12: Isothermal vapor-liquid equilibria of the binary system IPA-W at supercritical conditions with respect to IPA; experimental data [22]: (▼) vapor phase, (●) liquid phase.

conciseness and due to the similarity of both systems with respect to their thermodynamic properties the VLLE of the system *sec*-butyl alcohol and water with di-*sec*-butyl ether is not discussed in this work.

For the system diisopropyl ether-isopropyl alcohol-water two experimental VLLE data sets (Lladosa et al. [28], Verhoeye [29]), four data sets for the LLE (Chen and Dong [30], Chen and Zhang [31], Chen and Dong [32], Hwang et al. [33]), and one data set for the VLE (Arce et al. [34]) – all at 0.1 MPa – are found in literature. These data sets are used for fitting modified universal quasi-chemical (UNIQUAC-q') interaction parameters which are compiled in table 2.5. The parameter q' is 0.89 and 0.88 for C_3- and C_4-alcohols, respectively, unity for water and equates to the parameter q for all other components. Further reading on the modification of the UNIQUAC-q' model is provided by Anderson and Prausnitz [35].

Table 2.5: Binary UNIQUAC-q' interaction parameters of the ternary system DIPE-IPA-W for VLLE simulations based on the γ-φ-approach.

$i-j$	$a_{i,j}$ K	$a_{j,i}$ K	$b_{i,j}$	$b_{j,i}$	$c_{i,j}$ $10^{-3}\,\mathrm{K}^{-1}$	$c_{j,i}$ $10^{-3}\,\mathrm{K}^{-1}$
DIPE-IPA	−1582.0	230.3	−2.38	−0.077	25.8	−3.4
DIPE-W	1020.1	373.0	−0.858	0.059	3.8	−3.7
IPA-W	−1982.8	−342.5	10.0	1.694	−12.3	2.2

As heteroazeotropic distillation is usually carried out at moderate pressures (< 1 MPa) the application of the so-called γ-φ-approach as phase equilibrium condition is preferred here, i. e. eq. (2.4a) is chosen for reproducing liquid phase fugacities while for the vapor phase eq. (2.4b) is still used. Furthermore, the following simplifications are made:

i) the vapor phase is taken to be ideal ($\bar{\varphi}_i^{\mathrm{V}} = 1$),

ii) the standard fugacities of the pure liquid components are substituted by the corresponding vapor pressures ($f_i^0 = P_i^{\mathrm{sat}}$), and

iii) the LLE condition reduces to the isoactivity criterion ($x_i'\gamma_i' = x_i''\gamma_i''$).

The simulation of VLLE is by far more complex than the simulation of VLE or LLE. A VLLE is in almost all cases a non-isothermal problem, i. e. the heterogeneous liquid boiling surface (intersection of the LLE envelope with the VLE envelope) is not necessarily planar in T-$\underline{x}$ space. Furthermore, for a class of systems, which most often arise in heteroazeotropic distillation and of which type is also the system under consideration, the LLE envelope is

limited and closed for an upper critical solution temperature. This means, a liquid can be stable, metastable, or unstable and it must be distinguished between these different states. This phase stability problem is a classical issue in thermodynamics which has been addressed by many authors in the past, (e. g. Michelsen [36], Sun and Seider [37], Wasylkiewicz et al. [38]). However, the most reliable and fastest method that could be found is that of Pham and Doherty [39] although it is restricted to systems which have an upper critical solution temperature and exhibit at most two immiscible liquid phases.

The simple but very effective idea of this method is to scan in a temperature interval, $T_\mathrm{L} < T_\mathrm{max} < T_\mathrm{H}$, for the maximum temperature at which for a given composition, $\underline{x}' = \underline{x}^0$, the liquid is not yet stable. Transforming the isoactivity criterion into a set of differential equations in terms of the composition gradient of the second coexisting phase and of the temperature gradient

$$\frac{\mathrm{d}x_i''}{\mathrm{d}t} = x_i'\gamma_i' - x_i''\gamma_i'' \,, \qquad i = 1, 2, \ldots, n_\mathrm{c} - 1 \tag{2.14a}$$

$$\frac{\mathrm{d}T}{\mathrm{d}t} = x_{n_\mathrm{c}}'\gamma_{n_\mathrm{c}}' - x_{n_\mathrm{c}}''\gamma_{n_\mathrm{c}}'' \tag{2.14b}$$

wherein x_{n_c} is obtained from

$$x_{n_\mathrm{c}} = 1 - \sum_{i=1}^{n_\mathrm{c}-1} x_i \tag{2.14c}$$

the liquid mixture can be checked for stability. If for the complete range of temperatures only the trivial solution, $\underline{x}' = \underline{x}''$, is found or the trajectories run out of the composition space, the considered mixture will be stable and the following calculation will be a VLE simulation. If, otherwise, a separate solution is found it will be metastable.

The VLLE algorithm is as follows: the scan starts here at $T(0) = T_\mathrm{H}$ and at an initial guess for $\underline{x}''(0)$. If the integration of eq. (2.14) does not converge or converges to the trivial solution the temperature is reduced by, e. g. 10 K, and a new attempt is made. This procedure is repeated until a separate solution for $\underline{x}''$ is found. If the iteration converges already during the first attempt the liquid mixture will be completely unstable.

Once a temperature is found – at which heterogeneity is detected – the corresponding vapor phase mole fractions are calculated from

$$y_i = \frac{x_i'\gamma_i' P_i^\mathrm{sat}}{P} \,, \qquad i = 1, 2, \ldots, n_\mathrm{c} \tag{2.15}$$

If the sum over all vapor mole fractions is greater than unity the temperature must be reduced iteratively until the sum of vapor mole fractions will be unity

and the heterogeneous liquid boiling surface will be located. Now an LLE simulation can be performed to accomplish the solution of the VLLE problem. If, otherwise, the sum over all vapor mole fractions is less than unity the LLE and VLE envelopes are disjoint from each other and, hence, a VLLE is not existent. The algorithm is illustrated in fig. 2.13.

Results for the VLLE simulations are depicted in fig. 2.14. The simulation is in fair agreement with the experimental data of Lladosa et al. [28]. Only the ternary heterogeneous azeotrope is not reproduced by this simulation and for tie line No. 1 which is close to the plait point the model predicts a stable (homogeneous) liquid mixture. This is probably due to the uncertainty in the fitted UNIQUAC-q' interaction parameters as the ternary azeotrope is very close to the binary azeotrope of the system diisopropyl ether-water, i. e. the isopropyl alcohol content of the ternary azeotrope is only as low as 6.2 mol %.

To summarize, a fast and reliable method is used to check the stability of liquid mixtures which have an upper critical solution temperature and exhibit no more than two immiscible phases. Based on this stability algorithm solutions to VLLE problems are readily obtained. The VLLE of the system diisopropyl ether-isopropyl alcohol-water is sufficiently reproduced for studying the heterogeneous azeotropic distillation of this system by simulations.

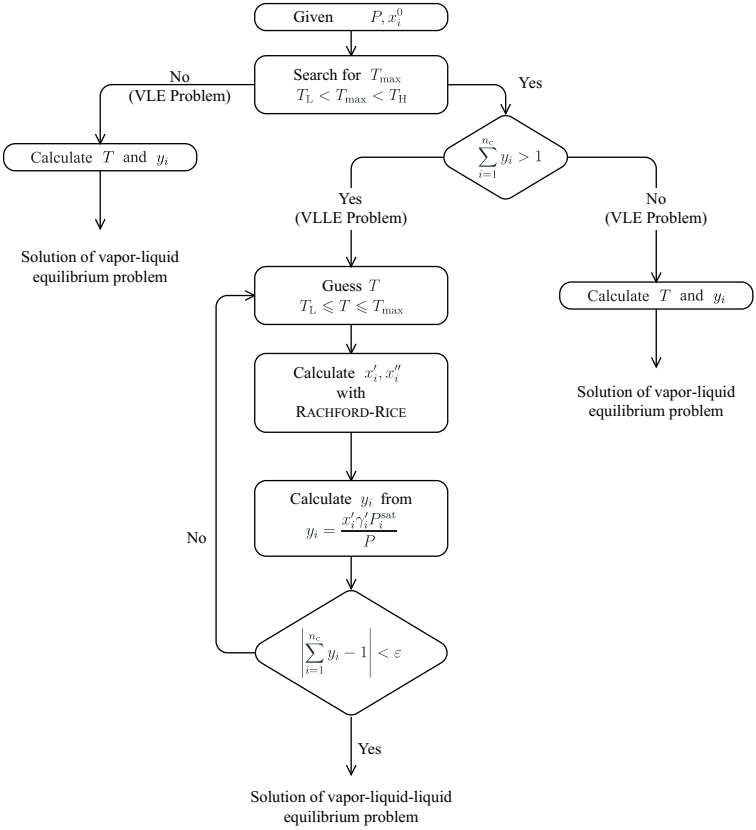

Figure 2.13: Flowchart of the VLLE algorithm (adopted from [39]).

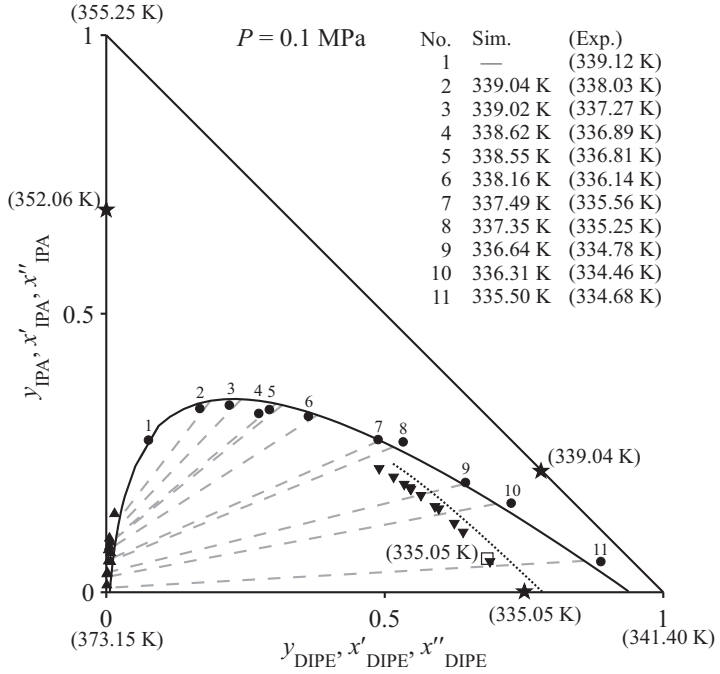

Figure 2.14: Isobaric vapor-liquid-liquid equilibrium of the ternary system DIPE-IPA-W; experimental data [28]: (▼) vapor phase, (●) organic liquid phase, (▲) aqueous liquid phase, (★) binary azeotrop, (□) ternary azeotrop.

2.2 Chemical Equilibria

Information on the simultaneous chemical and phase equilibria of the C_3- and C_4-hydration systems is important for a general understanding of the reactions and their course depending on temperature, pressure and reactant feed ratio. Their influence on the simultaneous chemical and phase equilibria is discussed and illustrated.

The composition of a reacting mixture at chemical equilibrium can be determined by minimization of the free (GIBBS) energy of the mixture for a given set of temperature and pressure. Due to stoichiometries the changes in the amount of the reacting species can simply be represented by the extent of reaction ε whereby the condition for chemical equilibrium can be expressed by

$$\left(\frac{\partial ng}{\partial \varepsilon}\right)_{T,P} = \sum_{i=1}^{n_c} \nu_i \mu_i = 0 \; . \tag{2.16}$$

Providing the definition of the activity

$$a_i = \frac{\bar{f}_i}{f_i^0} \tag{2.17}$$

and introducing eq. (2.17) into eq. (2.2) the partial molar chemical potential μ_i of component i can be expressed as

$$\mu_i = \mu_i^0(T, P^0) + RT \ln a_i \; . \tag{2.18}$$

The reference state for $\mu_i^0(T, P^0)$ and f_i^0 is arbitrary given that the partial molar fugacity $\bar{f}_i$ is calculated with eq. (2.4b). Data for $\mu_i^0(T, P^0)$ at the reference state of the ideal gas at 1 atm and, commonly at 298.15 K, are readily available in the open literature and the fugacity of the ideal gas reference state simplifies to $f_i^0 = 1\,\text{atm}$. For convenience, the ideal gas at 1 atm and 298.15 K is chosen as reference state. Chemical potentials and enthalpies at this ideal gas reference state are listed in table 2.6. For the calculation of chemical potentials at system temperature coefficients of a polynomial temperature function for ideal gas heat capacities at constant pressure are also provided in table 2.6. A survey on the necessary computations is given in appendix E.1.2.

Introducing further eq. (2.17) into eq. (2.18) the chemical equilibrium condition can be reshaped, by defining the chemical equilibrium constant as

$$-RT \ln K_a = \sum_{i=1}^{n_c} \nu_i \mu_i^0(T, P^0) \; , \tag{2.19}$$

into the common form of the mass action law

$$K_a = \prod_{i=1}^{n_c} a_i^{\nu_i} \ . \tag{2.20}$$

Table 2.6: Ideal gas reference enthalpies, free (GIBBS) energies, and polynomial coefficients for heat capacity temperature function $c_P/R = a_0 + a_1 T + a_2 T^2 + a_3 T^3 + a_4 T^4$, [40], pp. A.1-A.60.

Comp.	h^{ref} kJ mol	μ^{ref} kJ mol	a_0 -	a_1 $\times 10^3$	a_2 $\times 10^5$	a_3 $\times 10^8$	a_4 $\times 10^{11}$
P	20.0	62.5	3.834	3.893	4.688	−6.013	2.283
1B	−0.54	70.37	4.389	7.984	6.143	−8.197	3.165
*c*2B	−7.4	65.46	3.689	19.186	2.23	−3.426	1.256
*t*2B	−11.0	63.34	5.584	−4.89	9.133	−10.975	4.085
IPA	−272.7	−173.32	3.334	18.853	3.644	−6.115	2.543
SBA	−292.75	−167.71	3.86	28.561	2.728	−5.14	2.117
DIPE[a]	−319.9	−124.8	−3.256	96.097	−8.7	4.644	−1.049
W	−241.81	−228.72	4.395	−4.186	1.405	−1.564	0.632

[a] Cope [41]

The actual algorithm for computing simultaneous phase and chemical equilibria is subject to the assumption that the reaction takes place in the aqueous phase exclusively, provided that two immiscible phases exist at chemical equilibrium. This assumption is basing on the phenomenon that the aqueous phase separates the solid catalyst from the organic phase due to the wettability of the acidic catalyst by the aqueous phase which is superior compared to the organic phase.

The algorithm is based, primarily, on an inner loop which computes the compositions and ratio of amount of the formed light phase with respect to amount feed at phase equilibrium. This loop bases on the RACHFORD-RICE algorithm which is described more detailed in section 2.1.2. Secondly, an outer loop iterates the extent of reaction until a solution for the chemical equilibrium condition eq. (2.20) is found whereas the r. h. s. of eq. (2.20) is formed using the activities in the aqueous phase obtained from the phase equilibrium calculations of the inner loop. It should be noted here, eq. (2.20) is applied repeatedly according to the number of reactions considered in a chemical equilibrium calculation. This method for the computation of simultaneous phase and chemical equilibria is adopted from Walas [1] and found to be fast and robust. A solution is usually gained by five to eight iterations of the outer loop.

2.2.1 Results for the C_3-Hydration System

Figure 2.15 shows the distribution of the products isopropyl alcohol and diisopropyl ether between the two immiscible phases and the extent of reaction for both, the formation of isopropyl alcohol and diisopropyl ether. For pressures exceeding 15 MPa, the aqueous phase vanishes. It remains a homogeneous liquid mixture which is of organic nature. The extent of reaction for both, isopropyl alcohol and diisopropyl ether formation, are practically independent of pressure. This result is to be expected as the activities in the liquid phases are almost independent of pressure.

The dependence on temperature is illustrated in fig. 2.16. The extents of both reactions show the expectable trend of decreasing extent of reaction with decreasing temperature, but the trends are negligible small. However, the influence on phase equilibrium compositions is more considerable. The solubility for isopropyl alcohol in the aqueous phase increases and the diisopropyl ether content in the organic phase decreases with increasing temperature. The mixture is a homogeneous liquid for temperatures above 428 K.

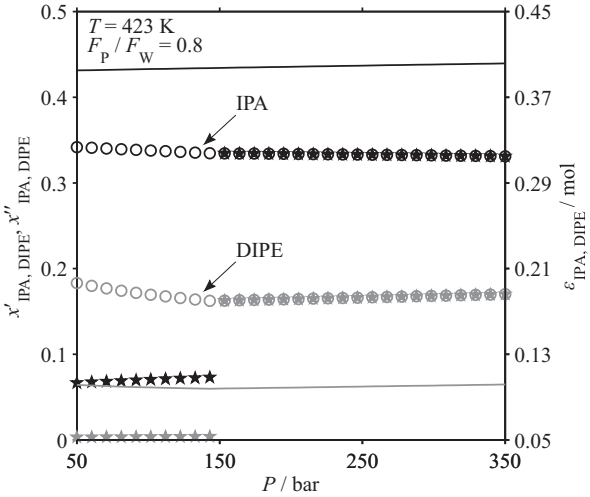

Figure 2.15: Distribution of IPA (black) and DIPE (gray) at chemical equilibrium as function of pressure; (★) aq. phase, (○) org. phase, (–) extent of reaction ε.

Figure 2.17 illustrates the dependence of chemical and phase equilibria on reactant feed ratio. The extents of reactions pass through a maximum close to the stoichiometric feed ratio. At this feed ratio the chemical equilibrium is finally

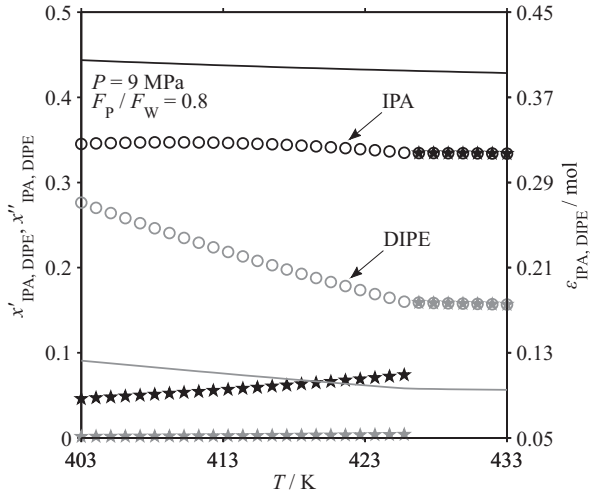

Figure 2.16: Distribution of IPA (black) and DIPE (gray) at chemical equilibrium as function of temperature; (★) aq. phase, (○) org. phase, (–) extent of reaction ε.

reached for a homogeneous liquid. The selectivity with respect to isopropyl alcohol at chemical equilibrium is low at this point which means that – following reactant feed ratios approaching unity – the additionally obtained isopropyl alcohol is consumed by the formation of diisopropyl ether. In spite of the increasing extents of reactions the compositions of the coexisting liquid phases remain constant. This is due to the increasing amount of organic phase which acts as a storage for isopropyl alcohol and diisopropyl ether. Furthermore, it can be seen for reactant ratios in the range 10^{-2} to 10^{-1} that extent of reaction and mole fractions of isopropyl alcohol coincide for identically scaled axes, thereby indicating full conversion of propene.

To summarize, temperature and pressure have only minor impact on yield and selectivity at chemical equilibrium. The only important effects are the loss in selectivity when a reactant feed ratio is used which is close to unity and the transition from a chemical equilibrium in multiple phases to an equilibrium in a single homogeneous phase.

2.2.2 Results for the C_4-Hydration System

The *n*-butenes (B) consists of the three isomers 1-butene (1B), *cis*-2-butene (*c*2B), and *trans*-2-butene (*t*2B). The isomerization is catalyzed by the acidic

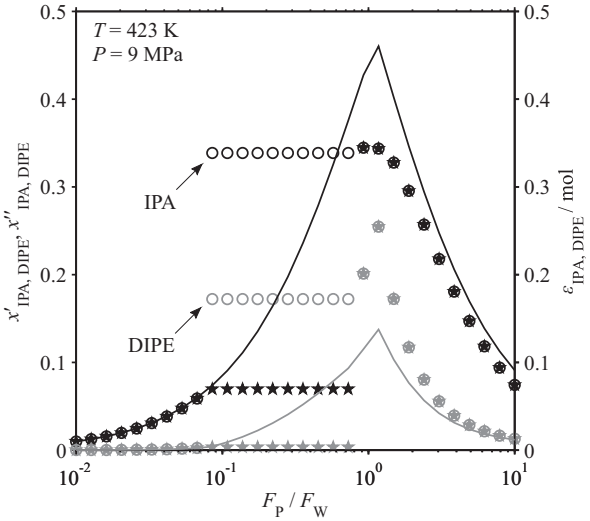

Figure 2.17: Distribution of IPA (black) and DIPE (gray) at chemical equilibrium as function of feed ratio; (★) aqueous phase, (○) organic phase, (–) extent of reaction ε.

catalyst as well as the hydration. From the detailed discussion in section 3.1.1 it can be concluded that the isomerization is remarkably faster than the hydration reaction and is – applying quasi-stationarity – at equilibrium. Therefore, the isomerization equilibrium can be incorporated into the chemical equilibrium constant for the formation of *sec*-butyl alcohol.

Starting at the common mass action law expressed in activities and in reciprocal form, and presuming further ideality for the mixture of the isomers the mass action law of the hydration reaction can be expanded as follows:

$$\frac{1}{K_a^{\mathrm{C_4}}} = \frac{a_{\mathrm{B}} a_{\mathrm{W}}}{a_{\mathrm{SBA}}} = \frac{(x_{1\mathrm{B}}^{\mathrm{iso}} + x_{c2\mathrm{B}}^{\mathrm{iso}} + x_{t2\mathrm{B}}^{\mathrm{iso}}) a_{\mathrm{B}} a_{\mathrm{W}}}{a_{\mathrm{SBA}}} \,. \tag{2.21}$$

Together with the mass action laws for the hydrations of each *n*-butene isomer which is expanded by the isomeric equilibrium composition of the isomer

$$\frac{K_{a,k\text{-SBA}}}{x_k^{\mathrm{iso}}} = \frac{a_{\mathrm{SBA}}}{x_k^{\mathrm{iso}} a_k a_{\mathrm{W}}} \,, \qquad k = \{1\mathrm{B}, c2\mathrm{B}, t2\mathrm{B}\} \tag{2.22}$$

it is possible to express the hydration equilibrium of an isomer mixture at equilibrium as a cumulative series of the hydration equilibria for the individual isomers by introducing eq. (2.22) into eq. (2.21)

$$\frac{1}{K_a^{\mathrm{C_4}}} = \frac{x_{1\mathrm{B}}^{\mathrm{iso}}}{K_{a,1\mathrm{B\text{-}SBA}}} + \frac{x_{c2\mathrm{B}}^{\mathrm{iso}}}{K_{a,c2\mathrm{B\text{-}SBA}}} + \frac{x_{t2\mathrm{B}}^{\mathrm{iso}}}{K_{a,t2\mathrm{B\text{-}SBA}}} \,. \tag{2.23}$$

The mole fractions in eqs. (2.21) to (2.23) are obtained from an equilibrium calculation for the isomerization equilibrium.

Using this chemical equilibrium constant the following results for the chemical equilibrium simulations of the *sec*-butyl alcohol formation are obtained. Generally speaking, the results for the C_4-hydration system are similar to those obtained for the C_3-hydration system. In figs. 2.18 and 2.19, the extent of reaction depends apparently stronger on pressure and temperature as for the C_3-hydration system, but it should be noted here that the axis limits are as narrow as 8×10^{-3} and 2×10^{-3}, respectively.

Figure 2.20 depicts the simulated dependency of equilibrium compositions and extent of reaction on reactant feed ratios. In these simulations the formation of di-*sec*-butyl ether is neglected. This is justified in section 3.4.2. From fig. 2.20 it might be deduced that a single phase operation is beneficial due to the high *sec*-butyl alcohol yield. But, for the single phase region the mentioned neglect is not valid, even more is a dramatic oversimplification. At relatively high *sec*-butyl alcohol concentrations the formation of di-*sec*-butyl ether increases drastically, similar to the C_3-hydration system, illustrated in fig. 2.17. Hence, for *sec*-butyl alcohol synthesis, the single phase situation shown in fig. 2.20

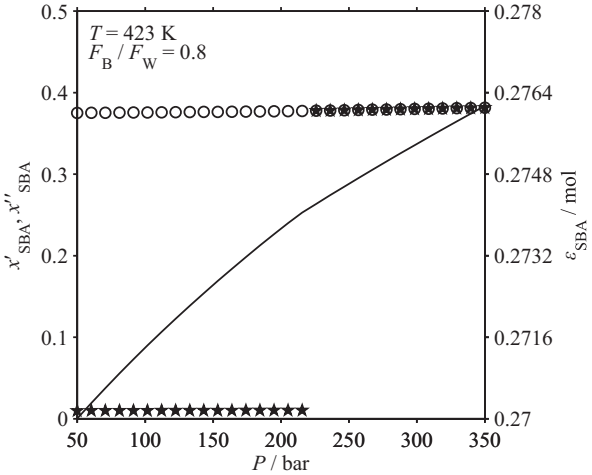

Figure 2.18: Distribution of SBA at chemical equilibrium as function of pressure; (★) aqueous phase, (○) organic phase, (–) extent of reaction ε.

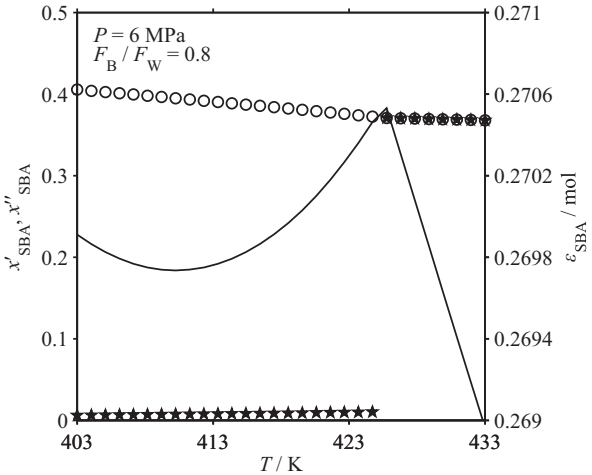

Figure 2.19: Distribution of SBA at chemical equilibrium as function of temperature; (★) aqueous phase, (○) organic phase, (–) extent of reaction ε.

should not be used for reasonable process design.

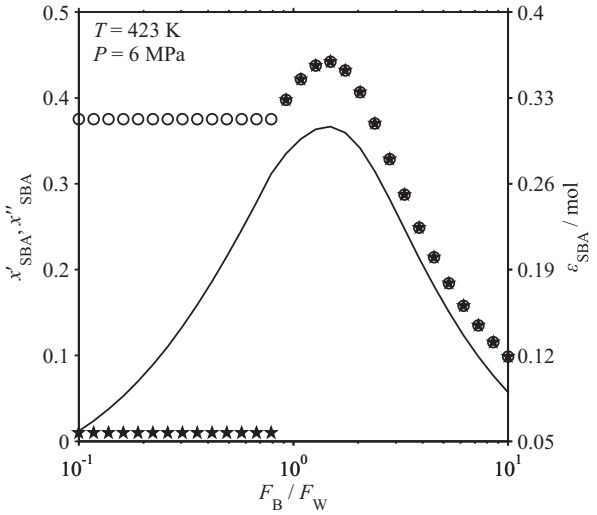

Figure 2.20: Distribution of SBA at chemical equilibrium as function of feed ratio; (★) aqueous phase, (○) organic phase, (–) extent of reaction ε.

2.3 Multicomponent Mass Transfer

The generalized Maxwell-Stefan equations (GMS) have been chosen to describe multicomponent mass transfer in nonideal fluid mixtures. As shown by many examples (cf. Krishna and Wesselingh [42]), the GMS confirm experimentally observed phenomena of multicomponent systems which are:

i) *reverse diffusion* of a component against its concentration gradient,

ii) *osmotic diffusion* of a component in the absence of a concentration gradient, and

iii) *diffusion barrier* which means no transport of a component occurs although its concentration gradient is nonzero.

Since these diffusional coupling effects are significant for liquid-liquid extraction systems as demonstrated experimentally and theoretically by Krishna et al. [43] and others (e. g. Haeberl and Blass [44], Uribe-Ramirez and Korchinsky

[45]), the GMS seem to be sufficient for the simulation of multicomponent extraction processes.

Following the detailed survey of Taylor and Krishna [46], a brief outline of the model equations used in this work is given. Neglecting external body forces but taking into account chemical potential gradients which should be a valid assumption for non-electrolytic mixtures processed by conventional extraction equipment, e. g., towers equipped with trays or structured packing, the film model equations for a nonideal fluid mixture are given by:

$$\frac{x_i}{RT}\nabla_{T,P}\mu_i = \sum_{\substack{j=1\\ j\neq i}}^{n_\mathrm{c}} \frac{x_i N_j - x_j N_i}{c_\mathrm{t}\,Đ_{i,j}}\ , \qquad i = 1, 2, \ldots, n_\mathrm{c}-1\ , \tag{2.24}$$

with $Đ_{i,j}$ the matrix of MAXWELL-STEFAN diffusivities, c_t the total molar concentration of the mixture, N_i the molar flux of component i, and $\nabla_{T,P}\mu_i$, the isothermal and isobaric partial molar chemical potential gradient of component i. Only $n_\mathrm{c}-1$ of the equations in eq. (2.24) are independent due to the GIBBS-DUHEM restriction that the sum of all chemical potentials during their isothermal and isobaric change remains constant:

$$\sum_{i=1}^{n_\mathrm{c}} x_i \frac{\mathrm{d}\mu_i}{\mathrm{d}z} = 0\ . \tag{2.25}$$

The term on the left hand of eq. (2.24) can be reformulated as follows:

$$\frac{x_i}{RT}\nabla_{T,P}\mu_i = \frac{x_i}{RT}\sum_{j=1}^{n_\mathrm{c}-1}\left.\frac{\partial\mu_i}{\partial x_j}\right|_{T,P,\Sigma}\nabla x_j\ , \qquad i = 1, 2, \ldots, n_\mathrm{c}-1 \tag{2.26a}$$

with

$$\mu_i = x_i RT \ln\bar{\varphi}_i \tag{2.26b}$$

to give

$$\frac{x_i}{RT}\nabla_{T,P}\mu_i = \frac{x_i}{RT}\sum_{j=1}^{n_\mathrm{c}-1} x_i RT\left.\frac{\partial \ln\bar{\varphi}_i}{\partial x_j}\right|_{T,P,\Sigma}\nabla x_j \tag{2.26c}$$

which can be simplified into

$$\frac{x_i}{RT}\nabla_{T,P}\mu_i = \sum_{j=1}^{n_c-1}\left(\delta_{i,j} + x_i \left.\frac{\partial \ln \bar{\varphi}_i}{\partial x_j}\right|_{T,P,\Sigma} \nabla x_j\right) \tag{2.26d}$$

where $\delta_{i,j}$ is the KRONECKER delta defined by

$$\delta_{i,j} = \begin{cases} 1 & \text{if } i = j \\ 0 & \text{if } i \neq j\ . \end{cases} \tag{2.26e}$$

Introducing the matrix of thermodynamic factors, $\Gamma_{i,j}$,

$$\Gamma_{i,j} = \delta_{i,j} + x_i \frac{\partial \ln \bar{\varphi}_i}{\partial x_j}\ , \qquad i,j = 1,2,\ldots,n_c - 1 \tag{2.27}$$

and combining eq. (2.27) with eq. (2.26d) results in

$$\sum_{j=1}^{n_c-1}\Gamma_{i,j}\nabla x_j = \sum_{j=1}^{n_c-1}\left(\delta_{i,j} + x_i \left.\frac{\partial \ln \bar{\varphi}_i}{\partial x_j}\right|_{T,P,\Sigma} \nabla x_j\right)\ . \tag{2.28}$$

Employing the steady state film model, eq. (2.24) reduces to a system of one-dimensional ordinary differential equations (ODE) describing the composition profiles across the film layer

$$\frac{\mathrm{d}x_i}{\mathrm{d}z} = [\Gamma]^{-1}\sum_{\substack{j=1\\ j\neq i}}^{n_c}\frac{x_i N_j - x_j N_i}{c_t \mathcal{D}_{i,j}}\ . \tag{2.29}$$

By substituting z with the dimensionless length coordinate, λ, of the film layer

$$\lambda = \frac{z}{\delta}\ , \tag{2.30}$$

we obtain

$$\frac{\mathrm{d}x_i}{\mathrm{d}\lambda} = [\Gamma]^{-1}\sum_{\substack{j=1\\ j\neq i}}^{n_c}\frac{x_i N_j - x_j N_i}{\frac{c_t}{\delta}\mathcal{D}_{i,j}} \tag{2.31}$$

where δ is the thickness of the film layer which must be estimated from appropriate fluid dynamic models. In this work, the model of Ruivo et al. [47] for a structured packing of the corrugated sheet type is employed, which is a modification to supercritical extraction of the mass transfer model of Rocha

et al. [48] for distillation. The film thickness is combined with diffusivities to give the matrix of mass transfer coefficients

$$\kappa_{i,j} = \frac{Đ_{i,j}}{\delta} , \qquad i,j = 1,2,\ldots,n_c - 1 . \tag{2.32}$$

The final working form of the multicomponent film model equations results from introduction of eq. (2.32) into eq. (2.31)

$$\frac{\mathrm{d}x_i}{\mathrm{d}\lambda} = [\Gamma]^{-1} \sum_{\substack{j=1 \\ j\neq i}}^{n_c} \frac{x_i N_j - x_j N_i}{c_t \kappa_{i,j}} . \tag{2.33}$$

2.3.1 Mathematical Model Implementation

The multicomponent film model equations, eq. (2.33), are implemented making the following assumptions:

i) the transport is in steady state, no accumulation or reaction of mass occurs in the films or at the interface,

ii) the mass transfer takes place under isothermal and isobaric conditions,

iii) the films are in equilibrium at the interface, and

iv) the equilibrium compositions at the interface are allowed to change dynamically during the extraction process.

From assumption (*i*), it is derived that the fluxes in both films surrounding the interface must be equal

$$N_i = N_i^{\mathrm{L1}} = N_i^{\mathrm{L2}} \tag{2.34}$$

and the fluxes remain constant throughout the thickness of the film layer

$$\frac{\mathrm{d}N_i}{\mathrm{d}\lambda} = 0 , \qquad i = 1,2,\ldots,n_c \tag{2.35}$$

where the superscripts $^{\mathrm{L1}}$ and $^{\mathrm{L2}}$ denote the organic and aqueous films, respectively. The two regions, namely the two films, may be folded at the interface to give one region for both the organic and the aqueous films whereby, on one hand, this region borders on the bulk phases and, on the other, it borders on the interface. When we further assume a positive flux to represent mass transfer from the organic into the aqueous phase, eq. (2.34) is cast into

$$N_i = N_i^{\mathrm{L1}} = -N_i^{\mathrm{L2}} \tag{2.36}$$

and, consequently, combining eq. (2.33) with eq. (2.36), we obtain for the organic film

$$\frac{\mathrm{d}x_i^{\mathrm{L1}}}{\mathrm{d}\lambda} = \left[\Gamma^{\mathrm{L1}}\right]^{-1} \sum_{\substack{j=1 \\ j\neq i}}^{n_\mathrm{c}} \frac{x_i^{\mathrm{L1}} N_j - x_j^{\mathrm{L1}} N_i}{c_\mathrm{t}^{\mathrm{L1}} \kappa_{i,j}^{\mathrm{L1}}} \tag{2.37a}$$

and, for the aqueous film

$$\frac{\mathrm{d}x_i^{\mathrm{L2}}}{\mathrm{d}\lambda} = \left[\Gamma^{\mathrm{L2}}\right]^{-1} \sum_{\substack{j=1 \\ j\neq i}}^{n_\mathrm{c}} \frac{-x_i^{\mathrm{L2}} N_j + x_j^{\mathrm{L2}} N_i}{c_\mathrm{t}^{\mathrm{L2}} \kappa_{i,j}^{\mathrm{L2}}} \ . \tag{2.37b}$$

Equation (2.35) and eq. (2.37) form a set of $3(n_\mathrm{c}-1)+1$ ordinary differential equations which are subject to the following boundary conditions:

$$x_{i,\lambda=1}^{\mathrm{L1}} = x_i' \ , \qquad i = 1, 2, \ldots, n_\mathrm{c} - 1 \tag{2.38a}$$

$$x_{i,\lambda=1}^{\mathrm{L2}} = x_i'' \ , \qquad i = 1, 2, \ldots, n_\mathrm{c} - 1 \tag{2.38b}$$

$$x_{i,\lambda=0}^{\mathrm{L1}} = K_i x_{i,\lambda=0}^{\mathrm{L2}} \ , \qquad i = 1, 2, \ldots, n_\mathrm{c} \tag{2.38c}$$

with K_i being the liquid-liquid distribution coefficient computed with the equilibrium model, i. e. VTPR-EoS. The molar equilibrium compositions at the interface, $x_{i,\lambda=0}$, may vary during an extraction process.

The property methods used for the estimation of diffusion coefficients at infinite dilution (Poling et al. [40]), the composition dependence of diffusivities, and viscosities (Martins et al. [49]) are listed in table 2.7. Krishna and van Baten [50, 51] recently investigated the composition dependence of self diffusivities in comparative experimental and molecular dynamics-based modeling studies on multicomponent mixtures. The authors used the Darken relation for obtaining multicomponent liquid-phase Maxwell-Stefan diffusivities from self diffusivities, which is also applied in this work.

In a series of papers [52–54], Krishna, Taylor, and their co-workers propose the so-called nonequilibrium cell model and demonstrate its application to reactive distillation, heterogeneous azeotropic distillation, and to a structured catalytically packed bed reactor. They use different implementations of the transport relation, eq. (2.24), depending on the simulation of steady state or dynamic operation. For the case of a steady state simulation, the chemical potential gradient of eq. (2.24) is approximated by finite differences. In contrast, the numerical solution strategy proposed here is based on the transformation of a multipoint boundary value problem (BVP) into a twopoint BVP, which is then solved by collocation. The model has been implemented in a package

Table 2.7: Property methods used for mass transfer simulations.

Property	Method	Ref.
Diffusivities at infinite solution $Đ^{\circ}_{i,j}$	Tyn and Calus	[40]
Multicomponent diffusivities $Đ_{i,j}$	Darken relation	[50, 51]
Dynamic viscosity η_i	Eyring	[49]
Mass transfer coefficients $\kappa_{i,j}$	Corrugated sheet packing	[47]

of MATLAB™ subroutines using the solver bvp4c (BVP for collocation) to compute the composition profiles in the films and the fluxes which are needed in the mass balances describing the actual extraction equipment.

2.3.2 Results

For the sake of conciseness, only results for the ternary system propene-isopropyl alcohol-water, as an example for an alkene-hydration reaction system, are presented here. This class of equilibrium reactions might be advantageously carried out in multifunctional reactors which offer improved yields by simultaneous product removal from the catalyst wetting aqueous phase. For the extraction of the product, no supplementary solvent is needed because the organic extract phase is already formed by the reactant, here: propene. Another important aspect is the water content of the organic extract phase with respect to a less energy-demanding product recovery process. If the water content could be sufficiently limited, a pre-concentration prior to heteroazeotropic drying would then become dispensable. It is therefore necessary to study the mass transport mechanisms in this heterogeneous reactive extraction system.

Figure 2.21 shows results for a simulation of the composition profiles in either film layer, where pure propene is contacted with an aqueous solution containing 20 mol % isopropyl alcohol at 428.15 K and 9.5 MPa. The fluxes from this simulation for the system P-IPA-W result in:

$$(N) = \begin{bmatrix} 0.101 \\ -2.284 \\ -0.264 \end{bmatrix} \text{mol}/(\text{m}^2\,\text{s}) \tag{2.39}$$

showing transport of propene into the aqueous phase, and extraction of isopropyl alcohol and water by the organic phase. Furthermore, in the aqueous film, water

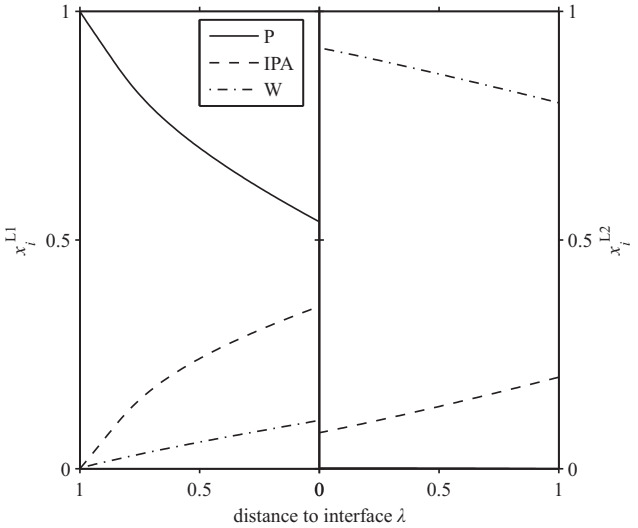

Figure 2.21: Concentration profiles in the films around the liquid-liquid interface of the ternary system P-IPA-W.

is diffusing against its concentration gradient, which is known as reverse diffusion. In this simulation, we rigorously considered the composition dependence of the MAXWELL-STEFAN diffusion coefficients, $Đ_{i,j}$, thermodynamic factors, $\Gamma_{i,j}$, and the total concentration, c_t, along the diffusion path. The concentration profiles are, however, nearly linear. According to Krishna [55], keeping these parameters constant over the diffusion path can, in many cases of technical relevance, lead to sufficiently accurate results. Nevertheless, the validity of this assumption should always be checked experimentally.

The transport of propene in the aqueous film exhibits some interesting characteristics. Figure 2.22 shows the course of the molar flux for propene during the equilibration process and concentration profiles for propene in the aqueous film at 5 selected points from the course of the molar flux of propene during equilibration. Profile (a) at the beginning of the process shows a slight maximum in the vicinity of the interface. The corresponding molar flux is positive. In this situation, the transport of propene is, therefore, controlled by a sequence of the mechanisms, reverse diffusion, osmotic diffusion, and normal diffusion. Profile (b) is controlled only by reverse diffusion. At the next point, (c), the maximum concentration of propene in the aqueous phase is reached and propene is forced to move back into the organic phase before

the binodal curve is reached (see fig. 2.23). This situation remains until point (e) is reached and the equilibration is finished. Point (d) marks the minimum of the flux where it turns back to zero flux. Results for a simple co-

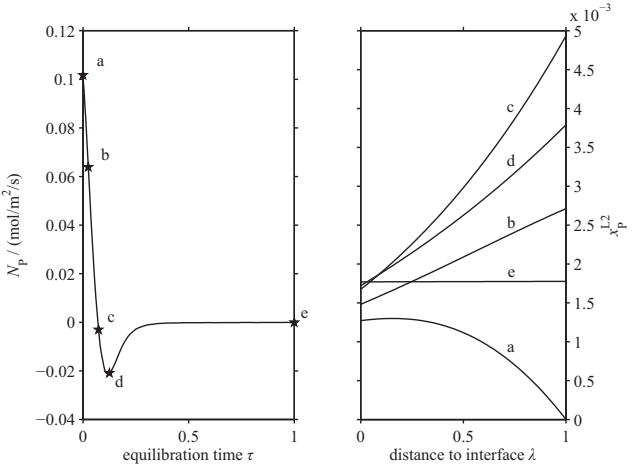

Figure 2.22: Molar flux of P, N_P, during equilibration (left); concentration profiles in the aqueous film for P at 5 different times ($\bigstar^a$, $\bigstar^b$, $\bigstar^c$, $\bigstar^d$, $\bigstar^e$) (right).

current extraction process are obtained in a column equipped with a structured packing. For convenience, neither fluid dynamics and related mass transfer coefficient correlations are discussed in detail here nor any geometric data for the structured packing of the corrugated sheet type, which is considered here, are given. Diaz and Brignole [56] present several papers in their review that deal with fluid dynamics and correlations for mass transfer coefficients for miscellaneous random and structured packing types. Hence, the discussion is more focused on extraction paths, concentration profiles in the films, and related diffusional coupling effects. Figure 2.23 shows extraction trajectories for both phases approaching the binodal curve which surrounds the region of liquid instabilities. The curvilinear extraction paths cannot be explained by a pseudo-binary diffusion model for interphase mass transfer. Initially, contacting the above mentioned phases, the matrices of mass transfer coefficients, $[\kappa']$ and

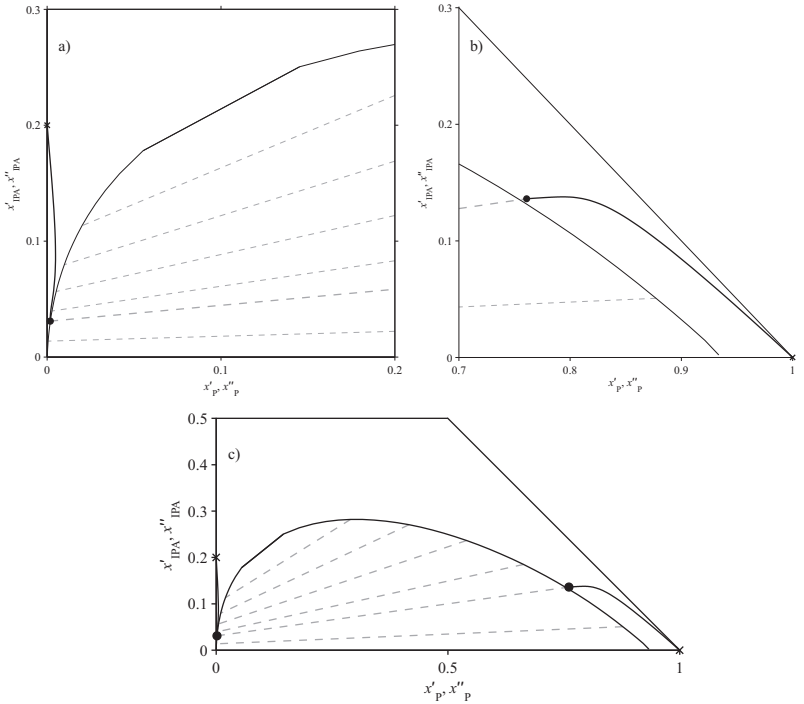

Figure 2.23: Equilibration trajectories at 428.15 K and 9.5 MPa for an aqueous solution containing 20 mol % IPA and pure supercritical P; (×) initial compositions, (●) end of equilibration.

$[\kappa'']$, and thermodynamic factors, $[\Gamma']$ and $[\Gamma'']$, in both phases (bulk) are:

$$\left[\kappa'\right] = \begin{bmatrix} 0.0 & 0.7197 \\ 0.7197 & 0.0 \end{bmatrix} 10^{-3}\,\mathrm{m/s} \tag{2.40a}$$

$$\left[\kappa''\right] = \begin{bmatrix} 1.118 & 1.1179 \\ 1.1179 & 0.6939 \end{bmatrix} 10^{-3}\,\mathrm{m/s} \tag{2.40b}$$

$$\left[\Gamma'\right] = \begin{bmatrix} 0.7003 & -0.3006 \\ 0.1258 & 1.3188 \end{bmatrix} \tag{2.40c}$$

$$\left[\Gamma''\right] = \begin{bmatrix} 1.0 & 0.0 \\ -0.8733 & 0.6592 \end{bmatrix} \tag{2.40d}$$

(2.40e)

The matrices of transport coefficients, $[\kappa']$ and $[\kappa'']$, are diagonal but the matrices of thermodynamic factors, $[\Gamma']$ and $[\Gamma'']$, are strongly nondiagonal. This emphasizes that the diffusional coupling effects are caused by the strongly nonideal thermodynamics of the system presented here. The result in eq. (2.39) reports an 8-times higher molar flux for the transport of isopropyl alcohol than for transport of water into the organic extract phase. From fig. 2.24, it can be seen that the two consecutive steps between the points, I-III, represent the same contacting time.

Taking these circumstances into account, it is important to control the residence time in an extraction column in order to minimize the water content of the extract phase, which might be of interest when isopropyl alcohol is being purified. Considering that diffusional coupling affects mass transfer, the simulation approach presented here is a useful tool for the design of supercritical or liquid extraction processes, as well as for optimization and process intensification studies. Further information on the presented model is provided by Pfeuffer et al. [57].

References

[1] Walas, S. M. *Phase equilibria in chemical engineering.* Butterworth, Boston, 1985.

[2] Valderrama, J. O. The State of the Cubic Equations of State. *Ind. Eng. Chem. Res.* **42**, (2003), 1603–1618. DOI: 10.1021/ie020447b.

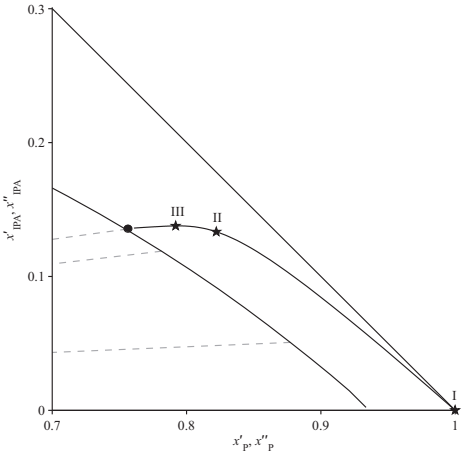

Figure 2.24: Equilibration trajectory of the organic phase when pure P is initially contacted with an aqueous solution of 20 mol % IPA at 428.15 K and 9.5 MPa; ($\bigstar^{I}$), ($\bigstar^{II}$), and ($\bigstar^{III}$) are consecutive points that intersect the trajectory into periods of equal contacting time.

[3] Ahlers, J. and J. Gmehling. Development of an universal group contribution equation of state: I. Prediction of liquid densities for pure compounds with a volume translated Peng-Robinson equation of state. *Fluid Phase Equilib.* **191**, (2001), 177–188. DOI: 10.1016/S0378-3812(01)00626-4.

[4] Ahlers, J. and J. Gmehling. Development of a Universal Group Contribution Equation of State. 2. Prediction of Vapor-Liquid Equilibria for Asymmetric Systems. *Ind. Eng. Chem. Res.* **41**, (2002), 3489–3498. DOI: 10.1021/ie020047o.

[5] Ahlers, J. and J. Gmehling. Development of a Universal Group Contribution Equation of State III. Prediction of Vapor-Liquid Equilibria, Excess Enthalpies, and Activity Coefficients at Infinite Dilution with the VTPR Model. *Ind. Eng. Chem. Res.* **41**, (2002), 5890–5899. DOI: 10.1021/ie0203734.

[6] Ahlers, J., T. Yamaguchi, and J. Gmehling. Development of a Universal Group Contribution Equation of State. 5. Prediction of the Solubility of High-Boiling Compounds in Supercritical Gases with the Group Contribution Equation of State Volume-Translated Peng-Robinson. *Ind. Eng. Chem. Res.* **43**, (2004), 6569–6576. DOI: 10.1021/ie040037i.

[7] Arce, A., A. Arce Jr., J. Martínez-Ageitos, E. Rodil, O. Rodríguez, and A. Soto. Physical and equilibrium properties of diisopropyl ether+isopropyl alcohol+water system. *Fluid Phase Equilib.* **170**, (2000), 113–126. DOI: 10.1016/S0378-3812(00)00328-9.

[8] Horstmann, S., A. Jabloniec, J. Krafcyk, K. Fischer, and J. Gmehling. PSRK group contribution equation of state: comprehensive revision and extension IV, including critical constants and α-function parameters for 1000 components. *Fluid Phase Equilib.* **227**, (2005), 157–164. DOI: 10.1016/j.fluid.2004.11.002.

[9] Gmehling, J. and U. Onken. *Vapor-Liquid Equilibrium Data Collection.* DECHEMA Chemistry Data Series. Dechema, Frankfurt, 1977.

[10] Fredenslund, A., L. Russell, J. Jones, and M. Prausnitz. Group-contribution estimation of activity coefficients in nonideal liquid mixtures. *AIChE J.* **21**, (1975), 1086–1099. DOI: 10.1002/aic.690210607.

[11] Abrams, D. S. and J. M. Prausnitz. Statistical Thermodynamics of Liquid Mixtures: A New Expression for the Excess Gibbs Energy of Partly or Completely Miscible Systems. *AIChE J.* **21**, (1975), 116–128. DOI: 10.1002/aic.690210115.

[12] Ahlers, J. Entwicklung einer universellen Gruppenbeitragszustandsgleichung. Ph.D. Thesis, University of Oldenburg, 2003.

[13] Péneloux, A., E. Rauzy, and R. Fréze. A consistent correction for Redlich-Kwong-Soave volumes. *Fluid Phase Equilib.* **8**, (1982), 7–23. DOI: 10.1016/0378-3812(82)80002-2.

[14] King, C. J. *Separation processes*, 2nd. McGraw-Hill, New York, 1980.

[15] Horstmann, S., R. Wollmann, C. Boldt, and K. Fischer. *Messung des Phasengleichgewichtsverhaltens des ternären Systems Propen (+Propan) + iso-Propanol + Wasser.* By order of Sasol Solvents Germany, Laboratory for Thermophysical Properties, 2005.

[16] Ihmels, C., P. Kamps, and S. Horstmann. *Messung des Phasengleichgewichtsverhaltens des ternären Systems Propen + Diisopropylether + Wasser und des quaternären Systems Propen + Diisopropylether + 2-Propanol + Wasser bei* 155 °C *und* 96 bar. By order of Sasol Solvents Germany, Laboratory for Thermophysical Properties, 2007.

[17] Ihmels, C., R. Wollmann, and S. Laue. *Messung des Phasengleichgewichtsverhaltens des ternären Systems Propen + 2-Propanol + Wasser und des quaternären Systems Propen + Diisopropylether + 2-Propanol + Wasser bei* 155 °C *und* 96 bar. By order of Sasol Solvents Germany, Laboratory for Thermophysical Properties, 2007.

[18] Horstmann, S., P. Kamps, and K. Fischer. *VLLE-Daten für das ternäre System Buten (technische Probe) + 2-Butanol + Wasser*. By order of Sasol Solvents Germany, Laboratory for Thermophysical Properties, 2002.

[19] Zabaloy, M. S., G. D. B. Mabe, S. B. Bottini, and E. A. Brignole. Isothermal vapor-liquid equilibrium data for the binaries propane-2-propanol and propylene-2-propanol. *J. Chem. Eng. Data* **38**, (1993), 40–43. DOI: 10.1021/je00009a009.

[20] Li, C. C. and J. J. McKetta. Vapor-Liquid Equilibrium in the Propylene-Water System. *J. Chem. Eng. Data* **8**, (1963), 271–275. DOI: 10.1021/je60017a040.

[21] Chamorro, C. R., J. J. Segovia, M. C. Martín, and M. A. Villamañán. Isothermal v.l.e. and excess molar Gibbs energy of binary and ternary mixtures containing diisopropyl ether, n-heptane and isopropanol at T=313.15 K. *J. Chem. Therm.* **34**, (2002), 13–28. DOI: 10.1006/jcht.2001.0840.

[22] Barr-David, F. and B. F. Dodge. Vapor-Liquid Equilibrium at High Pressures. The Systems Ethanol-Water and 2-Propanol-Water. *J. Chem. Eng. Data* **4**, (1959), 107–121. DOI: 10.1021/je60002a003.

[23] Prokopakis, G. J. and W. D. Seider. Dynamic simulation of azeotropic distillation towers. *AIChE J.* **29**, (1983), 1017–1029. DOI: 10.1002/aic.690290622.

[24] Prokopakis, G. J. and W. D. Seider. Feasible specifications in azeotropic distillation. *AIChE J.* **29**, (1983), 49–60. DOI: 10.1002/aic.690290107.

[25] Kovach, J. W. and W. D. Seider. Heterogeneous azeotropic distillation: Experimental and simulation results. *AIChE J.* **33**, (1987), 1300–1314. DOI: 10.1002/aic.690330807.

[26] Widagdo, S. and W. D. Seider. Journal review. Azeotropic distillation. *AIChE J.* **42**, (1996), 96–130. DOI: 10.1002/aic.690420110.

[27] Kovach, J. W. and W. D. Seider. Vapor-liquid and liquid-liquid equilibria for the system sec-butyl-alcohol-di-sec-butyl ether-water. *J. Chem. Eng. Data* **33**, (1988), 16–20. DOI: 10.1021/je00051a007.

[28] Lladosa, E., J. B. Monton, M. C. Burguet, and J. de la Torre. Isobaric (vapour plus liquid plus liquid) equilibrium data for (di-n-propyl ether plus n-propyl alcohol plus water) and (diisopropyl ether plus isopropyl alcohol plus water) systems at 100 kPa. *J. Chem. Therm.* **40**, (2008), 867–873. DOI: 10.1016/j.jct.2008.01.002.

[29] Verhoeye, L. A. System 2-Isopropoxypropane-2-Propanol-Water. *J. Chem. Eng. Data* **15**, (1970), 222–226. DOI: 10.1021/je60045a028.

[30] Chen, Y. and Y. H. Dong. Liquid-liquid equilibria of oxygenate fuel additives with water at 298.15 K: Ternary and quaternary aqueous systems of diisopropyl ether and hydrocarbons with 2-propanol. *J. Solution Chem.* **34**, (2005), 1445–1457. DOI: 10.1007/s10953-005-8517-8.

[31] Chen, Y. and S. L. Zhang. (Liquid plus liquid) equilibria of oxygenate fuel additives with water: (water plus diisopropyl ether plus 2,2,4-trimethylpentane plus ethanol) and (water plus diisopropyl ether plus 2,2,4-trimethylpentane plus 2-propanol). *J. Chem. Eng. Data* **51**, (2006), 1236–1241. DOI: 10.1021/je050541+.

[32] Chen, Y. and Y. H. Dong. Quaternary (liquid plus liquid) equilibria for (water plus 2-propanol plus 1,1-dimethylethyl methyl ether plus diisopropyl ether) at the temperature 298.15 K. *J. Chem. Therm.* **38**, (2006), 484–489. DOI: 10.1016/j.jct.2005.06.016.

[33] Hwang, I. C., S. J. Park, and J. S. Choi. Liquid-liquid equilibria for the binary system of di-isopropyl ether (DIPE) plus water in between 288.15 and 323.15 K and the ternary systems of DIPE plus water plus C-1-C-4 alcohols at 298.15 K. *Fluid Phase Equilib.* **269**, (2008), 1–5. DOI: 10.1016/j.fluid.2008.04.010.

[34] Arce, A., A. Arce, J. Martínez-Ageitos, E. Rodil, and A. Soto. (Vapour plus liquid) equilibrium of (DIPE plus IPA plus water) at 101.32 kPa. *J. Chem. Therm.* **35**, (2003), 871–884. DOI: 10.1016/s0021-9614(03)00018-1.

[35] Anderson, T. F. and J. M. Prausnitz. Application of the UNIQUAC Equation to Calculation of Multicomponent Phase Equilibria. 1. Vapor-Liquid Equilibria. *Ind. Eng. Chem. Process Des. Dev.* **17**, (1978), 552–561. DOI: 10.1021/i260068a028.

[36] Michelsen, M. L. The isothermal flash problem. Part I. Stability. *Fluid Phase Equilib.* **9**, (1982), 1–19. DOI: 10.1016/0378-3812(82)85001-2.

[37] Sun, A. C. and W. D. Seider. Homotopy-continuation method for stability analysis in the global minimization of the Gibbs free energy. *Fluid Phase Equilib.* **103**, (1995), 213–249. DOI: 10.1016/0378-3812(94)02579-P.

[38] Wasylkiewicz, S. K., L. N. Sridhar, M. F. Doherty, and M. F. Malone. Global Stability Analysis and Calculation of Liquid?Liquid Equilibrium in Multicomponent MixturesÂ. *Ind. Eng. Chem. Res.* **35**, (1996), 1395–1408. DOI: 10.1021/ie950049r.

[39] Pham, H. N. and M. F. Doherty. Design and Synthesis of Heterogeneous Azeotropic Distillations. 1. Heterogeneous Phase-Diagrams. *Chem. Eng. Sci.* **45**, (1990), 1823–1836. DOI: 10.1016/0009-2509(90)87058-Z.

[40] Poling, B. E., J. M. Prausnitz, and J. P. O'Connell. *The Properties of Gases and Liquids*, 5th. McGraw-Hill, New York, 2001.

[41] Cope, C. S. Equilibria in the Hydration of Propylene and of Butylenes. *J. Chem. Eng. Data* **11**, (1966), 379–383. DOI: 10.1021/je60030a027.

[42] Krishna, R. and J. A. Wesselingh. The Maxwell-Stefan approach to mass transfer. *Chem. Eng. Sci.* **52**, (1997), 861–911. DOI: 10.1016/S0009-2509(96)00458-7.

[43] Krishna, R., C. Y. Low, D. M. T. Newsham, C. G. Oliverafuentes, and G. L. Standart. Ternary Mass-Transfer in Liquid Liquid Extraction. *Chem. Eng. Sci.* **40**, (1985), 893–903. DOI: 10.1016/0009-2509(85)85003-X.

[44] Haeberl, M. and E. Blass. Multicomponent Effects in Liquid-Liquid Extraction. *Chem. Eng. Res. Des.* **77**, (1999), 647–655. DOI: 10.1205/026387699526584.

[45] Uribe-Ramirez, A. R. and W. J. Korchinsky. Fundamental theory for prediction of multicomponent mass transfer in single-liquid drops at intermediate Reynolds numbers (10<=Re<=250). *Chem. Eng. Sci.* **55**, (2000), 3319–3328. DOI: 10.1016/S0009-2509(99)00568-0.

[46] Taylor, R. and R. Krishna. *Multicomponent mass transfer*. Wiley, New York, 1993.

[47] Ruivo, R., M. J. Cebola, P. C. Simoes, and M. N. da Ponte. Fractionation of edible oil model mixtures by supercritical carbon dioxide in a packed column. 2. A mass-transfer study. *Ind. Eng. Chem. Res.* **41**, (2002), 2305–2315. DOI: 10.1021/ie0106579.

[48] Rocha, J. A., J. L. Bravo, and J. R. Fair. Distillation Columns Containing Structured Packings: A Comprehensive Model for Their Performance. 2. Mass-Transfer Model. *Ind. Eng. Chem. Res.* **35**, (1996), 1660–1667. DOI: 10.1021/ie940406i.

[49] Martins, R. J., M. Cardoso, and O. E. Barcia. A new model for calculating the viscosity of pure liquids at high pressures. *Ind. Eng. Chem. Res.* **42**, (2003), 3824–3830. DOI: 10.1021/ie021017o.

[50] Krishna, R. and J. M. van Baten. The darken relation for multicomponent diffusion in liquid mixtures of linear alkanes: An investigation using molecular dynamics (MD) simulations. *Ind. Eng. Chem. Res.* **44**, (2005), 6939–6947. DOI: 10.1021/ie050146c.

[51] Krishna, R. and J. M. van Baten. MD simulations of diffusivities in methanol-n-hexane mixtures near the liquid-liquid phase splitting region. *Chem. Eng. Technol.* **29**, (2006), 516–519. DOI: 10.1002/ceat.200500376.

[52] Higler, A., R. Krishna, and R. Taylor. Nonequilibrium cell model for multicomponent (reactive) separation processes. *AIChE J.* **45**, (1999), 2357–2370. DOI: 10.1002/aic.690451111.

[53] Higler, A. P., R. Krishna, J. Ellenberger, and R. Taylor. Counter-current operation of a structured catalytically packed-bed reactor:: Liquid phase mixing and mass transfer. *Chem. Eng. Sci.* **54**, (1999), 5145–5152. DOI: 10.1016/S0009-2509(99)00229-8.

[54] Springer, P. A. M., R. Baur, and R. Krishna. Composition trajectories for heterogeneous azeotropic distillation in a bubble-cap tray column - Influence of mass transfer. *Chem. Eng. Res. Des.* **81**, (2003), 413–426. DOI: 10.1205/026387603765173682.

[55] Krishna, R. Generalized Film Model for Mass-Transfer in Non-Ideal Fluid Mixtures. *Chem. Eng. Sci.* **32**, (1977), 659–667. DOI: 10.1016/0009-2509(77)80232-7.

[56] Diaz, M. S. and E. A. Brignole. Modeling and optimization of supercritical fluid processes. *J. Supercrit. Fluids* **47**, (2009), 611–618. DOI: 10.1016/j.supflu.2008.09.006.

[57] Pfeuffer, B., U. Kunz, U. Hoffmann, and T. Turek. Multicomponent Mass Transfer Model for Supercritical Extraction: Application to Isopropyl Alcohol Production. *Chem. Eng. Technol.* **32**, (2009), 1384–1391. DOI: 10.1002/ceat.200900204.

3 Experimental

This chapter describes the experiments which have been undertaken during this work. The objective of the experimental work is the exploration of the reaction kinetics of the hydration of linear C_3- and C_4-alkenes using an acidic ion exchange resin as catalyst.

Starting at some preliminaries on further work on kinetics in this field and some fundamental aspects of reaction conditions the following sections describe properties of the used acidic ion exchange resin and reactants, reaction networks, experimental equipment, procedures, and particularly the important fluid dynamic characterization of the equipment. Finally, the results from the experiments, discussion and rate model development are presented.

3.1 Preliminaries

Since the works of Petrus et al. [1, 2], Klein and Widdecke [3] no kinetic data related to the hydration of propene and *n*-butenes were published. Both research groups studied the rates of alkene hydration with alkene-saturated aqueous feeds in fixed bed tubular reactors. This approach is hardly comparable with the real system which comprises mass transfer of all components between the two immiscible phases. The amount of converted alkene is low because of the very limited solubility of linear alkenes in water (P: 1.0 mol %, B: 0.1 mol %) and the authors do not state if the aqueous inlet feed was checked for saturation with the alkene. It is for this reason why the studies reported by this work were conducted in a multiphase continuously stirred tank reactor (CSTR).

More recently, Mahajani et al. [4, 5] compared zeolite and acidic ion exchange resin (AMBERLYST 15™) catalysts for alkene hydration purposes. They found the zeolite catalyst to be more active than the ion exchange resin catalyst, but the activity of the zeolite catalyst decreases dramatically with time. However, Amberlyst 15 is not sufficiently stable for alkene hydration because, from an economical point of view, its usability is limited to a temperature of 120 °C.

In a series of papers Panneman and Beenackers [6–9] investigated the effect of sulfolane as a solubility promoting agent on reaction kinetics and equilibria in the acidic ion exchange resin catalyzed liquid phase hydration of cyclohexene. Although the macrokinetic rate is enhanced remarkably, by adding sulfolane to an extent of 60 mol % to 90 mol % the observed equilibrium conversion is decreased by a factor of 3 to 6. Because of the disadvantageous effect on

equilibrium conversion an industrial application of such an expensive co-solvent is rather not conceivable. Nevertheless, other co-solvents may be more suitable and screening of co-solvents may be a promising way for further improvements in liquid phase olefin hydration processes. Anyway, this study does not consider the use of co-solvents at all.

Heese et al. [10, 11] investigated the formation of diisopropyl ether as fuel oxygenate (octane enhancer). They used AMBERLYST 15™ as catalyst for their study. As reactants stoichiometric mixtures of P/W and P/IPA were employed. Unfortunately, the authors provide the reader neither with a kinetic model nor tabulated experimental data. Hence, their work can only be comprehended qualitatively.

The reactants alkenes and water are nearly immiscible and due to the hydrophilic nature of the acidic ion exchange resin only the aqueous phase wets the catalyst. The liquid or liquid-like supercritical state of the alkenes can be maintained by a pressure of 4.5 MPa which is slightly above the critical pressure of the alkenes. However, in order to maximize the amount of dissolved reactant alkene in the aqueous phase pressures up to 10 MPa are applied. In fact, for the typical range of reaction conditions the density of liquid or supercritical alkenes, respectively, is a considerable function of temperature and pressure (cf. Ihmels et al. [12]), especially for supercritical alkenes. This affects also the solubility in water. The reaction product alcohol is formed in the aqueous pore liquid of the catalyst, and is transferred through the aqueous bulk phase into the organic phase. That means the alkenes are reactants as well as extractants. The simultaneous extraction of alcohol from the reacting aqueous phase is a beneficial feature with respect to selectivity, reaction kinetics, and the limitation on equilibrium conversion. This aspect is analyzed by simultaneous phase and chemical equilibrium calculations in chapter 2.

3.1.1 Reaction Networks

The principle chemical reaction mechanism is described detailed in section 1.2. All reactions are equilibrium reactions which is already analyzed in section 2.2.

Figure 3.1 shows the reaction network of the C_3-hydration system. Considering propene as the starting point of the reaction the formation of isopropyl alcohol by addition of water to propene is accompanied by two consecutive paths for the formation of the by-product diisopropyl ether. One path is the condensation reaction of two isopropyl alcohol molecules which will produce one molecule of diisopropyl ether and one of water. The other route to diisopropyl ether is the reaction between propene and isopropyl alcohol.

The reaction network of the C_4-hydration system is generally very similar to the C_3-hydration system. Also here the formation of *sec*-butyl alcohol from water and *n*-butenes is accompanied by two possible routes for the consecutive

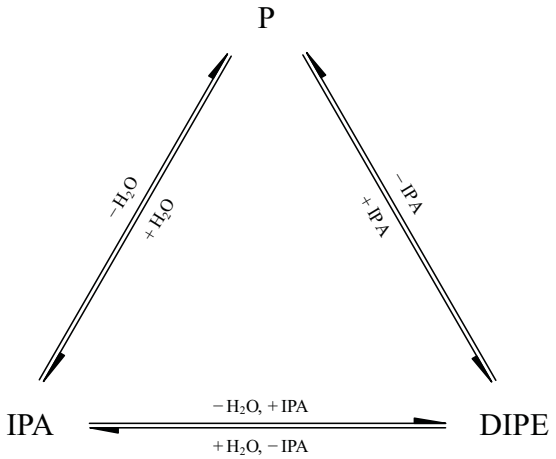

Figure 3.1: Reaction network of the C_3-hydration system.

formation of diisopropyl ether. But, as the linear C_4-alkenes comprise three isomers 1-butene, *cis*-2-butene, and *trans*-2-butene, the simultaneously proceeding isomerization must be considered. The formation of *sec*-butyl alcohol and di-*sec*-butyl ether can originate from each of the C_4-alkene isomers. The C_4-hydration network is illustrated in fig. 3.2.

3.1.2 Properties of the Ion Exchange Resin Catalyst

For many years the major drawback for the application of ion exchange resins for the hydration of linear alkenes was the limited thermal stability. But, nowadays improved resins are available which can be operated at temperatures exceeding 420 K (e. g. Amberlyst 70™, Amberlyst DT™, Rohm & Haas). For these resins no kinetic data for the hydration of linear C_3- and C_4-alkenes are available from public literature resources. In this study Amberlyst DT™ is used as catalyst whereas no differences in the ion exchange capacity related activity of both catalysts Amberlyst DT™ and Amberlyst 70™ could be found by a few comparative measurements.

However, even these for high temperatures improved ion exchange resin catalysts show deactivation caused by a logarithmically decaying loss of acid sites. The deactivation of acidic ion exchange resin catalysts has been studied by Petrus et al. [13] for various commercially available resins. Figure 3.3 shows a typical course for the ion exchange capacity loss for Amberlyst DT™ as function of time on stream compared to data from an industrial plant. The

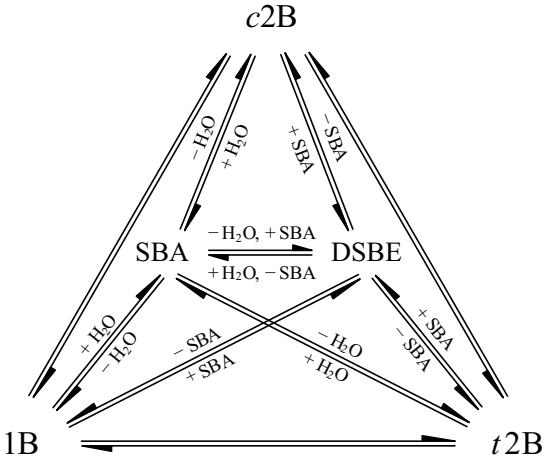

Figure 3.2: Reaction network of the C_4-hydration system.

period of using the catalyst for kinetic experiments within its life cycle is illustrated as well. A further loss of the ion exchange capacity during the period of usage for the kinetic investigations could not be found by according capacity measurements prior to and after the experiments.

In order to obtain reliable kinetic data not being influenced by catalyst deactivation an already employed catalyst sample from an industrial unit is employed. This sample has a run time of 130 days. After this period no further significant catalyst deactivation occurs. In an industrial plant the catalyst lasts for more than one year. Detailed data of the used catalyst sample are compiled in table 3.1.

Table 3.1: Properties of AMBERLYST DT™ (water-swollen state, after 130 d run-time, own measurements).

Manufacturer	ROHM & HAAS
Structure	macroporous
Particle size fraction (wet)	0.5 mm to 0.7 mm
SO_3H-concentration (wet)	1.1 eq/kg
Density (wet)	1150 kg/m^3_{cat}
Water content	approx. 50 wt%

Acidic ion exchange resins are subject to swelling in polar solvents whereas

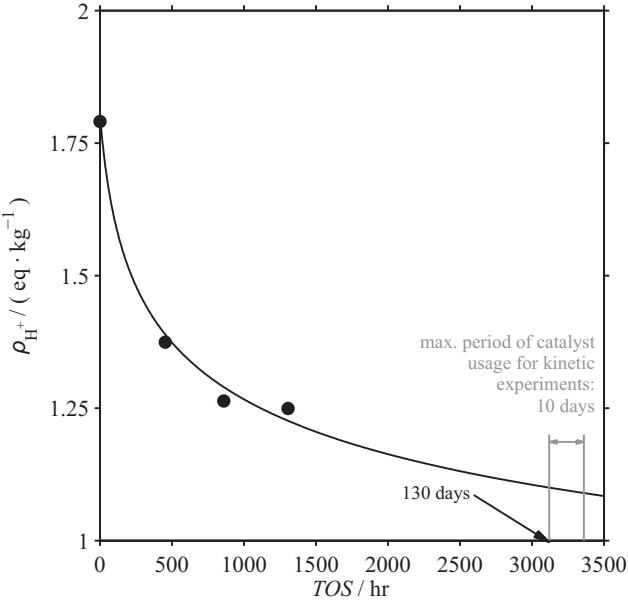

Figure 3.3: Loss of ion exchange capacity as function of time on stream. The gray colored part highlights the period in which the catalyst was used for experiments. Experimental data from [14].

water as common solvent shows the strongest polarity and marks the maximum extent of swelling for an acidic ion exchange resin. As can be deduced from table 3.1 the wet acidic ion exchange resin contains as much as 50 wt% water. For practical situations where reactions are processed with acidic ion exchange resins in solvent-reactant mixtures with widely varying compositions swelling is a serious issue.

However, in the case of this work, where an aqueous phase co-exists together with an organic phase, the catalyst is preferentially wetted by the aqueous phase which usually contains more than 95 mol % water. As a result, the catalyst is no subject to changing states of swelling.

The very intensive uptake of water by the acidic ion exchange resin leads to a change in the catalytic mechanism. In relatively unpolar solvents the acid sites remain bonded to the polymer matrix of the resin. The sites are not shielded by attracted solvent molecules, so the sites are easily accessible for the reactants and the activity of the polymer bonded acid sites is several times stronger than in water dissolved oxonium ions. This case is referred to as *general catalysis*.

If the acidic ion exchange resin is saturated with water or similar polar species, e. g. methanol, the acid sites become obviously solvated by the polar solvent molecules. At such conditions, the activity is comparable with that of dissolved oxonium ions. This is referred to as *specific catalysis* and is the case for the systems studied in this work. A comprehensive survey on the properties of acidic ion exchange resins provides Pitochelli [15].

3.2 Equipment

3.2.1 Laboratory Plant for High Pressure Multiphase Kinetic Experiments

For the kinetic investigation of olefin hydration a special CSTR was developed. This reactor (100 cm^3 excluding internals) can be operated up to 10 MPa and 500 K. The catalyst is arranged in two spinning baskets (max. total catalyst load (wet): 5.5 g) on the stirrer shaft (fig. 3.4), which is based on the well known concept introduced by Carberry [16]. The stirrer drive is linked via magnetic coupling thus avoiding any shaft sealing. All equipment is made of stainless steel; gaskets are either made of polymers (PTFE,FFKM/FFPM) or metal (gold, copper, stainless steel).

Measurement and control of the whole experimental setup is managed via a National Instruments Fieldpoint™ programmable automation controller and a computer which are both based on the system control software package National Instruments Labview™. The clearance between the two catalyst baskets – in combination with two oppositely aligned Sitec™ sapphire windows (2a) – provides a free view across the reactor (2). This feature allows controlling

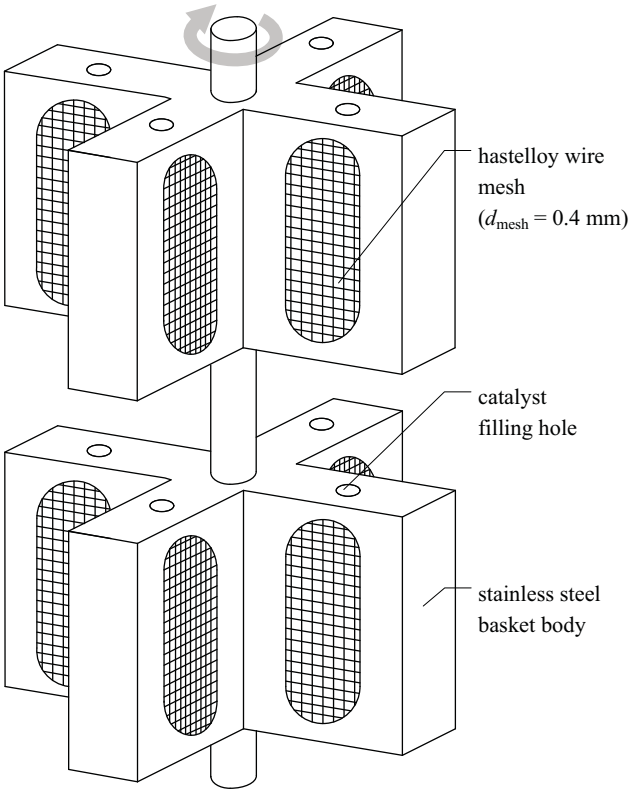

Figure 3.4: Modified CARBERRY reactor (clearance between spinning catalyst baskets provides a free view across the reactor).

the hold-up ratio of the two immiscible liquid phases. Figure 3.5 shows the essential parts of the experimental setup.

The reactant alkene is dosed into the reactor by means of a VARIAN SD-1™ high pressure piston pump (1b). A second pump (1a) of the same type is used for dosing the reactant water or mixtures of water with the product alcohol, respectively. Both pumps are high precision metering devices.

The reactor has an upper and a lower outlet in order to allow for hold-up control of both liquid phases. Two alternately switching magnetic valves (3a,b) control the hold-up ratio by an appropriate switch timing (on-off ratio). For a particular experiment, an appropriate on-off ratio needs to be found by trial and error. To check this, the stirrer turbine is stopped temporarily and the on-off ratio is adjusted accordingly. Once a ratio is found which keeps the hold-up at the desired level and steady state operation has been achieved, the system is ready for measurements of the actual experiment with a continuously running stirrer. Furthermore, the hold-up can be maintained independently from the residence time of each phase. The total reactor effluent flows to the decanter(4) (50 cm^3) where it is separated into an organic and an aqueous phase. The organic phase has the lower density. The decanter is necessary to provide the analytical system with settled phases. Both phases can be analyzed simultaneously by gas chromatography. The decanter is equipped with two aligned SCHOTT MAXOS™ borosilicate windows (4a) for observation of the liquid-liquid interface. The interface in the decanter is observed by a camera. With the help of image processing it is possible to locate the position of the liquid-liquid interface. This information is used to control the decanter hold-up with the magnetic valves (6a,b).

The gas chromatographic analysis of all components – in combination with the known feed streams – permits a detailed reactor balance. Nevertheless, the balance is checked additionally by measuring the aqueous effluent mass flow with a BRONKHORST CORIFLOW™ mass flow meter. Both phases are then merged and depressurized. The formed gas is flared whereas the remaining liquid is sent to the laboratory waste disposal.

Two rapid online sample injector (ROLSI) (supplied by LTP GMBH OLDENBURG) high pressure online-sampling devices are used to supply the HEWLETT-PACKARD 5890™ gas chromatograph with samples. These sampling devices provide small liquid samples (mm^3 domain) which are instantaneously evaporated into the carrier gas (helium) afterwards. The gas chromatograph is equipped with two capillary columns for independent analysis of samples from both phases (C_3-hydration: poly(ethylene glycol), SUPELCO CARBOWAX 20M™; C_4-hydration: poly(dimethyl siloxane), SUPELCO SPB-1™). The separated species are completely quantified by two thermal conductivity detectors. Reactor, decanter, camera and the two ROLSI sampling devices are shown in fig. 3.6.

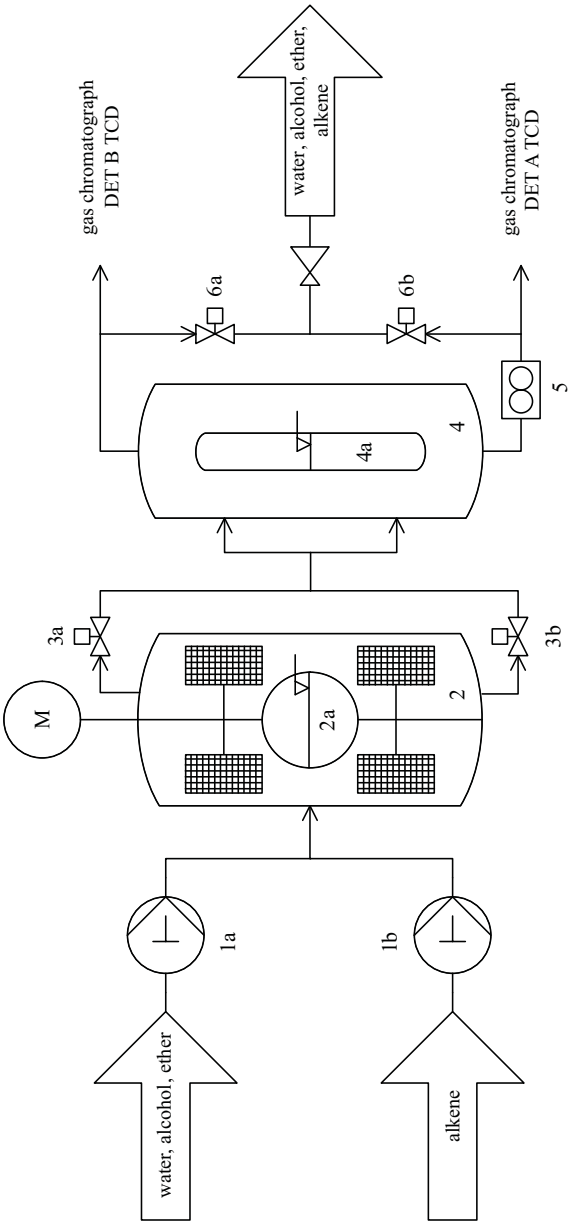

Figure 3.5: Simplified flow chart of the lab-scale plant for kinetic experiments.

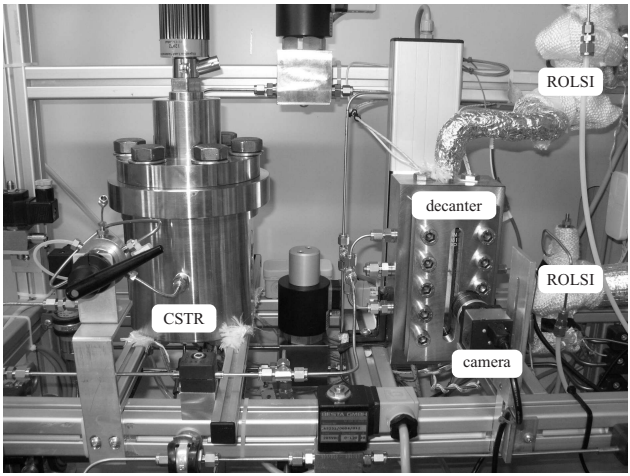

Figure 3.6: Picture of the main parts of the laboratory plant for kinetic measurements of systems with multiple liquid phases.

In an earlier work on the kinetics of the ion exchange resin catalyzed hydration of *n*-butenes, Petre [17] also used the previously described reactor. But, no decanter was used for the separation of phases, samples for gas chromatography were only taken from the organic phase, no mass flow measurement was available and a single pump was used to feed the separating liquid reactants into the reactor. The feeding of reactants was irreproducible and due to the missing mass flow measurement in either reactor effluent phase and composition analysis of the aqueous reactor effluent, respectively, a proper mass balancing of the reactor was practically impossible. In the new multiphase reactor setup these problems are completely resolved and a reliable investigation of the kinetics is now possible.

3.2.2 Residence Time Distribution and Reactor Balance

The development of a rate equation requires a verified model for the laboratory reactor. This is conducted by residence time distribution (RTD) experiments. In principle both phases should be fed and characterized. But, as the aqueous phase is exclusively in contact with the catalyst, and as its viscosity is higher than that of the organic phase, only the residence time of the aqueous phase is analyzed. Initially, alkenes are fed into the water-filled reactor. The feeding of alkenes is stopped after reaching a hold-up of 50 %. Then, the aqueous phase

is continuously fed into the reactor while only the lower reactor outlet is used. Tracer concentrations are measured by a Mettler Toledo ReactIR 4000™ FTIR-ATR spectrometer. A self-designed flow cell with a small detector volume ($0.1\,\mathrm{cm}^3$) is applied for connecting the probe of the spectrometer to the process (fig. 3.7).

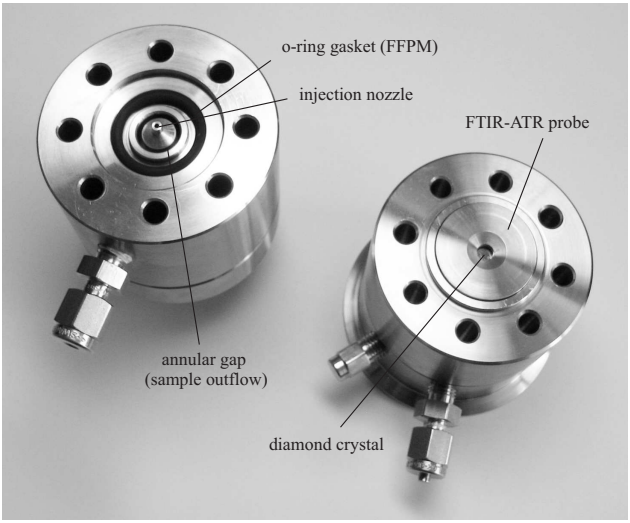

Figure 3.7: Flow cell for RTD measurements.

As infrared detectable tracer sodium acetate is used. Sodium acetate is an easily water soluble salt which is not transferred into the organic phase. This is essential for obtaining reliable phase-specific RTD data. An aqueous solution containing $6.5\,\mathrm{mol/dm}^3$ sodium acetate as tracer is injected by a HPLC-sample injection valve with a sample loop of $10\,\mathrm{cm}^3$. Figure 3.8 shows a flow chart of the RTD test rig. In addition to the output signal the input signal is measured as well (fig. 3.9). The measured input signal is described by a cubic spline interpolation for mathematical representation. This spline function is used as input signal ($c_{\mathrm{tracer,input}}(t)$) in the dynamic CSTR material balance:

$$\frac{\mathrm{d}c_{\mathrm{tracer,output}}}{\mathrm{d}t} = \frac{F''}{h''_{\mathrm{L}} V_{\mathrm{R}}} \left(c_{\mathrm{tracer,input}} - c_{\mathrm{tracer,output}} \right) \tag{3.1a}$$

with the initial conditions

$$c_{\text{tracer,output}} = c_{\text{tracer,output,0}} \qquad \text{at} \qquad t = 0\,. \tag{3.1b}$$

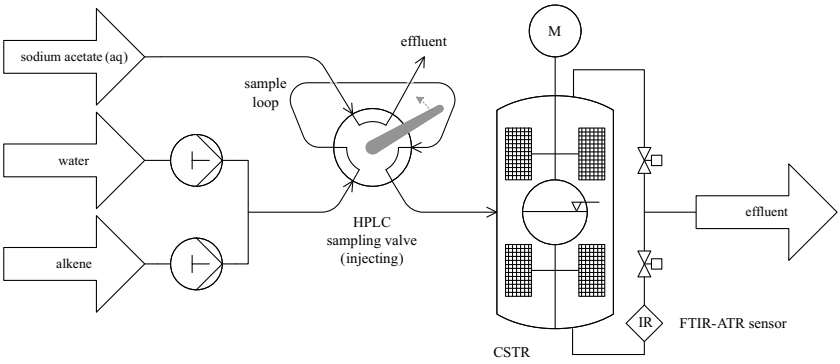

Figure 3.8: Flow chart of the RTD test rig as set-up for reactor feedback measurements.

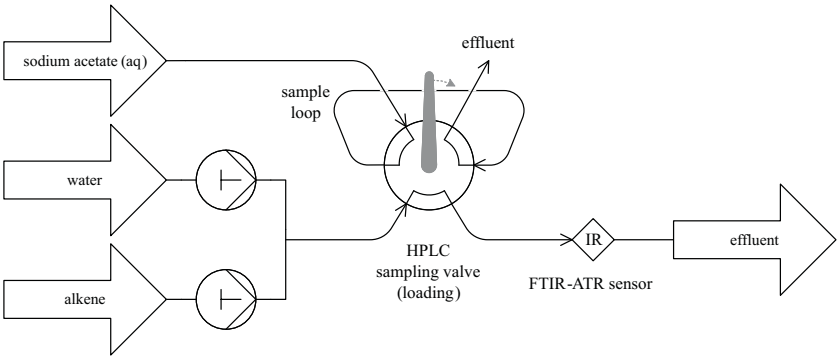

Figure 3.9: Flow chart of the RTD test rig as set-up for reactor test signal acquisition.

The dynamic CSTR material balance is used for the prediction of an expectable tracer response for a given tracer input signal. The obtained tracer response is given in fig. 3.10 and fits the measured data points exactly. Measured data and the cubic spline curve of the inlet signal are also given in fig. 3.10.

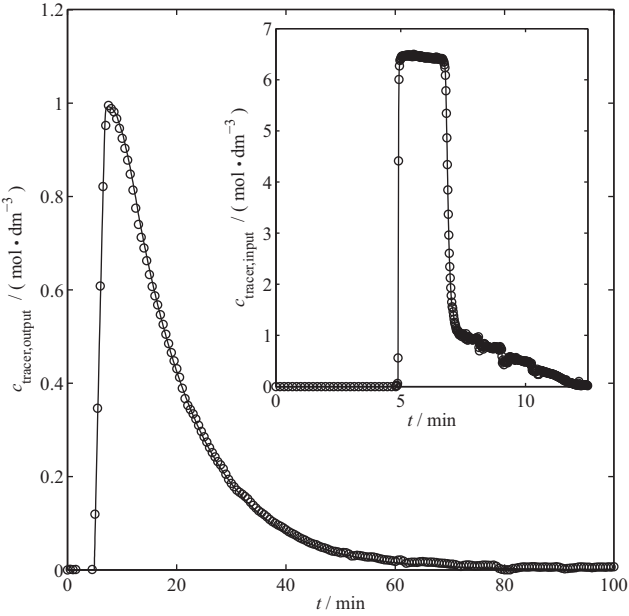

Figure 3.10: Observed and calculated input and output tracer signals in residence time distribution analysis of aqueous phase.

As the ideal flow behavior of the used CSTR is proofed by the undertaken RTD experiments the observed reaction rate can reasonably be obtained from the following set of equations representing time-invariant material balances of a multiphase CSTR:

Organic phase

$$M_i' \equiv F_i' - x_i' E' - \mathbb{N}_i^{\mathrm{I}} = 0 \,, \qquad i = 1, 2, \ldots, n_{\mathrm{c}} \tag{3.2a}$$

Aqueous phase

$$M_i'' \equiv F_i'' - x_i'' E'' + \mathbb{N}_i^{\mathrm{I}} + \nu_i r_{\mathrm{obs}} = 0 \,, \qquad i = 1, 2, \ldots, n_{\mathrm{c}} \tag{3.2b}$$

In eq. (3.2) $'$, $''$ denote the organic and the aqueous phase, respectively. F_i is the feed flow of component i in either phase, x_i is the mole fraction of component i in either phase measured by gas chromatography, E is the total exit flow of either phase, ν_i is the stoichiometric coefficient of component i, and $r_{\mathrm{obs,global}}$ is the observed global rate of the hydration reaction. The rate term appears only in eq. (3.2b) as only the aqueous phase wets the ion exchange resin due to its hydrophilic surface. $\mathbb{N}_i^{\mathrm{I}}$ denotes the interfacial mass transfer rate of component i, whereas a positive value indicates mass transfer from the organic to the aqueous phase. Equation (3.2) are coupled by the interfacial mass transfer rate. If at least not a single total effluent stream is measured the component reactor effluent streams can implicitly be calculated by solving this linear system of equations. This procedure has the advantage of excluding an additional experimental uncertainty by a mass flow measurement. However, as declared in section 3.2.1, the redundant mass flow measurement of the aqueous reactor effluent stream is used to indicate unstable operation of the reactor.

3.3 Procedures

3.3.1 Exclusion of mass transfer limitations

Overall 18 (9 for each reaction system) experimental series with varying stirring speed are performed to investigate the external mass transfer influence. It is found, by studying the dependence of the reaction rate on stirring speed in the range 300/min to 900/min and by varying the temperature in the range 393 K to 433 K that a rotational frequency of 1000/min is sufficient to exclude interparticle and liquid-liquid interface mass transfer limitations for both reaction systems in the mentioned temperature range. Exemplary results for the C_4-hydration system are provided in fig. 3.11. It is found that the diffusive

mass transfer in the films surrounding the liquid-liquid interphase and in the NERNST-layer around the catalyst bead (hypothetical film layer in which mass transfer between bulk of fluid phase and catalyst surface is provided by diffusion only) determines the overall rate of reaction up to a rotational frequency of 900/min.

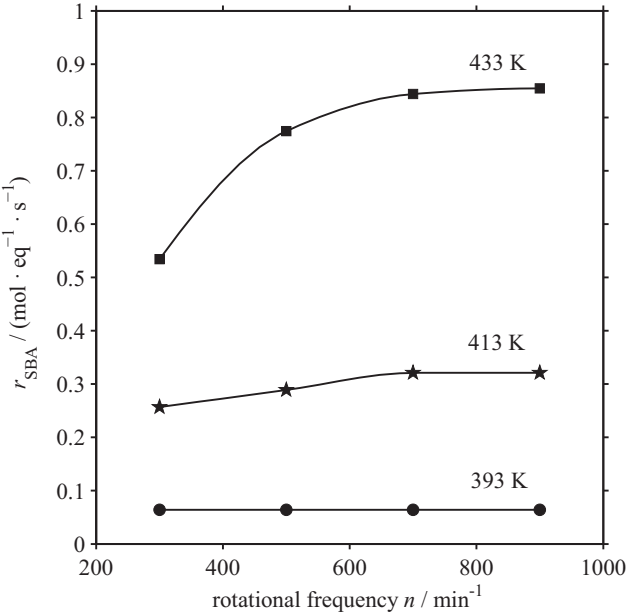

Figure 3.11: Test results for external mass transfer limitations (NERNST-layer around catalyst bead and interphase mass transfer) in the C_4-hydration system; observed rate as function of stirring speed.

Intraparticle mass transfer was also studied by varying the particle size in the range 0.5 mm to 1.2 mm and temperature in the range 393 K to 413 K. For a catalyst particle diameter fraction of 0.5 mm to 0.7 mm and a capacity of the water-saturated acid ion exchange catalyst of 1.1 eq/kg no intra particle diffusion limitations are observed for temperatures up to 413 K. For the experimental test of internal mass transfer limitations exemplary results for the C_4-hydration system are depicted in fig. 3.12.

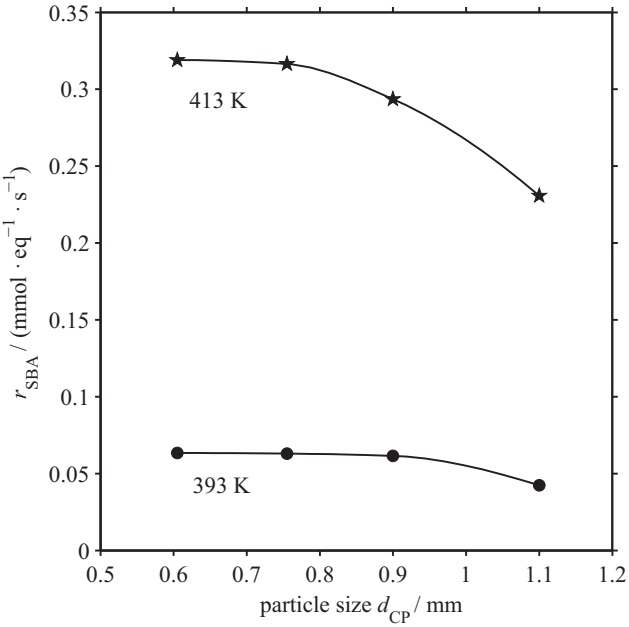

Figure 3.12: Test results for internal mass transfer limitations in the C_4-hydration system; observed rate as function of mean catalyst particle size.

3.3.2 Microkinetic investigations

This study comprises 36 experimental runs for the investigation of the microkinetics of the C_3-hydration system and 24 experimental runs for the investigation of the microkinetics of the C_4-hydration system, where each run consists of at least 40 repeated determinations, i. e. at least 40 samples are taken for gas chromatographic analysis from each phase. 3 experimental runs in the C_4-hydration system are carried out under intraparticle mass transfer influence. For the C_3-hydration system experiments influenced by mass transfer were not conducted.

Each run is started by filling the reactor with water at ambient temperature until the desired pressure is reached. The stirring is started and the dosage of water or water/alcohol mixtures, respectively, is continued. Then the heating of the reactor is initiated. During reactor heat-up the dosage of the liquid alkenes is also started. In all runs the hold-up ratio is 1:1 by volume and the flow rate for each reactant mixture is fixed to 0.5 cm^3/min or 1 cm^3/min, respectively.

The used catalyst amount is 4.5 g to 5.5 g (wet) at an ion exchange capacity of 1.1 eq/kg. To ensure steady state operation the first experiment is taken after a period of 12 h. Temperature is varied within the range 398 K to 433 K, whereas pressure is set to 6 MPa and 8 MPa, respectively, using a manually driven back pressure regulator(Tescom 26-1700™).

The influence of product concentration on the reaction rates is studied using 6 different inlet concentrations (0.0 mol %, 1.0 mol %, 3.0 mol %, 5.0 mol %, 10.0 mol % and 20.0 mol %) of isopropyl alcohol and 4 different inlet concentrations (0.0 mol %, 0.5 mol %, 1.5 mol % and 2.5 mol %) of *sec*-butyl alcohol, both with respect to the aqueous feed stream. The actual aqueous phase concentrations of the alcohols at steady state are much lower due to the simultaneous extraction of the alcohols by the organic phase. Setting the concentrations of alkenes and water in the reactor – relevant for the rate – cannot be achieved by simple adjustment of feed ratio because the concentrations in the coexisting liquids are primarily governed by phase equilibria. The influence of the phase split on each phase composition causes restrictions on the variation of reactant concentrations in an experiment. At least the product concentration can be varied due to full miscibility of the product with each reactant at typical reaction conditions. But, the limited mutual miscibility of the reactants determines their actual concentrations in either phase. Nevertheless, in order to obtain reasonably measurable product yields, which is hardly achievable if an alkene saturated single aqueous phase is used, the experiments were conducted in the described CSTR operated at multiphase conditions.

3.3.3 Reactants

Water is purified by ion exchange (conductivity $< 5\,\mu S$). Propene is supplied by Linde as Propen 2.5 having a purity of $\geq 99.5\,\%$. The kinetic experiments for the hydration of *n*-butenes are conducted using an industrial *n*-butenes feedstock, supplied by Sasol Solvents Germany. The composition of this feedstock is provided in table 3.2.

Table 3.2: Composition of industrial butenes feedstock (mass fractions).

1-Butene	51.5 %
cis-2-Butene	13.3 %
trans-2-Butene	33.2 %
iso-Butene	1.0 %
Butanes	$< 1.0\,\%$

Isopropyl alcohol and *sec*-butyl alcohol are of analytical grade, supplied by Fluka with a purity of $\geq 99\,\%$. Diisopropyl ether and di-*sec*-butyl ether are supplied by Sasol Solvents Germany having a purity of $\geq 97\,\%$.

3.4 Results

3.4.1 Microkinetics of the C_3-hydration system

The experimental kinetic data for the C_3-hydration system, which are obtained under exclusion of mass transfer limitations, are used for the development of a rate model. All experimental data and corresponding reaction conditions are compiled in table C.1.

The following assumptions are made during development of the rate equation:

i) the chemical reaction is the rate limiting step as mikrokinetic rate data are used for parameter adjustment,

ii) the reaction takes place in the water swollen gel phase of the ion exchange resin,

iii) the catalytically active acid sites are completely hydrated by water molecules, and

iv) the solvated protons remain locally associated to their polymer-bonded counterions (cf. Helfferich [18], pp. 14-16).

Generally, it can be assumed for the chemical equilibrium and the reaction kinetics that the reaction takes place in the water swollen gel phase of the

catalyst microspheres. Due to the large excess of water in the gel phase the compositions in the gel phase, in the macropore fluid, and in the catalyst surrounding aqueous phase are assumed to be identical. Attempts to use heterogeneous models (i. e. Langmuir-Hinshelwood, Eley-Riedel) failed because the sorption constants, which were gained from accordant adjustment calculations, were accompanied by confidence intervals having the same order of magnitude as their corresponding model parameters. This result confirms that an equilibrium distribution of the components between the macropore fluid and the fluid mixture in the gel phase of the microspheres does not exist.

Furthermore, solvation of the acid protons is well known to occur in the presence of strongly polar solvents (i. e. water, alcohols). This special case of catalysis in an acidic ion exchange resin is referred to as *specific catalysis*, whereas in the case of *general catalysis*, i. e. in the presence of an unpolar solvent, the acid protons remain polymer-bonded (Chakrabarti and Sharma [19]). Gates and Rodriguez [20] experimentally demonstrated the difference between specific and general catalysis for the dehydration of tertiary butyl alcohol with an acidic ion exchange resin. In addition, polymer-bonded acid protons are catalytically more active than hydrated protons. The work of Rehfinger and Hoffmann [21] on the kinetics of methyl tertiary butyl ether synthesis from methanol and isobutene confirms this behavior also. They found the reaction rate to decrease with increasing methanol concentration which is explained by an increasing degree of solvation of protons. If water is present only at infinite dilution the selectivity shifts towards the formation of diisopropyl ether, oligomers and other byproducts. Hence, the catalyst is less active when excessive amounts of water are present within the catalyst, but the selectivity for the hydration reaction is superior under these conditions. As a result, the hydration reaction proceeds in a pseudo-homogeneous manner when the catalyst is wetted by an aqueous phase.

From data fitting attempts wherein all three reaction pathes are considered it was concluded that the reaction network – the basis for the rate model development – can be simplified as is shown in fig. 3.13.

When both routes for the formation of diisopropyl ether are considered for data fitting purposes the resulting confidence intervals of the rate model parameters of the diisopropyl ether formation reactions are unacceptably large. Hence, the system is obviously over-determined for the limited range of experimental conditions. As this work considers only multiphase operation, whereas the reaction takes place in a low propene containing environment, a concentration range at which the concentration of propene reaches a similar extent as the isopropyl alcohol concentration is not available. This leads to the presumption that only one reaction path is significant here. Testing this by trying to fit the experimental data alternatively to rate equations for both reaction pathes satisfying results are found when considering the condensation reaction of two

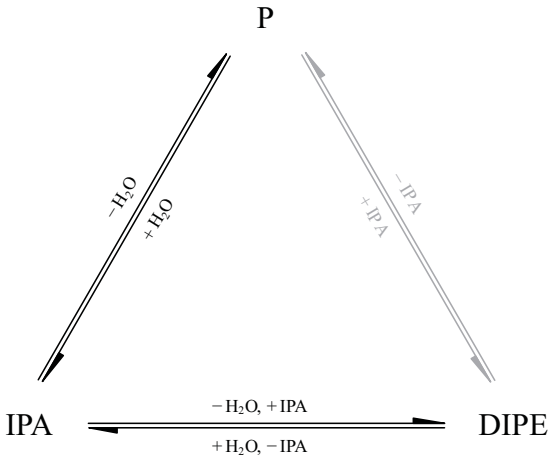

Figure 3.13: Reduced reaction network for the C_3-hydration system (grey colored reaction path is insignificant for IPA formation in aqueous reaction mixtures).

isopropyl alcohol molecules. The other reaction path, wherein propene reacts with isopropyl alcohol forming diisopropyl ether, may become important when the reaction is no longer proceeding under excess of water with very low propene concentrations. At relatively high isopropyl alcohol concentrations, the reaction mixture is a homogeneous liquid and the concentration of propene can be varied over wide ranges. This situation is possible if the objective is the production of diisopropyl ether, not isopropyl alcohol.

Both reactions, the formation of isopropyl alcohol from propene and water and the formation of diisopropyl ether and water from two isopropyl alcohol molecules are sufficiently described by the following pseudo-homogeneous reaction rate laws expressed in aqueous phase activities

$$r_{\text{rev, IPA}} = k_{+,\text{IPA}} \left(a''_{\text{P}} a''_{\text{W}} - \frac{a''_{\text{IPA}}}{K_{a,\text{IPA}}} \right) \tag{3.3a}$$

$$r_{\text{rev, DIPE}} = k_{+,\text{DIPE}} \left({a''_{\text{IPA}}}^{2} - \frac{a''_{\text{DIPE}} a''_{\text{W}}}{K_{a,\text{DIPE}}} \right) . \tag{3.3b}$$

In eq. (3.3), k_+ is the rate constant of the forward reaction in $\text{mmol}_{\text{IPA}}/(\text{eq s})$

which is a function of temperature according to the ARRHENIUS equation

$$k_+ = k_+^0 \exp\left(\frac{-E_\mathrm{a}}{RT}\right) . \tag{3.4}$$

The pre-exponential factors k_+^0 and the activation energies E_a are used for adjustment calculations of the reaction rate models. The obtained parameter values and approximate individual confidence intervals for both reactions (IPA and DIPE) are given in tables 3.3 and 3.4. The activities in eq. (3.3) are defined by eq. (2.17). As the heats of reaction are only weak functions of the temperature, at least for the considered range of temperatures, the computation of K_a is simplified by applying the VAN'T HOFF equation which describes the temperature dependency of the chemical equilibrium constant

$$\frac{\mathrm{d}\ln K_a}{\mathrm{d}T} = \frac{\Delta h_\mathrm{r}}{RT^2} \tag{3.5}$$

whereas the following relation is derived by integration of eq. (3.5):

$$\ln \frac{K_a}{K_a^{398}} = -\frac{\Delta h_\mathrm{r}}{R}\left(\frac{1}{T} - \frac{1}{398\,\mathrm{K}}\right) . \tag{3.6}$$

The reference value of the equilibrium constant at 398 K K_a^{398} and the reaction enthalpy for both reactions (IPA and DIPE) are also listed in tables 3.3 and 3.4.

The residuals of the model-experiment comparison are symmetrically distributed and the distribution exhibits a gaussian-like shape (fig. 3.14). This confirms the general adequacy of the developed rate model with respect to reproduction of the experimental data.

Equation (3.3a) shows the rate of the forward reaction to be first order with respect to the activities of propene and water and that of the reverse reaction to be first order with respect to the activity of isopropyl alcohol. The order of the activity of water has no kinetic significance as water is always excessively present in the polymer network of the acidic ion exchange resin, and thus, could generally be eliminated from the left term of eq. (3.3a).

However, elimination of the activity of water would mean dividing the entire eq. (3.3a) by the activity of water to keep this reversible rate expression consistent with respect to chemical equilibrium. The equilibrium constant would be subject to a modification if the activity of water is canceled from the rate equation. In order to preserve the generality of the chemical equilibrium constant an apparent simplification of eq. (3.3a) is not made.

Equation (3.3b) shows the rate of the forward reaction to be second order with respect to the activity of isopropyl alcohol and that of the reverse reaction

Table 3.3: Intrinsic IPA formation rate model parameter for eqs. (3.3a) and (3.4).

Parameter		Unit	Value	App. individual confidence limit (95 %)
1	k_+^0	$\mathrm{mmol_{IPA}/(eq\,s)}$	1.16×10^{12}	$\pm 9.2 \times 10^{9}$
2	E_a	kJ/mol	115.3	±1.8
3	$K_{a,\mathrm{IPA}}^{398}$	–	9.45×10^{-2}	–
4	Δh_r	kJ/mol	−51.6	–
r_0(418 K, 8 MPa)[a]		$\mathrm{mmol_{IPA}/(eq\,s)}$	2.31	–
		$\mathrm{mol_{IPA}/(m^3\,s)}$	1.91	–

[a] $x_\mathrm{P}'' = 0.2\,\mathrm{mol\,\%}$

Table 3.4: Intrinsic DIPE formation rate model parameter for eqs. (3.3b) and (3.4).

Parameter		Unit	Value	App. individual confidence limit (95 %)
1	k_+^0	$\mathrm{mmol_{DIPE}/(eq\,s)}$	6.56×10^{8}	$\pm 3.8 \times 10^{7}$
2	E_a	kJ/mol	85.6	±18.2
3	$K_{a,\mathrm{DIPE}}^{398}$	–	3.57	–
4	Δh_r	kJ/mol	−14.7	–
r_0(418 K, 8 MPa)[a]		$\mathrm{mmol_{DIPE}/(eq\,s)}$	2.6×10^{-2}	–
		$\mathrm{mol_{DIPE}/(m^3\,s)}$	2.1×10^{-2}	–

[a] $x_\mathrm{P}'' = 0.2\,\mathrm{mol\,\%}$, $x_\mathrm{IPA}'' = 2.0\,\mathrm{mol\,\%}$

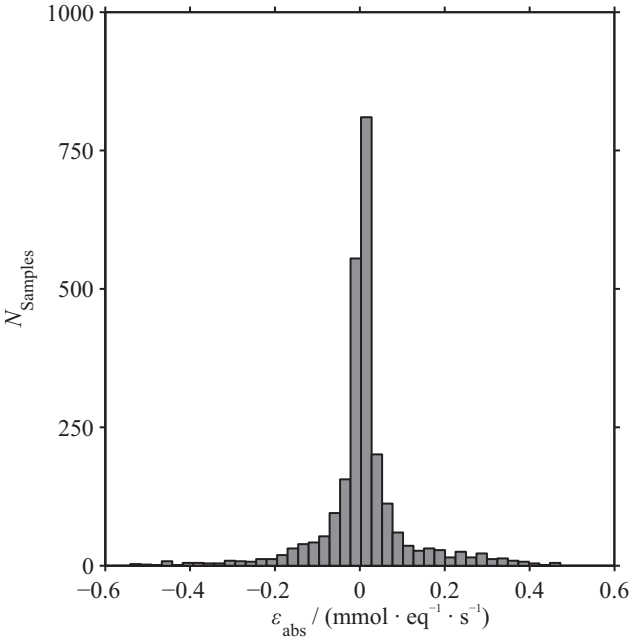

Figure 3.14: Distribution of model-experiment residuals.

to be first order with respect to the activities of diisopropyl ether and water.

Hence, both reaction rate equations (eq. (3.3)) are elementary in nature with respect to the dependence on concentration or activity, respectively.

The accuracy of the proposed model for the reaction rates of the formation of isopropyl alcohol and diisopropyl ether is illustrated by the parity plots provided in figs. 3.15 and 3.16. It can be seen that the model represents the measured data fairly well for the entire temperature range of 125 °C to 160 °C. Due to the strong extraction of isopropyl alcohol from the reacting aqueous phase it was impossible to measure dehydration rates at all with only one exception.

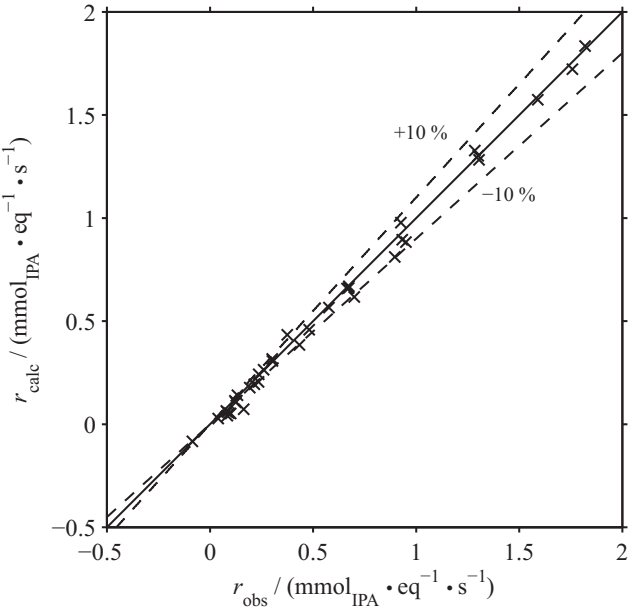

Figure 3.15: Parity plot of measured and simulated IPA formation rate.

The activities in eq. (3.3) are obtained from the VTPR-EoS as described in section 2.2. Adjusting the parameters of a model according to eq. (3.3), but expressed in mole fractions, unsatisfactory results are obtained. Obviously, the activities are essential for a physically reasonable description of the concentration dependence of the reaction rate when the reaction is carried out in a nonideal liquid mixture. This is also demonstrated in the work of Rehfinger and Hoffmann [21] for methyl tertiary butyl ether synthesis and is discussed in detail by

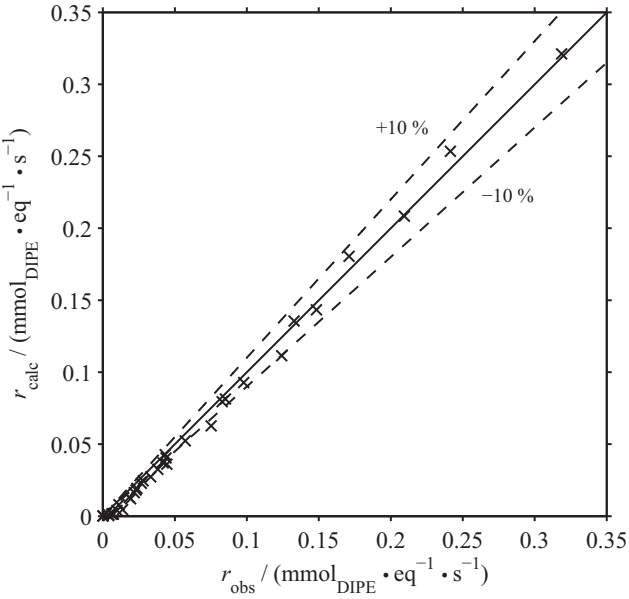

Figure 3.16: Parity plot of measured and simulated DIPE-formation rate.

Kondepudi and Prigogine [22].

Figure 3.17 illustrates the course of the reaction resistance from initial conditions towards equilibrium with increasing isopropyl alcohol concentration.

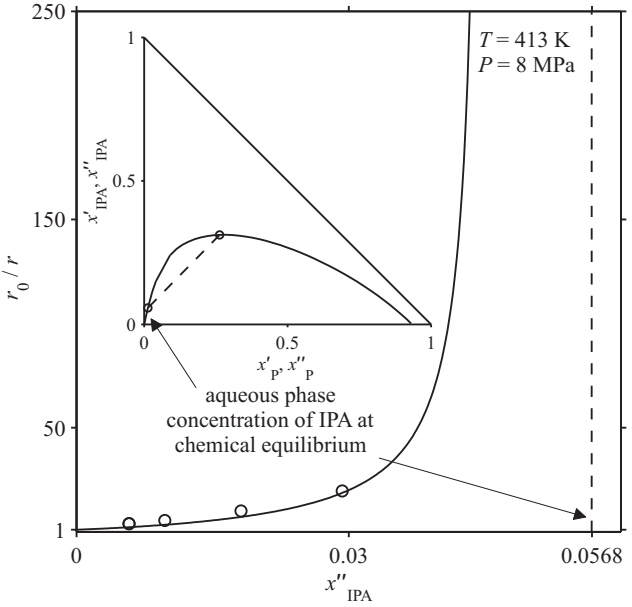

Figure 3.17: Reaction resistance as function of product concentration in the aqueous phase.

It can be seen that the shown experiments are obtained in a sufficient distance to the equilibrium in order to gain reliable kinetic data. Moreover, the equilibrium is reached for relatively small amounts of isopropyl alcohol. As can be expected from the second order dependence for the diisopropyl ether formation rate with respect to the activity of isopropyl alcohol the selectivity to the formation of isopropyl alcohol strongly depends on the aqueous phase concentration of isopropyl alcohol as is illustrated in fig. 3.18. It should be noted here that the presented data are obtained in an ideally mixed flow reactor. Performing the C_3-hydration in an integral reactor the resulting total selectivity will be remarkably greater.

The effect of the aqueous phase mole fraction of isopropyl alcohol on the extent of equilibrium conversion and on selectivity emphasizes the importance of simultaneous product extraction into the organic phase.

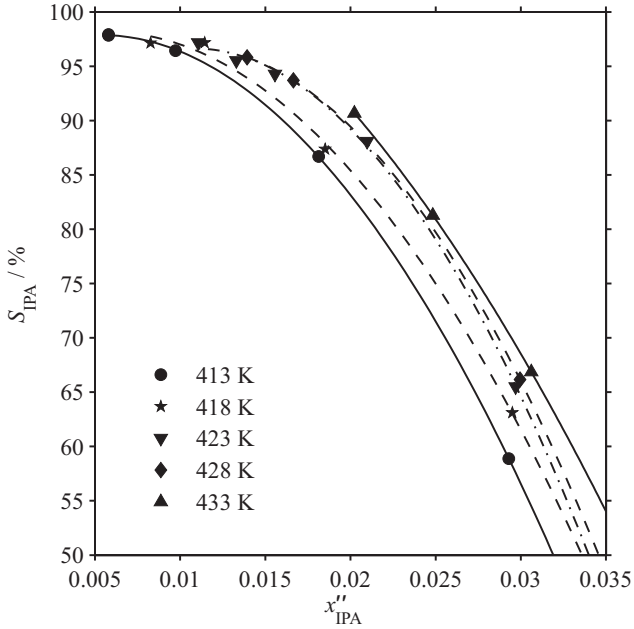

Figure 3.18: Selectivity of IPA formation as function of the aqueous phase mole fraction of IPA.

Figure 3.19 provides a comparison of calculated initial reaction rates of this work with those of Petrus et al. [1]. The initial rate of this work for the formation of isopropyl alcohol exceeds that of Petrus et al. [1] whereas the activation energy determined in this work is approximately 7.5 % greater. As Petrus et al. [1] used an intermediate type acidic ion exchange resin between gel phase and macroporous and the range for pore diffusion limitations is checked by an estimation method the lower rate is probably caused by internal mass transfer.

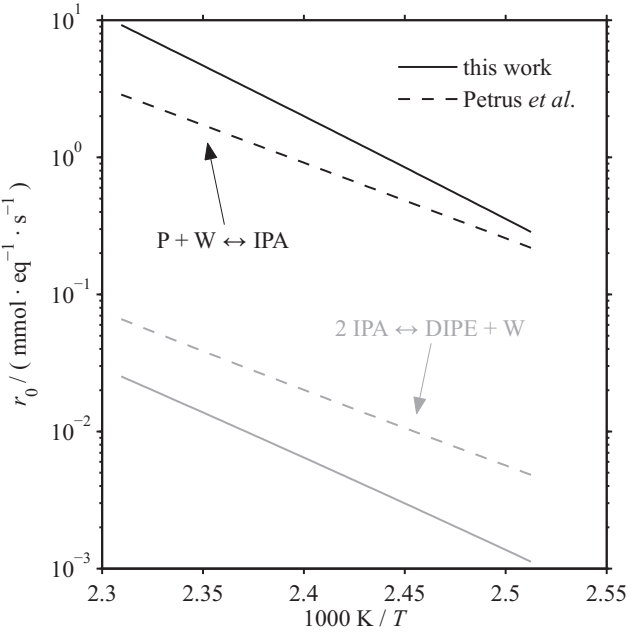

Figure 3.19: Temperature dependency of initial reaction rates.

Furthermore, while the used bead size fraction is similar to that of this work the capacity of the wet resin used by Petrus et al. [1] (2.3 eq/kg) is approximately two times greater than of the resin used in this work (1.1 eq/kg).

However, the magnitudes of the initial diisopropyl ether formation rate from Petrus et al. [1] are remarkably greater than those found in this work.

A comparison of the equilibrium constants of Petrus et al. [1] and of this work with respect to temperature is given in fig. 3.20. The course of the equilibrium constants with temperature of both studies are very similar. Petrus et al. [1]

obtained the equilibrium constants experimentally whereas those of this work are calculated using the methods presented in section 2.2.

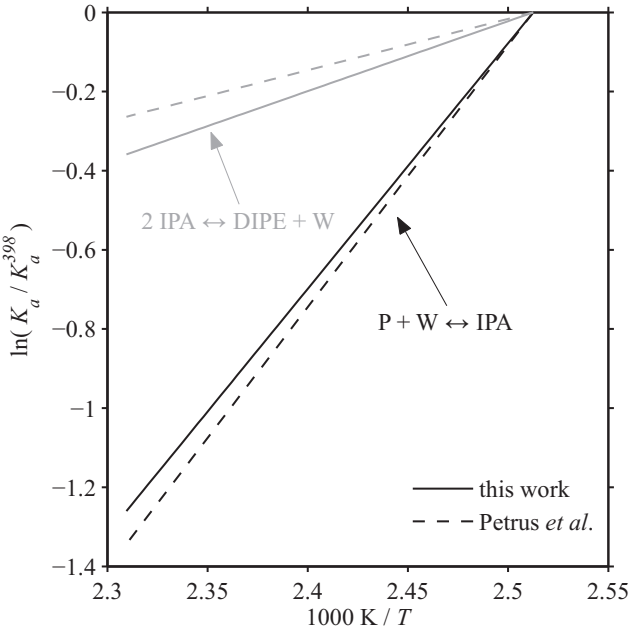

Figure 3.20: Temperature dependency of equilibrium constants (this work: based on theoretical considerations and on data provided in tables 2.1 and 2.2; Petrus et al. [1]: based on measured data).

However, a comparative validation of the experimental data from this work with that of Petrus et al. [1] is impossible as these authors neither provide experimental data nor give any comparison of their model and experimental data.

3.4.2 Microkinetics of the C_4-hydration system

The experimental kinetic data for the C_4-hydration system, which are obtained under exclusion of mass transfer limitations, are used for the development of a rate model. All experimental data and corresponding reaction conditions are compiled in table C.2.

The following assumptions which are essentially the same as for the C_3-hydration system - are made during development of the rate equation:

i) the chemical reaction is the rate limiting step as mikrokinetic rate data are used for parameter adjustment,

ii) the reaction takes place in the water swollen gel phase of the ion exchange resin,

iii) the catalytically active acid sites are completely hydrated by water molecules,

iv) the solvated protons remain locally associated to their polymer-bonded counterions (cf. Helfferich [18]),

v) the byproduct di-*sec*-butyl ether will not be considered in the rate model, and

vi) the isomerization of the butenes is significantly faster than the hydration reaction. Due to the strong polarity of the used catalytic resin it is mainly wetted by the aqueous phase.

The first four preceding assumptions are already explained in section 3.4.1 and, therefore, only listed for the sake of completeness.

As di-*sec*-butyl ether was never detected during the kinetic experiments for the C_4-hydration system of this work the reaction network – the basis for the rate model development – can be simplified as shown in fig. 3.21.

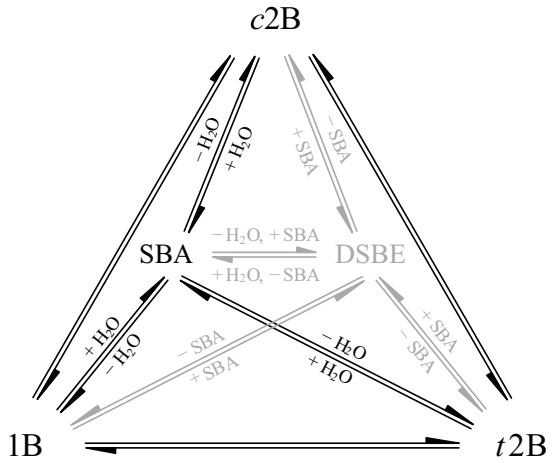

Figure 3.21: Reaction network (neglecting DSBE formation).

Furthermore, the butene isomer mixture in the feed used in this work (cf. table 3.2) is rather far from an equilibrium composition for the isomerization.

But, in all experiments provided in table C.2 the butenes are analyzed by gas chromatography to be in equilibrium even in the organic phase. This result provides evidence of the last assumption in which isomerization of the butenes is considered to be at equilibrium. This phenomenon can be explained by the matter of fact that isomerization simply proceeds via reduction of the unstable carbenium ion which must occur more frequently than reaction of water with the carbenium ion. As a conclusion, the reaction of linear butenes with water can be illustrated by the following finally simplified reaction network (fig. 3.22).

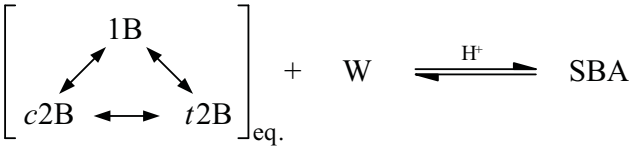

Figure 3.22: Reaction network (isomerization in equilibrium).

A pseudo-homogeneous 3-parameter rate expression in aqueous phase activities of stoichiometric orders represents the experimental data well

$$r_{\text{rev, SBA}} = k_+ \left(a''_{\text{B}} a''_{\text{W}} - \frac{a''_{\text{SBA}}}{K_{a,\text{SBA}}} \right) . \tag{3.7}$$

In eq. (3.7), k_+ is the rate constant in $\text{mmol}_{\text{SBA}}/(\text{eq}\,\text{s})$ which is a function of temperature according to the ARRHENIUS equation

$$k_+ = k_+^0 \exp\left(\frac{-E_{\text{a}}}{RT} \right) . \tag{3.8}$$

The pre-exponential factor k_+^0, the activation energy E_{a}, and the chemical equilibrium constant $K_{a,\text{SBA}}$ were used for adjustment calculations of the reaction rate model. The obtained parameter values and approximate individual confidence intervals are given in table 3.5. It should be noted here that the confidence interval of $K_{a,\text{SBA}}^{398}$ is relatively large (approx. 20 % of the corresponding parameter). This is most probably due to the low range of rate values of the reverse reaction which, in turn, results from the limited range of feasible *sec*-butyl alcohol concentrations in the feed (cf. table C.2). The activities in eq. (3.7) are defined by eq. (2.17).

Table 3.5: Intrinsic rate model parameter for eqs. (3.7), (3.8) and (3.10).

Parameter		Unit	Value	App. individual confidence limit (95 %)
1	k_+^0	$\mathrm{mmol_{SBA}/(eq\,s)}$	1.14×10^{11}	$\pm 2.2 \times 10^5$
2	E_a	kJ/mol	108.0	± 6.8
3	$K_{a,\mathrm{SBA}}^{398}$	–	1.3×10^{-2}	$\pm 2.8 \times 10^{-3}$
4	Δh_r	kJ/mol	-39.9	–
$r_0(418\,\mathrm{K},\ 8\,\mathrm{MPa})$[a]		$\mathrm{mmol_{SBA}/(eq\,s)}$	0.63	–
		$\mathrm{mol_{SBA}/(m^3\,s)}$	0.52	–

[a] $x_\mathrm{B}'' = 0.07\,\mathrm{mol\,\%}$

Equation (3.7) shows the rate of the forward reaction to be first order with respect to the activities of *n*-butenes and water and that of the reverse reaction to be first order with respect to the activity of *sec*-butyl alcohol. According to the explanations in section 3.4.1, the activity of water is not canceled from eq. (3.7).

Although the chemical equilibrium constant could be obtained readily from ideal gas thermodynamics (cf. section 2.2.2), the absolute value of the theoretically calculated equilibrium constant $K_{a,\mathrm{SBA}}$ does not lead to a satisfying fit with the kinetic model. For this constant, only the temperature dependence correlates well with experimental data of this work and data provided in literature. A comparison of the temperature dependence with the work of Petrus et al. [2] is given in fig. 3.23.

For strongly limited solubilities, as is the case for *n*-butenes in water, uncertainties of the fitted binary interaction parameters of the UNIQUAC model become significant. Furthermore, the equilibrium concentration of *n*-butenes in the aqueous phase is very small ($< 0.1\,\mathrm{mol\,\%}$) and the activity coefficient of *n*-butenes is sensitive to changes in mole fractions. Thus, possible errors in the concentration measurements are amplified by computation of related activities. Finally, the calculation of fugacities is based only on the isomer 1-butene because the available experimental phase equilibrium data are also based on 1-butene. All these error sources may cause inconsistencies of the activities with the theoretically calculated chemical equilibrium constant.

The chemical equilibrium constant $K_{a,\mathrm{SBA}}$ in eq. (3.7) is, therefore, used as adjustable parameter in the rate model. Starting from the VAN'T HOFF equation describing the temperature dependence of the chemical equilibrium

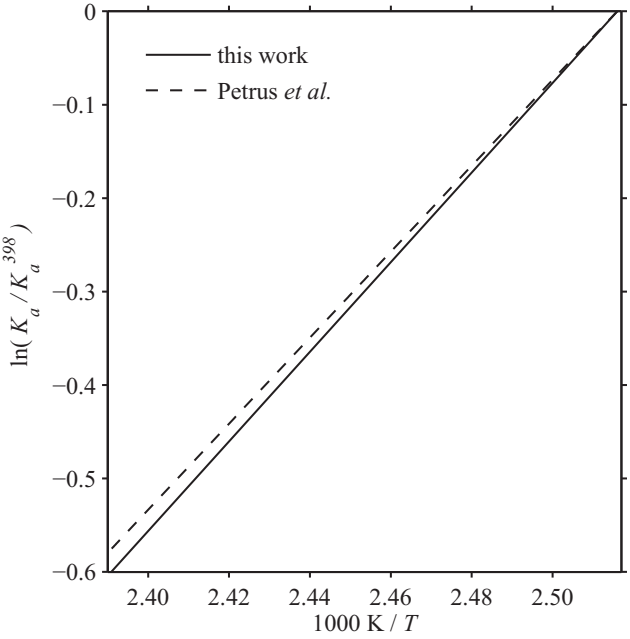

Figure 3.23: Temperature dependency of the equilibrium constant (this work: based on theoretical considerations and on data provided in tables 2.1 and 2.3; Petrus et al. [2]: based on their measured data).

constant:

$$\frac{\mathrm{d}\ln K_a}{\mathrm{d}T} = \frac{\Delta h_\mathrm{r}}{RT^2} \tag{3.9}$$

the following relation is derived by integration of eq. (3.9):

$$\ln \frac{K_a}{K_a^{398}} = -\frac{\Delta h_\mathrm{r}}{R}\left(\frac{1}{T} - \frac{1}{398\,\mathrm{K}}\right) . \tag{3.10}$$

The parameter K_a^{398} in eq. (3.10) was adjusted together with the other parameters of the rate model. All parameters are given in table 3.5. The accuracy of the proposed model is illustrated by a parity plot provided in fig. 3.24. It can be seen that the model represents the measured data fairly well at least for the more important temperature range of 130 °C to 145 °C. The variation of reaction rate data measured at temperatures below 130 °C is less narrow, but the data points are almost equally distributed around the locus of an exact match. The three data points in the lower left corner of fig. 3.24 correspond to the dehydration of *sec*-butyl alcohol. Due to the strong extraction of *sec*-butyl alcohol from the reacting aqueous phase it was impossible to measure dehydration rates at higher levels.

The activities in eq. (3.7) are obtained from the VTPR-EoS as described in section 2.2. It is assumed that the linear butene isomers form ideal liquid mixtures. The pure component parameters of 1-butene are used to represent the pseudo-component *n*-butenes, i. e. isomeric equilibrium mixture of linear butenes, because data of pure 1-butene are also used for the adjustment calculations of the thermodynamic model. Adjusting the parameters of a model according to eq. (3.7), but expressed in mole fractions, unsatisfactory results are obtained. This is also demonstrated in the work of Rehfinger and Hoffmann [21] for methyl tertiary butyl ether synthesis and is discussed in detail by Kondepudi and Prigogine [22]. Figure 3.25 illustrates the course of the reaction resistance from initial conditions towards equilibrium with increasing *sec*-butyl alcohol concentration.

It can be seen that the presented experiments are obtained in a sufficient distance to the equilibrium in order to gain reliable kinetic data. Moreover, the equilibrium is reached for very small amounts of *sec*-butyl alcohol which emphasizes the importance of simultaneous product extraction. Figure 3.26 provides a comparison of calculated initial reaction rates of this work with those of Petrus et al. [2]. The rather small differences between the initial rates of both studies may originate from experimental uncertainties especially at low temperatures. It is assumed that the experimental data from this work are more reliable because in this study higher amounts of *sec*-butyl alcohol

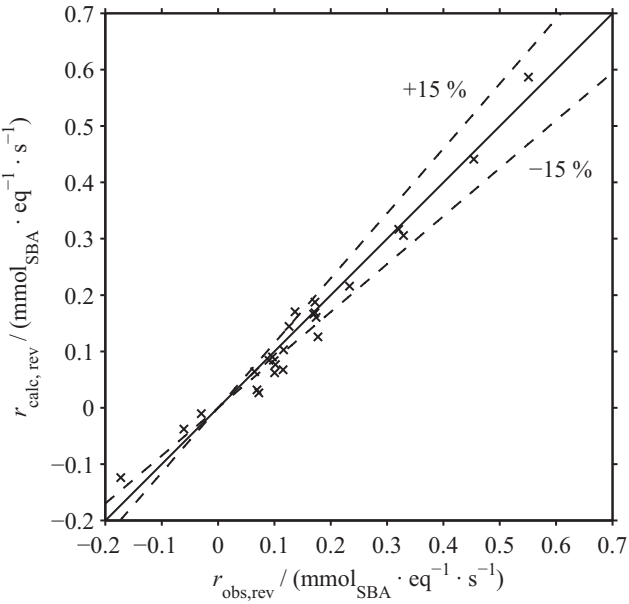

Figure 3.24: Parity plot of measured and simulated reaction rate data.

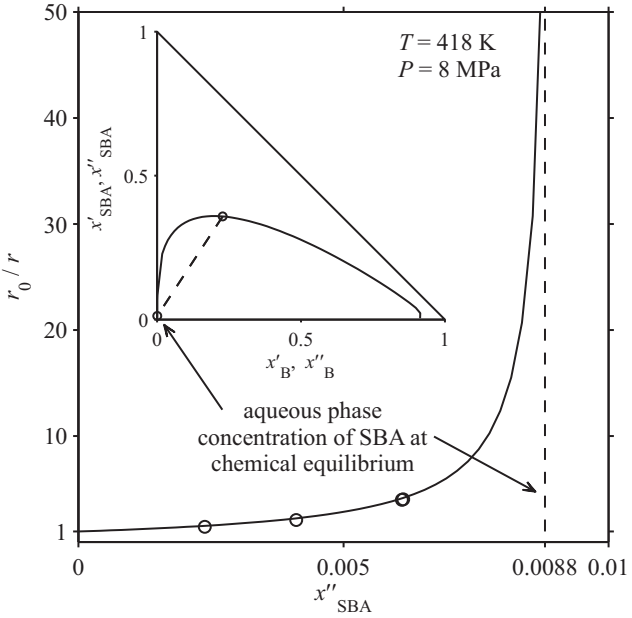

Figure 3.25: Reaction resistance as function of product concentration in the aqueous phase.

are obtained due to multiphase operation in the reactor. The continuous transport of *n*-butenes from the organic to the aqueous phase at multiphase conditions provides higher *sec*-butyl alcohol yields compared to a reactor fed with butene-saturated aqueous mixtures.

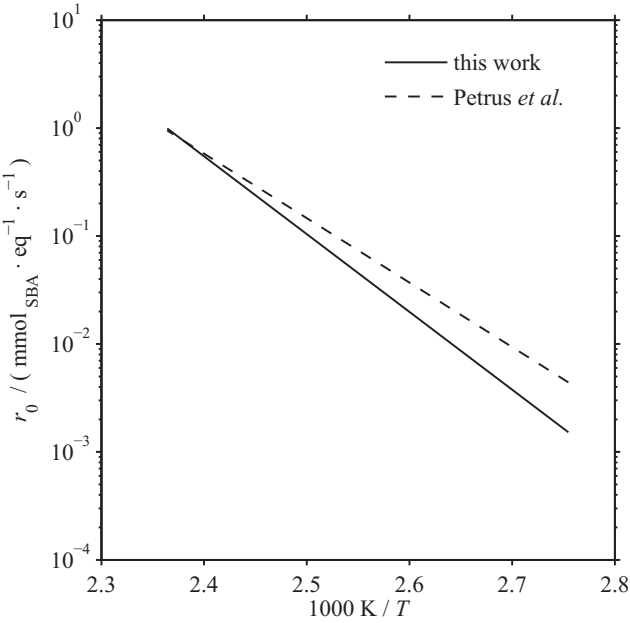

Figure 3.26: Temperature dependency of initial reaction rates.

The presented microkinetic study of the C_4-hydration system catalyzed by an acidic ion exchange resin has also been published elsewhere (cf. Pfeuffer et al. [23]).

3.4.3 Macrokinetics of the C_4-hydration system

For the description of nonideal multicomponent mass transfer in the pores of the catalyst the dusty-fluid model is used. The dusty-fluid model ((cf. Krishna and Wesselingh [24])) is a generalization of the well known dusty-gas model ((cf. Mason and Malinauskas [25])) to pore structures which are filled with nonideal fluid mixtures.

The dusty-fluid model equations are based on the generalized Maxwell-Stefan equations (GMS). Considering exclusively bulk diffusion inside the

catalyst pores the dusty-fluid model equations reduce to the GMS except that the bulk phase diffusivities are subject to a transformation in order to account for the pore volume fraction and shape. The resulting model equations are (see also section 2.3)

$$\frac{x_i}{RT}\nabla_{T,P}\bar{\mu}_i = \sum_{\substack{j=1\\ j\neq i}}^{n_c} \frac{x_i N_j - x_j N_i}{c_t \mathit{Đ}^e_{i,j}} \qquad i = 1, 2, \ldots, n_c - 1 \tag{3.11a}$$

with the effective diffusivity $\mathit{Đ}^e_{i,j}$

$$\mathit{Đ}^e_{i,j} = \frac{\varepsilon_{cat}}{\tau_{cat}} \mathit{Đ}_{i,j} \tag{3.11b}$$

In eq. (3.11b) ε_{cat} is the porosity (pore volume fraction) of the catalyst and τ_{cat} is the tortuosity (labyrinth factor) which accounts for a non-cylindrical shape of the pores (cylindrical pore: $\tau_{cat} = 1$).

Mass transfer in the NERNST diffusion layer surrounding the catalyst bead is modeled according to eq. (2.24).

Following the survey given in section 2.3 and using the identical mathematical implementation, whereas the following assumptions are taken as a basis:

i) the transport is in steady state, no accumulation occurs in the NERNST layer surrounding the catalyst and in the catalyst,

ii) reaction of mass occurs in the catalyst only,

iii) the mass transfer takes place under isothermal and isobaric conditions,

iv) the catalyst is spherically shaped,

v) the center of the catalyst is subject to symmetry, and

vi) the actual bimodal pore structure of the acidic ion exchange resin is treated as homogeneous pore structure,

the final set of model equations obtained from eq. (3.11a) for the catalyst is

$$\frac{\mathrm{d}x_i^S}{\mathrm{d}\lambda} = \left[\Gamma^S\right]^{-1} \sum_{\substack{j=1\\ j\neq i}}^{n_c} \frac{-x_i^S \mathbb{N}_j + x_j^S \mathbb{N}_i}{c_t^S \frac{2 s_{CP} \lambda^2}{d_{CP}} \mathit{Đ}^e_{i,j}} \qquad i = 1, 2, \ldots, n_c - 1 \tag{3.12a}$$

and, for the NERNST film layer from eq. (3.11a) we obtain

$$\frac{\mathrm{d}x_i^{L2S}}{\mathrm{d}\lambda} = \left[\Gamma^{L2S}\right]^{-1} \sum_{\substack{j=1\\ j\neq i}}^{n_c} \frac{x_i^{L2S} N_j - x_j^{L2S} N_i}{c_t^{L2S} \kappa_{i,j}^{L2S}} \qquad i = 1, 2, \ldots, n_c - 1\,. \tag{3.12b}$$

using the following set of equations describing the diffusion path dependency of the mass transfer rate throughout the radius of the catalyst

$$\frac{\mathrm{d}\mathbb{N}_i}{\mathrm{d}\lambda} = -s_{\mathrm{CP}} \frac{d_{\mathrm{CP}}}{2} \lambda^2 c_{\mathrm{H+}} \nu_i r_{\mathrm{rev}} \qquad i = 1, 2, \ldots, n_{\mathrm{c}} \tag{3.13a}$$

and for the fluxes in the NERNST film layer

$$\frac{\mathrm{d}N_i}{\mathrm{d}\lambda} = 0 \qquad i = 1, 2, \ldots, n_{\mathrm{c}} \tag{3.13b}$$

with the volume specific acid site concentration of the catalyst specified by

$$c_{\mathrm{H+}} = \rho_{\mathrm{H+}} \rho_{\mathrm{cat,\ wet}} \ . \tag{3.14}$$

The $\mathbb{N}_i$ are mass transfer rates which are preferred over fluxes in order to account for a geometrically related change of cross section for mass transfer along the diffusion path. The mass transfer coefficients $\kappa_{i,j}^{\mathrm{L2S}}$ for the aqueous NERNST film layer around the catalyst are calculated from bulk phase diffusivities as described in section 2.3 and using a trickle-bed reactor SHERWOOD-function from Krevelen and Krekels [26] as discussed by Goto et al. [27].

Equations (3.12) and (3.13) form a set of $4(n_{\mathrm{c}} - 1) + 2$ ODE which are subject to the following boundary conditions, first for the catalyst related to eqs. (3.12a) and (3.13a)

$$x_{i,\lambda=1}^{\mathrm{S}} = x_{i,\lambda=1}^{\mathrm{L2S}} \qquad i = 1, 2, \ldots, n_{\mathrm{c}} - 1 \tag{3.15a}$$

$$\mathbb{N}_{i,\lambda=0} = 0 \qquad i = 1, 2, \ldots, n_{\mathrm{c}} \tag{3.15b}$$

and secondly for the NERNST film layer related to eqs. (3.12b) and (3.13b)

$$x_{i,\lambda=0}^{\mathrm{L2S}} = x_i'' \qquad i = 1, 2, \ldots, n_{\mathrm{c}} - 1 \tag{3.15c}$$

$$N_{i,\lambda=1} = -\frac{\mathbb{N}_{i,\lambda=1}}{s_{\mathrm{CP}}} \qquad i = 1, 2, \ldots, n_{\mathrm{c}} \ . \tag{3.15d}$$

Figure 3.27 gives exemplary results for the mole fraction profiles of *n*-butenes and *sec*-butyl alcohol inside the catalyst and throughout the NERNST diffusion film layer around the catalyst. The profiles clearly illustrate that the main mass transfer resistance is located rather in the pores of the catalyst than in the film layer.

The model is tested with experimental data from the kinetic study of the C_4-hydration system. The results are presented in an ARRHENIUS plot showing experimental data and according micro- and macrokinetic data computed with the proposed models (fig. 3.28). The ratio $\frac{\varepsilon_{\mathrm{cat}}}{\tau_{\mathrm{cat}}}$ which relates the bulk phase diffusivity to the effective diffusivity is taken as 0.4. The porosity $\varepsilon_{\mathrm{cat}}$ of the used

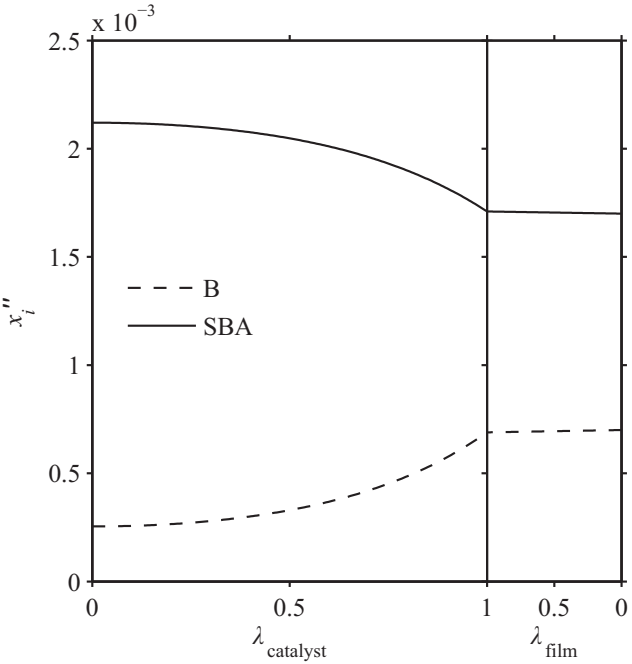

Figure 3.27: Composition profiles of B and SBA inside the catalyst and in the NERNST diffusion layer surrounding the catalyst.

ion exchange resin is 36 % in the dry state. The volumetric degree of swelling in water is approximately 100 % which results in a porosity of approximately 70 %. Under these conditions the tortuosity is approximately 1.8. However, as porosity and tortuosity cannot be determined separately and exactly, the ratio $\frac{\varepsilon_{cat}}{\tau_{cat}}$ is adjusted to the experimental data which are obtained under internal mass transfer influence.

Furthermore, mass transfer within a macroreticular ion exchange resin can be classified among two types: macropore diffusion and diffusion in micropores which are formed in the intermolecular space of the gel phase (cf. Sundmacher et al. [28]). However, the number of applicable ion exchange resin catalysts for alkene hydration is low and properties which have an influence on the inner structure of the catalyst, e. g. degree of cross-linking, do not vary much among these catalyst types. Hence, in this work, there is no need to distinguish between the two regimes of mass transfer within the catalyst.

The data points from all three sources are in close agreement for temperatures up to 418 K. For higher temperatures the only experimental and computed macrokinetic data points are still correlating while the microkinetic data points follow the linear course of the low temperature data points. For the two lowest temperatures the deviation of the experimental data from the computed data is due to experimental uncertainties (see also fig. 3.24).

3.5 Conclusions

As the reaction rates of this important reaction class, the alkene hydration reactions, as a synthesis route for secondary alcohols are rather low the attractiveness of this reaction is based on the fact that the alkenes do not only act as reactants but also as extracting agents for the formed product secondary alcohol, e. g. isopropyl alcohol, *sec*-butyl alcohol. Only by a continuous removal of the sparely formed product from the aqueous phase this synthesis route becomes interesting not only from chemical reaction engineering aspects but primarily for an economic industrial production.

The here designed and operated laboratory reactor proofed to be a suitable tool for analyzing the kinetics of isopropyl alcohol and *sec*-butyl alcohol synthesis. The independent control of feed flow rate and hold-up of the two liquid phases in the CSTR ensures sufficient conversion for reliable kinetic measurements. Due to the low solubility of alkenes in water this reactor is superior compared to single phase reactors operating with olefin saturated aqueous phases.

The microkinetics of the C_3- and C_4-hydration systems are well described by pseudo-homogeneous global rate expressions in liquid phase activities which is methodically in line with the theory of *specific catalysis* in water-swollen acidic ion exchange resins (cf. Chakrabarti and Sharma [19]).

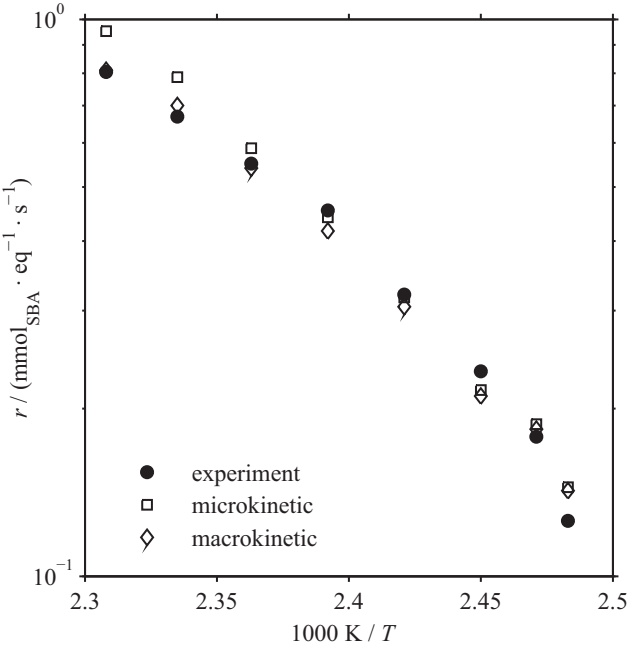

Figure 3.28: ARRHENIUS-plot showing macrokinetic and microkinetic model predictions and corresponding measurements.

The presented macrokinetic model seems to be a valuable tool for simulating the interrelation of chemical reaction rate and nonideal multicomponent mass transfer in the pores of the catalyst.

This study reveals the key role of phase equilibria in the considered reaction systems. The evaluation of the importance of extraction and liquid phase nonidealities on the reaction kinetics confirms the necessity to rigorously consider phase equilibrium thermodynamics. In the first place, the co-existence of two immiscible liquids in combination with a heterogeneous catalyst and secondly an effective extractive product removal are prerequisites for a reliably designed industrial alkene hydration reactor.

Taking into account low pressure drop, sufficient wetting of the catalyst and large interfacial areas the application of a structured catalytic packing seems to be a promising approach towards intensified isopropyl alcohol and *sec*-butyl alcohol production processes which could be named heterogeneous reactive extraction.

References

[1] Petrus, L., R. W. De Roo, E. J. Stamhuis, and G. E. H. Joosten. Kinetics and equilibria of the hydration of propene over a strong acid ion exchange resin as catalyst. *Chem. Eng. Sci.* **39**, (1984), 433–446. DOI: 10.1016/0009-2509(84)80041-X.

[2] Petrus, L., R. W. De Roo, E. J. Stamhuis, and G. E. H. Joosten. Kinetics and equilibria of the hydration of linear butenes over a strong acid ion-exchange resin as catalyst. *Chem. Eng. Sci.* **41**, (1986), 217–226. DOI: 10.1016/0009-2509(86)87002-6.

[3] Klein, J. and H. Widdecke. *Verfahren zur Umsetzung von n-Butenen mit Festsäurekatalysatoren.* DGMK Projekt-Bericht 328, 1987.

[4] Mahajani, S. M., M. M. Sharma, and T. Sridhar. Extractive hydration of n-butene with solid acid catalysts in the liquid phase and under supercritical conditions. *Chem. Eng. Sci.* **56**, (2001), 5625–5633. DOI: 10.1016/S0009-2509(01)00172-5.

[5] Mahajani, S. M., M. M. Sharma, and T. Sridhar. Direct hydration of propylene in liquid phase and under supercritical conditions in the presence of solid acid catalysts. *Chem. Eng. Sci.* **57**, (2002), 4877–4882. DOI: 10.1016/S0009-2509(02)00293-2.

[6] Panneman, H. J. and A. Beenackers. Solvent Effects on the Hydration of Cyclohexene Catalyzed by a Strong Acid Ion-Exchange Resin. 1. Solubility of Cyclohexene in Aqueous Sulfolane Mixtures. *Ind. Eng. Chem. Res.* **31**, (1992), 1227–1231. DOI: 10.1021/ie00004a039.

[7] Panneman, H. J. and A. Beenackers. Solvent Effects on the Hydration of Cyclohexene Catalyzed by a Strong Acid Ion-Exchange Resin. 2. Effect of Sulfolane on the Reaction-Kinetics. *Ind. Eng. Chem. Res.* **31**, (1992), 1425–1433. DOI: 10.1021/ie00006a001.

[8] Panneman, H. J. and A. Beenackers. Solvent Effects on the Hydration of Cyclohexene Catalyzed by a Strong Acid Ion-Exchange Resin. 3. Effect of Sulfolane on the Equilibrium Conversion. *Ind. Eng. Chem. Res.* **31**, (1992), 1433–1440. DOI: 10.1021/ie00006a002.

[9] Panneman, H. J. and A. Beenackers. Solvent Effects in the Liquid-Phase Hydration of Cyclohexene Catalyzed by a Macroporous Strong Acid Ion-Exchange Resin. *Chem. Eng. Sci.* **47**, (1992), 2635–2640. DOI: 10.1016/0009-2509(92)87105-Y.

[10] Heese, F. P., M. E. Dry, and K. P. Möller. Single stage synthesis of diisopropyl ether - an alternative octane enhancer for lead-free petrol. *Catal. Today* **49**, (1999), 327–335. DOI: 10.1016/S0920-5861(98)00440-4.

[11] Heese, F. P., M. E. Dry, and K. P. Möller. The mechanism of diisopropyl ether synthesis from a feed of propylene and isopropanol over ion exchange resin. *Stud. Surf. Sci. Catal.* **130**, (2000), 2597–2602.

[12] Ihmels, E. C., K. Fischer, and J. Gmehling. Thermodynamic properties of the butenes: Part I. Experimental densities, vapor pressures, and critical points. *Fluid Phase Equilib.* **228-229**, (2005), 155–171. DOI: 10.1016/j.fluid.2004.09.013.

[13] Petrus, L., E. J. Stamhuis, and G. E. H. Joosten. Thermal deactivation of strong-acid ion-exchange resins in water. *Ind. Eng. Chem. Prod. Res. Dev.* **20**, (1981), 366–371. DOI: 10.1021/i300002a026.

[14] Rozek, M. Reaktionstechnische Untersuchungen zur heterogen-katalysierten Direkthydratisierung von Buten zu 2-Butanol. Diploma Thesis, Fachochschule Niederrhein, 2001.

[15] Pitochelli, A. R. *Ion Exchange Catalysis and Matrix Effects*. tech. rep., Rohm and Haas, Philadelphia, 1980.

[16] Carberry, J. J. Designing Laboratory Catalytic Reactors. *Ind. Eng. Chem.* **56**, (1964), 39–46. DOI: 10.1021/ie50659a007.

[17] Petre, D. Kinetic Investigations on Direct Hydration of *n*-Butene in a Multiphase Reactor. Ph.D. Thesis, Clausthal University of Technology, 2006.

[18] Helfferich, F. G. *Ion exchange*. McGraw-Hill, New York, 1962.

[19] Chakrabarti, A. and M. M. Sharma. Cationic ion exchange resins as catalyst. *React. Polym.* **20**, (1993), 1–45. DOI: 10.1016/0923-1137(93)90064-M.

[20] Gates, B. C. and W. Rodriguez. General and specific acid catalysis in sulfonic acid resin. *J. Catal.* **31**, (1973), 27–31. DOI: 10.1016/0021-9517(73)90266-2.

[21] Rehfinger, A. and U. Hoffmann. Kinetics of methyl tertiary butyl ether liquid phase synthesis catalyzed by ion exchange resin - I. Intrinsic rate expression in liquid phase activities. *Chem. Eng. Sci.* **45**, (1990), 1605–1617. DOI: 10.1016/0009-2509(90)80013-5.

[22] Kondepudi, D. and I. Prigogine. *Modern Thermodynamics - From Heat Engines to Dissipative Structures*. John Wiley & Sons, Chichester, 1998.

[23] Pfeuffer, B., U. Kunz, U. Hoffmann, T. Turek, and D. Hoell. Heterogeneous reactive extraction for secondary butyl alcohol liquid phase synthesis: Microkinetics and equilibria. *Chem. Eng. Sci.* **66**, (2011), 777–787. DOI: 10.1016/j.ces.2010.11.040.

[24] Krishna, R. and J. A. Wesselingh. The Maxwell-Stefan approach to mass transfer. *Chem. Eng. Sci.* **52**, (1997), 861–911. DOI: 10.1016/S0009-2509(96)00458-7.

[25] Mason, E. A. and A. P. Malinauskas. *Gas transport in porous media : the dusty-gas model*. Elsevier, Amsterdam, 1983.

[26] Krevelen, D. W. van and J. T. C. Krekels. Rate of dissolution of solid substances. *Recl. Trav. Chim. Pays-Bas* **67**, (1948), 512.

[27] Goto, S., J. Levec, and J. M. Smith. Trickle-Bed Oxidation Reactors. *Catal. Rev.* **15**, (1977), 187–247. DOI: 10.1080/03602457708081725.

[28] Sundmacher, K., H. Künne, and U. Kunz. Contribution of Gel Phase Diffusion to Mass Transfer in Supported Ion Exchange Catalysts. *Chem. Eng. Technol.* **21**, (1998), 494–498. DOI: 10.1002/(SICI)1521-4125(199806)21:6<494::AID-CEAT494>3.0.CO;2-Y.

4 Process Intensification by Reactive Extraction

4.1 On the Need for Efficiency Improved Chemical Production Processes

After an era of meanwhile more than 200 years of industrial manufacturing the still growing demand for energy due to the growth of economy forces engineers to develop improved efficient processes and engines. In 2007, more than 50 % of the global energy demand was caused by industry whereas the usage grows at an annual rate of 1.3 %. The chemical industry is the most energy consuming sector using 22 % of the industrial energy demand (Conti and Doman [1]).

Despite the discussion on the extent of environmental impact imposed by greenhouse gases and the trend of shrinking resources of fossil fuels (cf. Schaub and Turek [2], pp. 133-138) it can generally be stated that a reduction of the energy demand of processes and engines is beneficial from an economical point of view. Especially in the field of petrochemical processing – wherein energy makes approximately 60 % of the operational costs – reducing the energy demand always improves profit.

This holds especially for the manufacture of bulk chemicals. Profits per mass unit are usually small and the fraction of energy related costs from overall costs is high. Therefore, improvements for bulk chemical manufacture processes with respect to energy demand reductions can be profitable and are helpful in reducing pollution of the environment. Furthermore, such arrangements enhance the acceptance of chemical processing by population.

There are many examples for modern chemical reaction engineering concepts which focus on the objectives of process intensification, e. g. micro reactors for heat exchange intensive applications (cf. Ehrfeld et al. [3]), structured catalytic packings as – for instance – monolith catalyst supports operated at Taylor flow regime for improved mass transfer performance (cf. Cybulski and Moulijn [4], Part I), or reaction and separation integrated processes which are able to circumvent equilibrium or selectivity related limitations on the extent of conversion (cf. Schmidt-Traub and Górak [5]).

Increasing the field of application of such concepts is one of the most important challenges for chemical engineers today. Therefore, process intensification is also a major concern of this work with respect to the manufacture of secondary

alcohols from linear alkenes which is an established synthesis route for quite a long time.

4.2 Hybrid Processes Unifying Separation and Reaction Processes

Hybrid (integrated) processes which unify the unit operations reaction and separation into one apparatus can be a very effective concept for the manufacture of chemical products. An overview of integrated processes is given by numerous examples in Sundmacher et al. [6]. Practically all kind of thermal separation operations can be combined with homogeneously and heterogeneously catalyzed conversions (fig. 4.1).

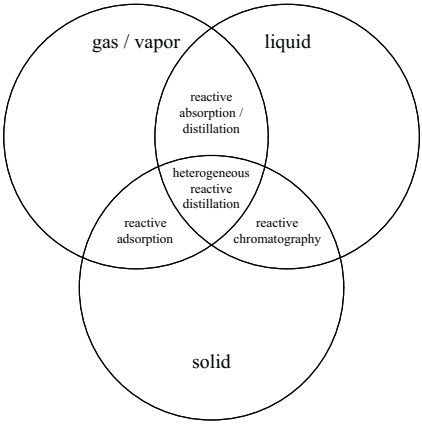

Figure 4.1: Classification of multifunctional reactors according to participating phases [7].

However, in the scheme of Agar [7] the combination of reaction and extraction was not considered. Seizing this suggestion, Kenig et al. [8] extended this scheme towards reactive extraction (fig. 4.2). This scheme is now extended another time by this work considering the use of heterogeneous catalysts for reactive extraction (fig. 4.3).

For chemical engineers the advantages of integrated reaction and separation processes are obvious. All kind of integrated reaction and separation processes have some common characteristics. At least two immiscible phases (gas–liquid, gas–solid, liquid–solid or liquid–liquid) interact by undertaking mass, heat and momentum transfer. Usually, the reaction takes place in one of the co-existing

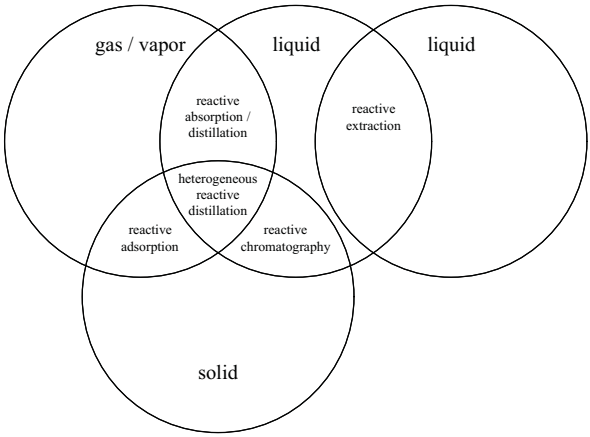

Figure 4.2: 1st extension of classification of multifunctional reactors according to participating phases [8].

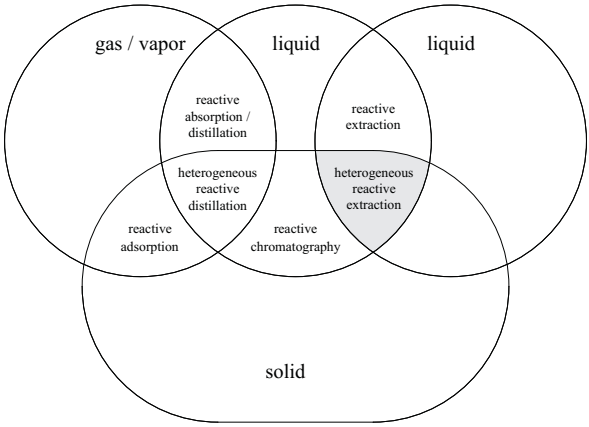

Figure 4.3: 2nd extension of classification of multifunctional reactors according to participating phases.

phases. The benefit of the process is mostly based on the simultaneous removal of product from the reacting phase by the second non-reactive phase leading to:

i) an improved selectivity when consecutive reactions of the main-product to undesired by-products occur,

ii) a shift of the chemical equilibrium thereby enabling higher levels of conversion, and

iii) a transcending of distillation borders thereby circumventing azeotrops in down-stream separation units.

On the other hand, there is a major disadvantage when reaction and separation are integrated: the reduction of the degree of freedom. Operation conditions such as pressure, temperature, concentrations and fluid dynamics must be selected in a way fulfilling the requirements of both operations, reaction and separation.

The most common and industrially applied type of integrated reaction and separation processes is reactive (catalytic) distillation. Etherification for the manufacture of fuel oxygenates, e. g. methyl *tert*-butyl ether (MTBE), ethyl *tert*-butyl ether (ETBE), and *tert*-amyl methyl ether (TAME), and esterification for manufacturing of acetates, e. g. methyl acetate, are the most important applications among others (cf. Sundmacher and Kienle [9], pp. 3-26). Reactive distillation for the hydration of linear alkenes, particularly for propene has been proposed by Xu [10], Wang and Wong [11]. But, one may doubt that a catalytic distillation process for the hydration of propene is feasible at all. The reasons are manifold:

i) considering the remarks in section 3.4.1 reasonable reaction rates are obtained for temperatures exceeding 130 °C which is much above the critical temperature of propene (cf. table 2.1) above which propene cannot be condensed or evaporated vice versa;

ii) the ion exchange resin is saturated with water and, hence, propene reacts as aqueous dissolved matter which requires rather supercritical pressures (cf. section 2.1.2);

iii) the liquid phase will be unstable in parts of the reactive zone of the reactive distillation column inducing incalculable difficulties;

iv) the volatilities of the involved species spread over a wide temperature range which reduces the effective length of a reasonable reactive zone in the column thereby leading to unfeasible short contact times (cf. section 5.1.2).

The latter item is a general restriction to the feasibility of reactive distillation processes. The other system-specific issues are knock-out criteria for the manufacture of isopropyl alcohol from propene by reactive distillation. These limitations hold also for the manufacture of *sec*-butyl alcohol.

Considering reactive extraction it is possible to select appropriately high temperatures obtaining reasonable reaction rates but, otherwise, requiring sufficiently high pressures to avoid evaporation of any reactant or solvent. Due to the miscibility gap between the reactants propene and water and due to the extractive potential of propene with respect to isopropyl alcohol the alkene hydration reaction system naturally points towards a reactive extraction process thus avoiding the use of any additional solvent.

Therefore, this work considers reactive extraction as a reasonable approach for process intensification in the field of acidic ion exchange resin catalyzed alkene hydration.

4.3 Key Issues of Multiphase Packed Bed Reactors for *sec*-Alcohol Synthesis

Sasol Solvents Germany (formerly Deutsche Texaco AG) applies the direct hydration of propene with strong acidic ion exchange resins on a large scale since 1972. The reactor consists of a co-currently operating trickle bed subdivided into multiple trays with intersectional injection of cooling water (fig. 4.4).

Regarding the ion exchange resin catalyzed liquid phase hydration of linear alkenes various patents (Brandes et al. [12, 13], Carls et al. [14, 15], Henn et al. [16], Neier et al. [17]) address several difficulties to the trickle bed reactor which comprise polymerization of propene deactivating the catalyst, hot spots by polymerization and oligomerization and a high pressure drop. In general, due to the highly selective sorption of water by the catalyst no polymerization of the alkene occurs. However, the mentioned patents report a remarkable loss of selectivity for isopropyl alcohol of about 50 % when the catalyst gets dry. The patent authors recommend to use high water to propene feed ratios as mentioned in the previous paragraph in order to overcome the problem of an unacceptably low selectivity. Trickle-bed reactors as used for isopropyl alcohol production often show incomplete catalyst wetting (cf. Pangarkar et al. [18]). The related results, therefore, indicate incomplete wetting of the catalyst which leads to direct contact of concentrated (liquefied) alkene to dry catalyst. The patent authors use the mentioned high water to propene feed ratio in order to overcome the problem of a poor wetting performance which results in a large water recycling stream.

Another characteristic property of a randomly packed fixed bed containing

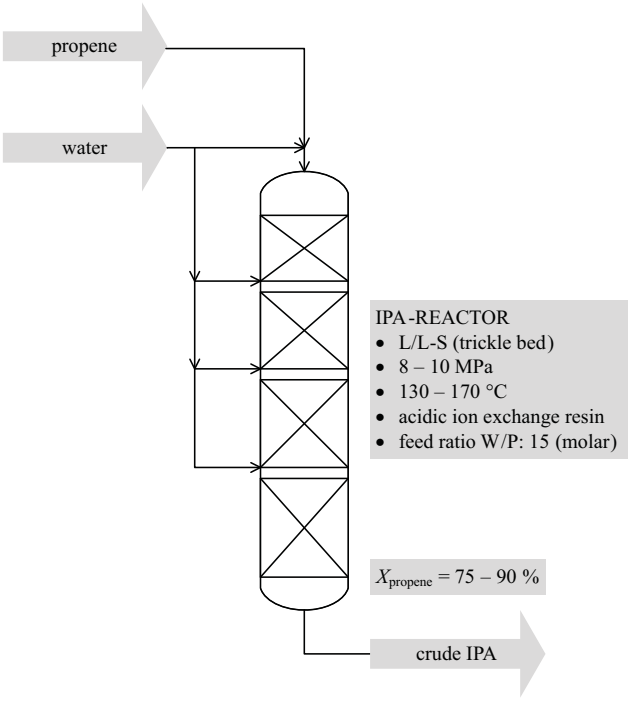

Figure 4.4: Trickle bed reactor for direct hydration of P.

wet acidic ion exchange resin beads (approx. 1 mm OD) and free water in the void space of the bed imposes some more undesirable effects on fluid dynamics. The free water which completely fills the void space between the catalyst beads acts as an adhesive agent on the catalyst forming a kind of pasty lump. Figure 4.5 illustrates the strong adhesive forces between water and the acidic ion exchange resin.

Figure 4.5: Illustration of strongly sticking wet ion exchange resin beads.

Thus, there is no space for the alkene to pass the catalyst bed, and as a consequence, the alkene accumulates in front of the catalyst bed leading to a rising pressure drop. As the pressure drop reaches a sufficiently high level only a few channels are formed in the bed and the accumulated alkene slug then rapidly flows off through these few channels. The channels in the bed will relock when the high pressure drop is released and the described cycle restarts. Figure 4.6 illustrates this behavior for the flooded bed reactor (co-currently upstream) which was found in a video analysis by Horstmann et al. [19]. The actual behavior in the trickle bed reactor is assumed to be similar to that of the flooded bed reactor, at least with respect to the accumulation of the alkene in front of the catalytic bed.

Adjacent to the high pressure drop maldistribution of alkene in the bed and a small interfacial area degrade the mass transfer performance of the trickle bed reactor. The only advantage of the trickle bed reactor for the case considered here seems to be the high catalyst loading capacity. Nevertheless, for the given application the trickle bed reactor is probably the worst choice of currently

available multiphase reactor types.

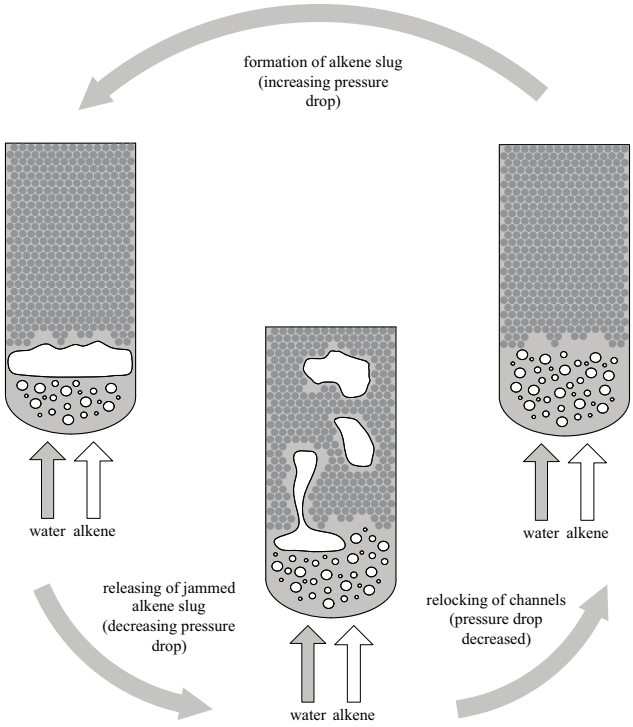

Figure 4.6: Cycle of alkene accumulation and release in randomly packed fixed bed reactors.

The flooded bed reactor which is used for the hydration of *n*-butenes has an improved wetting performance for which a molar feed ratio of water to *n*-butenes of about 1 : 2 is feasible without any loss in selectivity (fig. 4.7). However, the flooded bed reactor still shows some unfavorable behavior in a similar manner as the trickle bed reactor, e. g. high pressure drop and formation of large alkene slugs in the catalyst bed which causes maldistribution of alkenes in the reactor, rather small interfacial areas, and, hence, a relatively low reactor performance. For the ion exchange resin catalyzed hydration of linear alkenes this reactor type is an improvement, of course, but still seems to be an improper reactor concept for a reliable and efficient manufacture process.

The mentioned issues of fixed bed reactors are probably the reasons why the

ion exchange catalyzed liquid phase hydration is not as common as the sulfuric acid catalyzed indirect hydration process.

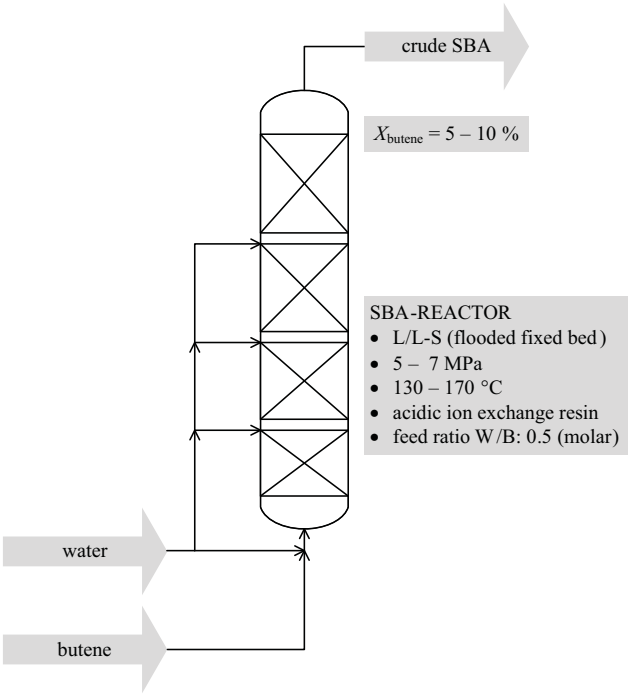

Figure 4.7: Flooded bed reactor for direct hydration of B.

4.4 Heterogeneous Reactive Extraction

Heterogeneous reactive extraction can be considered as an integrated reaction and separation process wherein the product is extracted by a second liquid phase which is immiscible with the other (reactive) liquid phase. Here, heterogeneous means that a solid catalyst phase is involved. In the case of the alkene hydration no additional co-solvent is needed for extraction because both reactants (alkenes and water) are only partially miscible forming two immiscible liquid phases. Due to the polarity of the employed acidic ion exchange resin catalyst it is selectively wetted by the aqueous phase. Hence, the alkenes need to be transferred through the aqueous phase thereby attaining to the catalyst surface and consecutively

through the pore system of the catalyst to the active sites. To sum all diffusive mass transfer steps the alkenes pass:

i) the organic film layer at the liquid-liquid interface,

ii) the aqueous film layer at the liquid-liquid interface,

iii) the aqueous film (NERNST) layer surrounding the catalyst beads, and, finally,

iv) through the pores of the catalyst.

It is worth to note that the other reactant water takes a similar way to the active sites, but, without passing the liquid-liquid interface. During extraction, both, the main product alcohol and the by-product ether take the reverse way of mass transfer of the alkenes. Each diffusive mass transfer step and the chemical reaction can be potentially rate determining. As all mass transfer steps are taking place in a liquid environment the govern mass transfer parameters, e. g. diffusivities and mass transfer coefficients, are in the same order of magnitude. The determining phenomenon in liquid phase mass transfer is, therefore, thermodynamic non-ideality. The largest deviation from ideal phase behavior in this system is found for alkenes dissolved in the aqueous phase which is indicated once more in the very low solubility of alkenes in water (cf. section 2.1.2). As a result, if the chemical reaction is not the rate determining step in the hydration process it is the diffusive mass transfer of the alkenes. This is particularly the case in the C_4-hydration system at high temperatures and high catalyst activities as is demonstrated in section 5.2.2. For the C_3-hydration system the chemical reaction is the rate determining step for practically all situations. Figure 4.8 illustrates the mass transfer steps that are involved in the heterogeneous reactive extraction process for the manufacture of *sec*-alcohols.

In view of the mentioned deficiencies of trickle bed and flooded bed reactors for this application a new multiphase reactor concept like heterogeneous reactive extraction is desirable. The main problem arising in randomly packed fixed bed multiphase reactor types is the lumping of the acidic ion exchange resin beads by water imposing high pressure drop, maldistribution of alkenes and incomplete catalyst wetting. Within this new reactor concept the main objective must be the generation of void space for the alkenes and large interfacial surface areas providing good mass transfer performance.

In a series of papers, Samant and Ng [20–23], Samant et al. [24] developed design concepts for the case of homogeneous reactive extraction. Such strategies do not exist for heterogeneous reactive extraction whereas the works on the conceptual design of heterogeneous reactive (catalytic) distillation processes can be taken as a basis (cf. Sundmacher and Kienle [9], Doherty and Malone [25], Subawalla and Fair [26]). This will be a task for future research work in the field of heterogeneous reactive extraction.

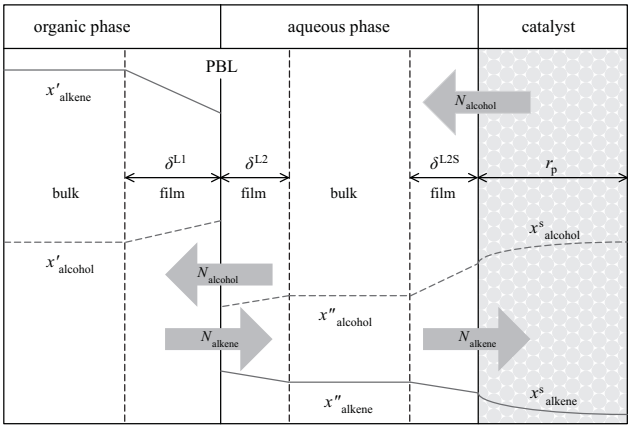

Figure 4.8: Mass transfer steps for alkene and alcohol in the heterogeneous reactive extraction process.

4.4.1 Structured Catalytic Packing

A possible solution can be the use of so-called open cross-flow structured catalytic packing (OCFS) which are commercially available and are widely used in heterogeneously catalyzed reactive distillation processes (Pangarkar et al. [18]). Structured catalytic packings, e. g. KATAPAK™ developed and manufactured by SULZER CHEMTECH (Götze et al. [27]), provide void space for the alkenes between catalyst filled wire gauze baskets and corrugated sheets significantly reducing pressure drop (fig. 4.9).

Furthermore, large specific packing areas, good radial mixing and flexibility regarding catalyst load are typical properties of these types of packing. Data of the open cross flow structured packing KATAPAK™-SP are compiled in table 4.1. Moreover, structured packings extend the applicability to mechanically less resistant ion exchange resin compounds.

The OCFS separates alkene and water streams whereas it provides sufficiently large packing surface areas. As the packing surface area acts as support for a film layer of one of the liquids the packing surface area corresponds to the effective liquid-liquid interface area if the packing is completely wetted. Which liquid the packing surface particularly wets depends strongly on the used packing material. Here, a hydrophilic construction material, e. g. stainless steel wire mesh, is beneficial because the aqueous phase must wet the packing surface.

As the two immiscible liquid phases flow through allocated parts of the cross

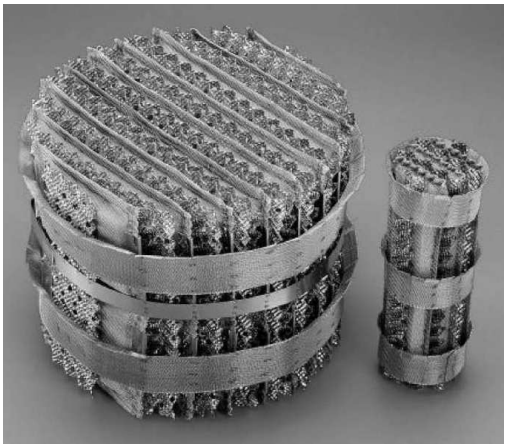

Figure 4.9: Open cross-flow structured packing KATAPAK™-SP, [27].

Table 4.1: Geometrical properties of OCFS KATAPAK™-SP [28].

Parameter	Unit	KATAPAK™-SP 11	KATAPAK™-SP 12
Column diameter, d_C	mm	100	100
Specific surface area, a_{SP}	m^2/m^3	210	282
Catalyst volume fraction, ψ	–	0.2	0.242
Void fraction, ε_{OC}	–	0.74	0.82
Inclination angle, θ	°	45	45
Corrugation side, S	mm	7.5	7.5

section of the packing some special aspects must be considered for the design of reactor injection equipment. Although between the hold-up pattern dispersive and continuous phase can not be distinguished in a way as within the flow pattern bubble and spray flow in an OCFS the aqueous phase can, however, be considered as dispersive phase while the organic phase is the continuous phase. This is justified by the fact that the wetting phase must be injected directly into the distributed catalyst baskets of the packing by, e. g. a distributor equipped with nozzles while the organic phase can simply be fed through an orifice. Figure 4.10 illustrates this principle schematically.

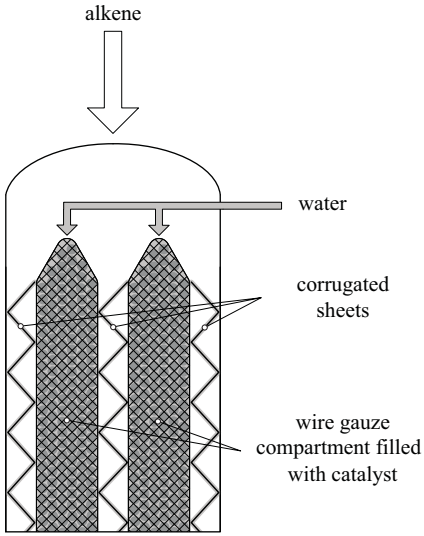

Figure 4.10: Longitudinal section through an open cross-flow structured catalytic packing (OCFS) depicting the flow paths for alkenes and water.

Furthermore, the load of the catalyst and of the packing wetting liquid determines the fraction of the effectively used catalyst amount, i. e. the fraction of the catalyst in the packing that contributes to the conversion at all. The flow of the liquid within the catalyst basket is driven by gravity. Depending on properties of liquid and catalyst there is a resistant force acting on the liquid and a certain flow rate results (cf. Moritz and Hasse [29]). If the actual load leads to a lower calculative flow rate as the theoretically possible flow rate stagnant zones are formed in the catalyst bed baskets. Catalyst which is located within such stagnant zones practically does not contribute to conversion

as reactants and products have to diffuse rather long distances to reach the active sites of the catalyst which lie within these stagnant zones. On the other hand, a part of the wetting liquid experiences a reduced catalyst contact time if the actual liquid load related flow rate exceeds the limiting flow rate of the packing. This is due to the effect that the excessive part of the wetting liquid escapes from the inner core of the catalyst basket and flows along the outer surface of the packing where it has no contact to the catalyst (fig. 4.11).

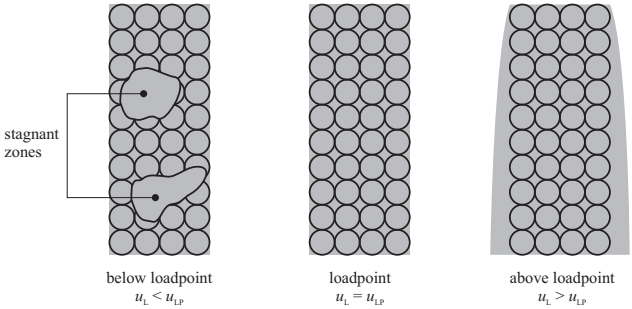

Figure 4.11: Flow regimes within a catalyst basket of an OCFS, inspired by [29, 30].

From earlier works on polymer/ceramic ion exchange resin composite packings being shaped as, e. g. RASCHIG-rings (cf. Kunz and Hoffmann [31]), it is also imaginable to use such random composite packings. Their practical advantage is obvious: the exchange of deactivated catalytic random packings can be conducted more easily than of structured packings. However, these packings are not yet commercially available and are, therefore, not considered in this work.

4.5 Proposal for an Intensified Alcohol Production Process

By changing the catalyst arrangement from a randomly packed fixed bed into a structured packing it is now possible to properly account for the extraction of the desired product alcohol by the organic phase. More precisely, while the catalyst is most effectively operated at a certain superficial mass flow velocity ($SMFV$) of the catalyst wetting aqueous phase the organic phase load is arbitrary. The organic phase load can be optimized with respect to mass transfer efficiency and residence time of the organic extract phase (cf. section 5.2.2). The simultaneous extraction of the formed alcohol is advantageous with respect to space time yield and selectivity. This is due to strong sorption of alcohol which takes place

in the catalyst phase leading to the formation of the undesired by-product ether and to the reverse reaction (Petrus et al. [32, 33]). Besides this, the organic extract phase dissolves approximately 15 times more moles alcohol than the coexisting aqueous phase. The alcohol might now be recovered from the organic extract phase. Figure 4.12 compares the trickle bed process with the proposed reactive extraction process.

First, a reboiled stripper recovers unconverted alkenes and produces a bottom product mainly containing alcohol and water in a molar ratio of at least 1 : 1. A heteroazeotropic distillation unit is then used for purification of the alcohol whereas an aqueous solution containing approximately 5 mol % to 7 mol % alcohol (as it is withdrawn from the trickle bed reactor) would have to be enriched before being passed to a heteroazeotropic distillation unit. Hence, the commonly used distillation column for enrichment of dilute aqueous alcohol solutions is substituted by a stripper with a significantly lowered energy demand.

4.6 Prearrangement and Recommendations for Future Research

4.6.1 Preliminary Reaction Experiments

In preliminary experiments two similar ion exchange resin catalysts have been compared in a randomly packed trickle bed and in a structured packed bed reactor for the hydration of propene at the production site of Sasol Solvents Germany in Moers (Urban et al. [34]). The setups for both reactors comprising the main physical and geometrical properties are shown in fig. 4.13. The results presented here were obtained for the C_3-hydration system. While operating the randomly packed bed in co-current down flow the structured packing was operating counter-currently with a continuous organic phase and a disperse aqueous phase trickling along the catalyst baskets and packing surfaces.

In all experiments the pressure was set to 9 MPa. Higher space time yield (STY) were observed for the structured catalytic packing for both catalysts and superficial mass flow velocity ($SMFV$) as given in table 4.2.

The slopes of space time yield (STY) with respect to temperature of both reactor configurations are almost the same indicating that the rate determining macro scale phenomena in both configurations are probably identical and that the improved STY of the structured packing are probably caused by an enlarged interfacial area. However, these presumptions need to be confirmed by further experiments. More experiments were carried out for a structured packing filled with Amberlyst 70™. Again, propene was used as the olefin for the comparison of different flow and hold-up situations. In fig. 4.14 the reactor 7 is fed by the olefin inlet stream1 and the water inlet stream 2. Stream 3 is the organic phase outlet and stream 4 is the aqueous phase outlet. The minor part

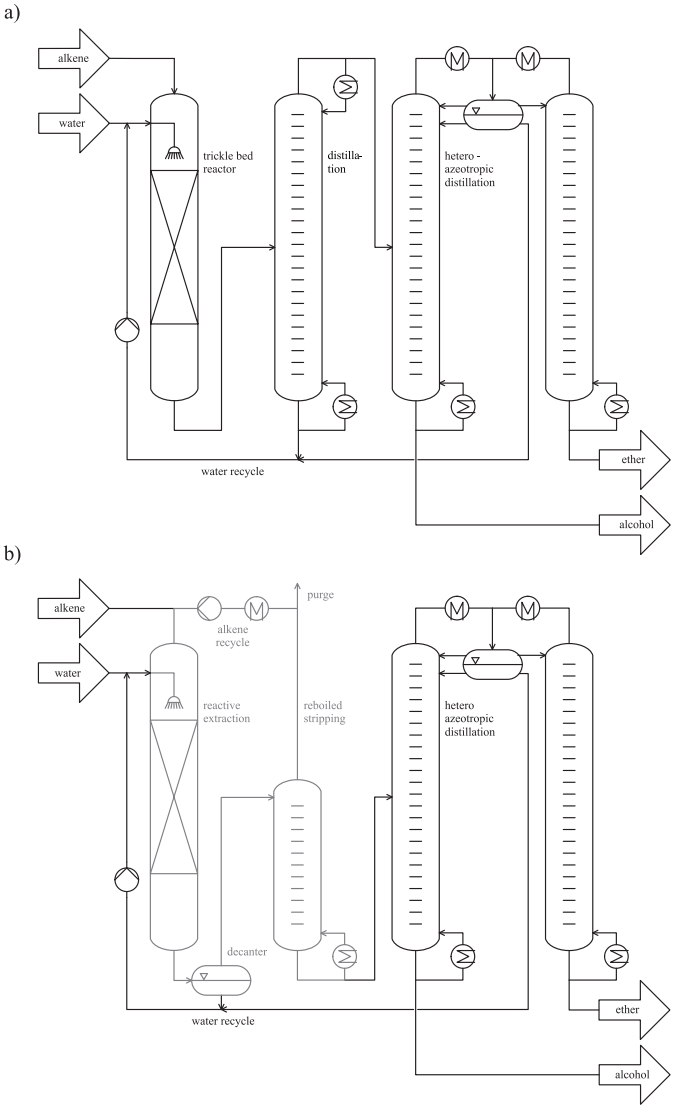

Figure 4.12: Flowcharts of trickle-bed (a) and reactive extraction (b) process.

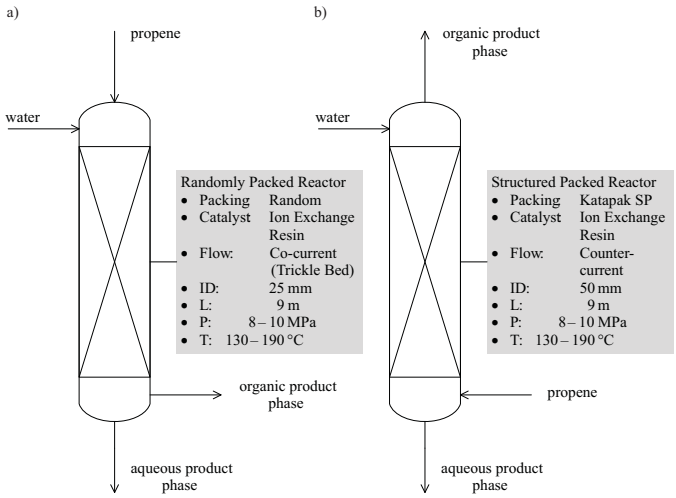

Figure 4.13: Properties of experimental high pressure reactors: (a) randomly packed reactor; (b) structured packed reactor.

Table 4.2: Comparison of random and structured packing for IPA production. Data from [34].

	Amberlyst DT™ (operated at 160 °C)		Amberlyst 70™ (operated at 170 °C)	
	random packing	structured packing	random packing	structured packing
STY $\mathrm{mol_{IPA}/(dm^3\,h)}$	3.34	5.37	4.79	7.96
$SMFV_{\mathrm{water}}$ $\mathrm{kg/(m^2\,s)}$	1.95	0.3	1.95	0.3
$SMFV_{\mathrm{propene}}$ $\mathrm{kg/(m^2\,s)}$	0.78	0.28	0.78	0.28

of stream 3 served as purge stream. The recycle stream 5 is driven by pump 8 and is combined with a feed stream to the reactor inlet stream 6. Number 9 marks the position of the phase boundary layer between the organic and aqueous phase. Four different operation modes were investigated: (a) Propene was the stationary phase and water was the mobile phase. The phase boundary layer 9 was below the catalytic packing. Recovery of isopropyl alcohol was done from the aqueous phase, stream 4. There was no recycle, stream 5 was zero. (b) Same conditions as described in (a), but recovery of isopropyl alcohol was done from the organic phase, stream 3. The major part of the aqueous phase outlet stream 4 was recycled by stream 5. (c) Water was the stationary phase and propene was the mobile phase. The phase boundary layer 9 was above the catalytic packing. Recovery of isopropyl alcohol was done from the aqueous phase, stream 4. The major part of the organic phase outlet stream 3 was recycled by stream 5. (d) Same conditions as described in (c), but recovery of isopropyl alcohol was done from the organic phase, stream 3. There was no recycle, stream 5 was zero.

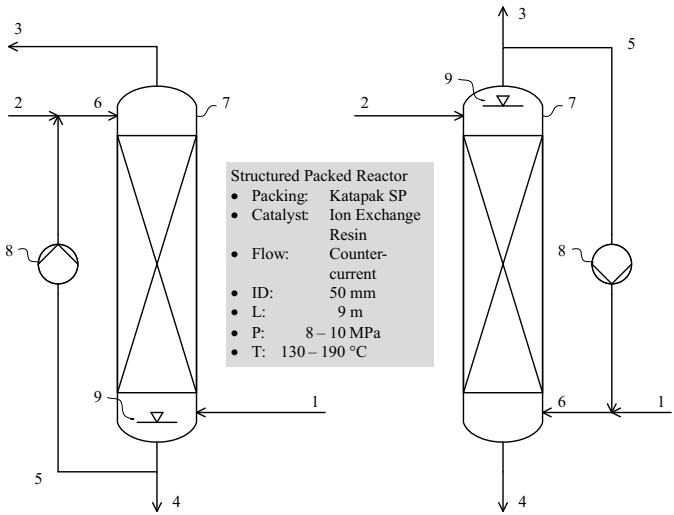

Figure 4.14: Experimental high pressure reactor equipped with a catalytic structured packing (7), olefin feed (1), water feed (2), organic phase exit (3), aqueous phase exit (4), recycle (5), recycle + feed (6), recycle pump (8), and phase boundary layer (9). (a) Recycling of aqueous phase (modes a & b, cf. table 4.3). (b) Recycling of organic phase (modes c & d, cf. table 4.3).

The results corresponding to these operation modes are summarized in table 4.3. When propene is used as the continuous phase and water is trickling along the structured catalytic packing (modes a & b) the highest STY are achieved. An increase in STY of up to 65 % was obtained by changing the reactor setup from a randomly packed trickle bed into a structured packing. The lower volume-related catalyst load of the structured packed reactor may partially be compensated by an improved STY. Furthermore, by application of a structured catalytic packing which provides space for the olefin flow the problem of transient high-level pressure drop is eliminated.

Table 4.3: Comparison of operation modes of the structured packing for IPA production catalyzed by AMBERLYST 70™. Data from [34].

		Mode a	Mode b	Mode c	Mode d
Flow		counter-current	counter-current	counter-current	counter-current
Disperse phase		aqueous	aqueous	organic	organic
Catalyst load	dm^3	0.6	0.6	0.54	0.54
Pressure, P	MPa	9.0	9.0	9.0	9.0
Temperature, T	°C	170	170	170	170
STY	$\frac{mol_{IPA}}{dm^3\,h}$	5.48	7.96	1.62	2.89
Stream #1	g/h	129[a]	2010	38[a]	980
Stream #2	g/h	1981	110[b]	978	42[b]
Stream #3	g/h	0	2120	0	1022
Stream #4	g/h	2110	0	1016	0
Stream #5	g/h	0	2000	2000	2000

[a] Approx. value, fed via pressure control system.
[b] Approx. value, fed via level control system for phase boundary layer.

However, detailed information on the actual disperse phase loading in the catalyst pockets of the structured packing is still missing for the application of a reactive extraction process. Hence, experiments providing data of real fluid dynamic characteristics are necessary in order to obtain fundamental data for the design of appropriate heterogeneous reactive extraction processes. Such investigations under relevant process conditions and detailed experiments on chemical reaction and mass transfer under broader variation of process variables are planned to be carried out for future research work.

4.6.2 Preliminary Experiments on Fluid Dynamics

Some fluid dynamic characteristics of the OCFS KATAPAK™-SP have been investigated preliminary for two co-currently flowing immiscible liquids (Cengiz Celik [35]). As model system for the fluid dynamic experiments water which had been colored with methyl orange as aqueous phase and cyclohexane as organic phase were used. This model system allowed for experiments at ambient pressure and temperature.

With these experiments basic information on the range of fluid dynamic operation variables should be resolved for the design of a laboratory plant for heterogeneous reactive extraction with structured catalytic packings. For this purpose, the experimental investigation focused on the following fluid dynamic parameters:

i) loading point of the catalytic packing (cf. fig. 4.11),

ii) hold-up by outflow experiments, and

iii) pressure drop.

For these experiments a 1 m long glass column with an inner diameter of 50 mm was used (fig. 4.15). The column was equipped with 10 10 cm long KATAPAK™-SP laboratory packing modules. The catalyst baskets of the packing were filled with a size fraction of 0.8 mm to 1.0 mm large beads of the acidic ion exchange resin AMBERLYST DT™.

The aqueous phase was fed to the structured packing by direct injection through a particularly designed distributor into the catalyst baskets of the first packing module on top (fig. 4.16). Both phases were separated in a decanter and recycled to the glass column.

The distributor is designed such that the liquid is equally distributed throughout all jets. The smooth distribution of liquid streams is maintained by the small inner diameter (0.1 mm) of the injection jets.

The loading point of the packing was found by increasing the aqueous phase load at a constant organic phase load. The result for 3 organic phase loads is shown in fig. 4.17. It can be seen that the pressure drop – which is very small for all selected experimental conditions – is constant up to a maximum aqueous phase load of approximately $5\,m^3/(m^2\,h)$. Beyond this point the pressure drop increases with an increasing aqueous phase load. This point marks, consequently, the loading point of the structured packing. Furthermore, from fig. 4.17 it can be concluded that the loading point is independent of the organic phase load.

The aqueous phase hold-up was investigated by outflow experiments. The experiments were undertaken as follows: After a stable steady state – indicated through the pressure drop gauge and through visual inspection of the flow

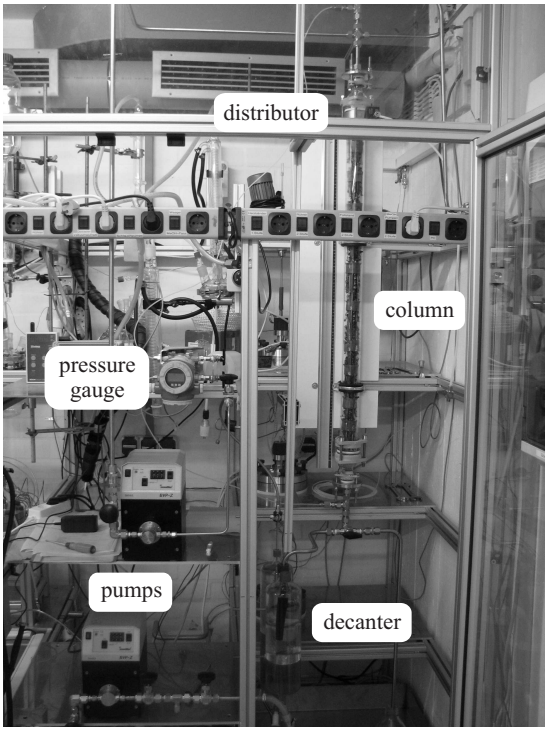

Figure 4.15: Photograph of the experimental setup for preliminary fluid dynamic experiments.

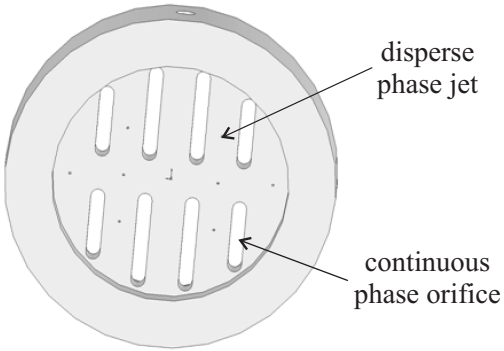

Figure 4.16: CAD-drawing of the disperse phase distributor.

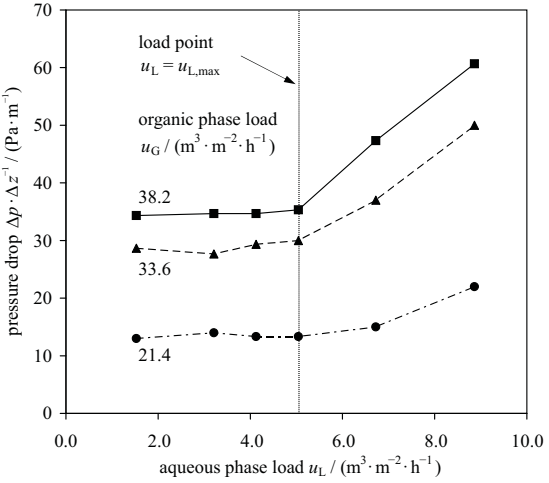

Figure 4.17: Pressure drop in structured packing as function of aqueous and organic phase load.

pattern inside the glass column – was reached, in the first instance, both recycle pumps were stopped and the column outlet valve at the bottom was simultaneously switched from the decanter to a sufficiently large sample container. Secondly, the column was aerated to allow for effluence of both phases. Finally the sampled liquids were separated by decantation and quantified volumetrically.

Figure 4.18 illustrates the results for the aqueous phase hold-up as function of aqueous phase and organic phase load. It was found that the aqueous phase hold-up is – with respect to measurement accuracy – independent of the organic phase load at least for aqueous phase loads below the loading point of the packing.

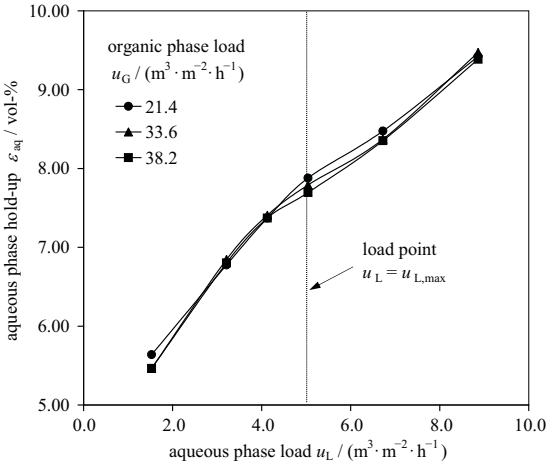

Figure 4.18: Aqueous phase hold-up in structured packing as function of aqueous and organic phase load.

However, it can be expected that an influence of the organic phase load increasingly establishes with increasing loads. Furthermore, from fig. 4.18 it can be seen that the slope of the hold-up curves is lower above the loading point. This phenomenon can be explained through a higher flow velocity of such fraction of the aqueous phase which flows outside the catalyst baskets as e. g. by-pass or film flow on packing element surfaces when the aqueous phase load exceeds the loading point.

The experimental results have been compared with a fluid dynamic model which is derived from the models proposed by Moritz and Hasse [29], Hoffmann et al. [36], Ratheesh and Kannan [37], Ellenberger and Krishna [38]. Details of the model are given in appendix D. A comparison of experimental and

simulation results provide table 4.4 and figs. 4.19 and 4.20.

Table 4.4: Comparison of experimentally obtained and calculated fluid dynamic data for KATAPAK^{TM}-SP.

Parameter	Unit	Experiment	Calculation
Specific surface area, a_{SP}	m^2/m^3	200[a]	–[b]
Volume fraction catalyst basket, ψ	vol%	23.1	–[b]
Void fraction catalyst bed, ε_{CB}	vol%	34.0[c]	–[b]
Void fraction *open channels*, ε_{OC}	vol%	74.5	–[b]
Flow velocity at load point, $u_{L,max}$	mm/s	4.04	4.09
Aqueous phase hold-up at load point, h_{LP}	vol%	7.9	8.0

[a] Estimated for laboratory KATAPAK^{TM}-SP (ID 50 mm).
[b] Value is unknown for laboratory KATAPAK^{TM}-SP (ID 50 mm), experimental value used.
[c] Typical value for relatively narrow size distributions ($\pm 10\,\%$ d_P) of spherically shaped particles.

From both parity plots figs. 4.19 and 4.20 it can be seen that experimental (observed) and simulated data for pressure drop and hold-up below and above the load point correlate fairly well. The model is a suitable tool for the important description of fluid dynamics in OCFS. The fitted model parameters are provided in appendix D.

It should be noted here that the obtained results – in view of the model character of employed liquids and conditions – can only serve for the design of a laboratory heterogeneous reactive extraction column. For scale-up purposes the data have to be revised for relevant process conditions and for actually, during the course of the alkene hydration reaction, present species.

4.6.3 Experimental Concept for Reactive Extraction

A laboratory plant for detailed experimental investigation of heterogeneous reactive extraction for the hydration of linear alkenes has been designed. The design is based on a structured packed extraction column equipped with a decanter which reflects the hold up in the bottom part of the column by two communicating pipelines or high pressure hoses, respectively (fig. 4.21).

Both the organic and the aqueous phase are recycled such that the reactor can be considered as a CSTR, i. e. the reactants are fed continuously to the

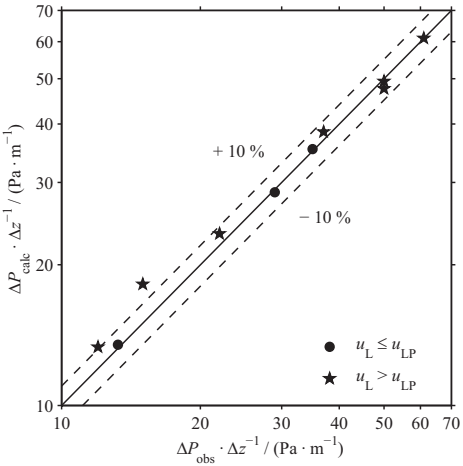

Figure 4.19: Parity plot of measured and calculated pressure drop data for KATAPAK™-SP.

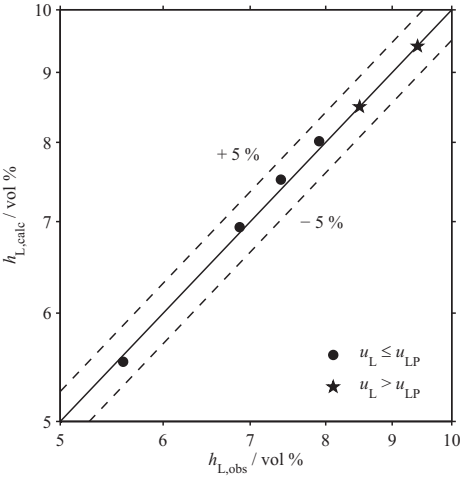

Figure 4.20: Parity plot of measured and calculated hold-up data for KATAPAK™-SP.

column at a much lower mass flow rate than the recycle streams. The hold-up in the decanter is kept constant by controlled outflow of organic and aqueous phase through a back pressure regulator.

The decanter is located parallel to the bottom of the column in order to display a stable hold-up reflecting the hold-up in the bottom of the column whereby the expectable formation of foam in the bottom of the column does not disturb the level measurement. The hold-up in the decanter is measured by means of image acquisition and processing.

While the aqueous phase always passes the column in downflow operation the organic phase can be directed in both directions, downflow and upflow, using the 4/2-way valve. As a result, the apparatus allows for the investigation of co-current and counter-current operation.

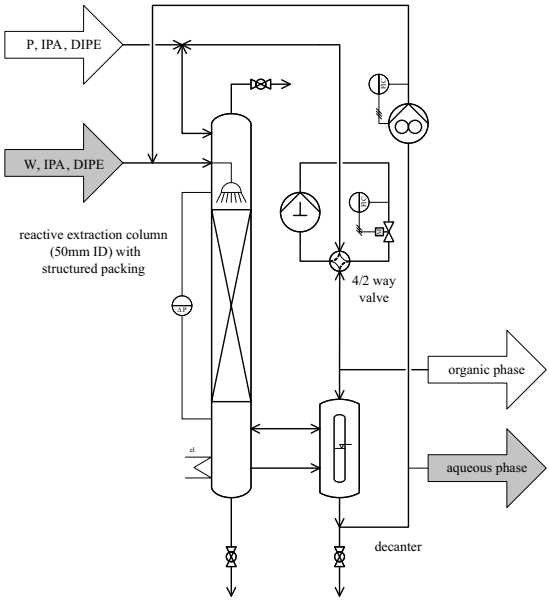

Figure 4.21: Flow chart of the laboratory reactive extraction plant for direct hydration (here: P).

The column is equipped with a liquid distributor which is particularly designed for the employed structured packing. Two oppositely in the reactor wall located windows allow for a visual investigation of the flow pattern in the reactor under operation (fig. 4.22). The developed reactive extraction setup is made of stainless steel and can be operated at temperatures and pressures up to 200 °C

and 150 MPa with respect to the column.

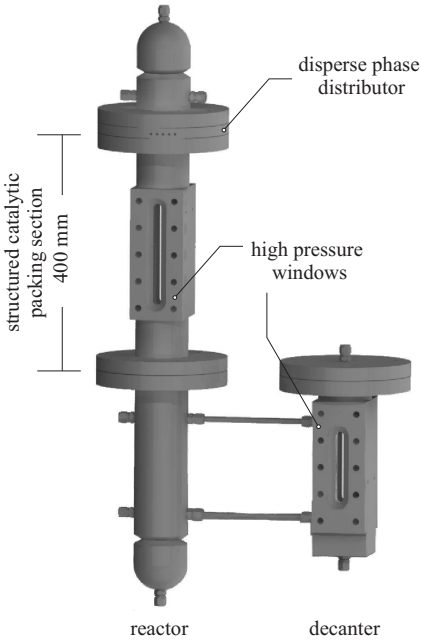

Figure 4.22: 3D-Model of the proposed reactive extraction column with decanter [39].

The following phenomena and properties of the heterogeneous reactive extraction for the hydration of linear C_3- and C_4-alkenes are to be investigated with the described apparatus:

i) loading point, pressure drop, and hold-up of the structured packing at relevant process conditions,

ii) liquid–liquid and liquid–solid mass transfer, and

iii) the effect of co-current and counter-current operation of the structured packing on fluid dynamics and mass transfer.

It should be noted that the small column diameter of only 50 mm imposes significantly different parameters to industrial scale structured catalytic packings due to the tight bending of this small diameter and consequential strong fringe effects. Hoffmann et al. [36] give a nice overview on the parameter shifts of a

structured catalytic packing during scale-up. They show that specific surface area a_P and void fraction ε_{OC} of the packing increase with increasing overall diameter of the packing. Hence, it can safely be assumed that the performance of the structured catalytic packing is improved along the scale-up. As a result this laboratory concept allows for a comprehensive and reasonable study of the with a meaningful experimental effort.

References

[1] Conti, J. J. and L. E. Doman. *International Energy Outlook 2010*, http://www.eia.gov/oiaf/ieo/index.html.

[2] Schaub, G. and T. Turek. *Energy Flows, Material Cycles and Global Development*. Springer, Berlin, 2011.

[3] Ehrfeld, W., V. Hessel, and H. Löwe. *Microreactors*, 1st. Wiley-VCH, Weinheim, 2000.

[4] Cybulski, A. and J. A. Moulijn. *Structured Catalysts and Reactors*. CRC Press, Boca Raton, 2006.

[5] Schmidt-Traub, H. and A. Górak. *Integrated Reaction and Separation Operations*. Springer, Berlin, 2006.

[6] Sundmacher, K., A. Kienle, and A. Seidel-Morgenstern. *Integrated Chemical Processes*. Wiley-VCH, Weinheim, 2005.

[7] Agar, D. W. Multifunctional reactors: Old preconceptions and new dimensions. *Chem. Eng. Sci.* **54**, (1999), 1299–1305. DOI: 10.1016/S0009-2509(99)00040-8.

[8] Kenig, E. Y., A. Górak, and H.-J. Bart. *Reactive Separations in Fluid Systems*, in: A. Stankiewicz and J. A. Moulijn (Eds.). *Re-engineering the Chemical Processing Plant*. Marcel Dekker, New York, 2004.

[9] Sundmacher, K. and A. Kienle. *Reactive Distillation*. Wiley-VCH, Weinheim, 2003.

[10] Xu, Y. Production of isopropyl alcohol by hydration of propylene in a catalytic distillation column. Ph.D. Thesis, University of Alberta, 2001.

[11] Wang, S. J. and D. S. H. Wong. Control of reactive distillation production of high-purity isopropanol. *J. Process Control* **16**, (2006), 385–394. DOI: 10.1016/j.jprocont.2005.06.015.

[12] Brandes, G., W. Neier, J. Wöllner, and W. Webers. Verfahren zur kontinuierlichen Herstellung von niederen Alkoholen, insbesondere Isopropanol. Ger. Pat. 2,147,740. 1973.

[13] Brandes, G., J. Wöllner, W. Neier, and W. Webers. Method of conducting reactions in a trickle-type reactor. U.S. Pat. 4,281,206. 1981.

[14] Carls, R. R., G. Osterburg, M. Prezelj, and W. Webers. Process for the production of isopropyl alcohol. U.S. Pat. 4,760,203. 1988.

[15] Carls, R. R., M. Dettmer, G. Osterburg, M. Prezelj, and W. Webers. Verfahren zur Herstellung von Isopropylalkohol und tertiären C4- bis C5-Alkoholen. E.U. Pat. 0,257,511. 1990.

[16] Henn, F., W. Neier, G. Strehlke, and W. Webers. Process for the continuous production of lower aliphatic alcohols. U.S. Pat. 4,831,197. 1989.

[17] Neier, W., W. Webers, M. Dettmer, and G. Osterburg. Process for the production of alcohols. U.S. Pat. 4,579,984. 1986.

[18] Pangarkar, K., T. J. Schildhauer, J. R. van Ommen, J. Nijenhuis, F. Kapteijn, and J. A. Moulijn. Structured Packings for Multiphase Catalytic Reactors. *Ind. Eng. Chem. Res.* **47**, (2008), 3720–3751. DOI: 10.1021/ie800067r.

[19] Horstmann, S., R. Wollmann, and K. Fischer. *Untersuchung des Strömungsverhalten von Wasser bzw. Wasser mit Emulgator (20-40 ppm) + Buten - Mischungen durch einen Ionenaustauscher B-23*. By order of Sasol Solvents Germany, Laboratory for Thermophysical Properties, 2003.

[20] Samant, K. D. and K. M. Ng. Synthesis of extractive reaction processes. *AIChE J.* **44**, (1998), 1363–1381. DOI: 10.1002/aic.690440615.

[21] Samant, K. D. and K. M. Ng. Effect of kinetics and mass transfer on design of extractive reaction processes. *AIChE J.* **44**, (1998), 2212–2228. DOI: 10.1002/aic.690441010.

[22] Samant, K. D. and K. M. Ng. Design of multistage extractive reaction processes. *AIChE J.* **44**, (1998), 2689–2702. DOI: 10.1002/aic.690441210.

[23] Samant, K. D. and K. M. Ng. Systematic Development of Extractive Reaction Processes. *Chem. Eng. Technol.* **22**, (1999), 877–880. DOI: 10.1002/(SICI)1521-4125(199910)22:10<877::AID-CEAT877>3.0.CO;2-D.

[24] Samant, K. D., D. J. Singh, and K. M. Ng. Design of liquid-liquid phase transfer catalytic processes. *AIChE J.* **47**, (2001), 1832–1848. DOI: 10.1002/aic.690470814.

[25] Doherty, M. F. and M. F. Malone. *Conceptual design of distillation systems*. McGraw-Hill, Boston, Mass., 2001.

[26] Subawalla, H. and J. R. Fair. Design Guidelines for Solid-Catalyzed Reactive Distillation Systems. *Ind. Eng. Chem. Res.* **38**, (1999), 3696–3709. DOI: 10.1021/ie9900081.

[27] Götze, L., O. Bailer, P. Moritz, and C. von Scala. Reactive distillation with KATAPAK™. *Catal. Today* **69**, (2001), 201–208. DOI: 10.1016/S0920-5861(01)00370-4.

[28] Aferka, S., A. Aviva, E. Brunazzi, P. Marchot, M. Crine, and D. Toye. Liquid Load Point Determination in a Reactive Distillation Packing by X-ray Tomography. *Can. J. Chem. Eng.* **88**, (2010), 611–617. DOI: 10.1002/cjce.20320.

[29] Moritz, P. and H. Hasse. Fluid dynamics in reactive distillation packing Katapak-S™. *Chem. Eng. Sci.* **54**, (1999), 1367–1374. DOI: 10.1016/S0009-2509(99)00078-0.

[30] Schmitt, M. Heterogen katalysierte Reaktivdestillation: Stoffdaten, Experimente, Simulation und Scale-up am Beispiel der Synthese von Hexylacetat. Ph.D. Thesis, University of Stuttgart, 2006.

[31] Kunz, U. and U. Hoffmann. Preparation of catalytic polymer/ceramic ionexchange packings for reactive distillation columns. *Stud. Surf. Sci. Catal.* **91**, (1995), 299–308. DOI: 10.1016/S0167-2991(06)81766-0.

[32] Petrus, L., R. W. De Roo, E. J. Stamhuis, and G. E. H. Joosten. Kinetics and equilibria of the hydration of propene over a strong acid ion exchange resin as catalyst. *Chem. Eng. Sci.* **39**, (1984), 433–446. DOI: 10.1016/0009-2509(84)80041-X.

[33] Petrus, L., R. W. De Roo, E. J. Stamhuis, and G. E. H. Joosten. Kinetics and equilibria of the hydration of linear butenes over a strong acid ion-exchange resin as catalyst. *Chem. Eng. Sci.* **41**, (1986), 217–226. DOI: 10.1016/0009-2509(86)87002-6.

[34] Urban, T., D. Hoell, H. Kohnz, U. Hoffmann, U. Kunz, and B. Pfeuffer. Process for the Production of Lower Alcohols by Olefin Hydration. EP Pat. 2208719 A1. 2010.

[35] Cengiz Celik, Y. Fluiddynamische Untersuchungen zur reaktiven Extraktion an strukturierten Packungen. Diploma Thesis, Clausthal University of Technology, 2009.

[36] Hoffmann, A., C. Noeres, and A. Górak. Scale-up of reactive distillation columns with catalytic packings. *Chem. Eng. Process.* **43**, (2004), 383–395. DOI: 10.1016/s0255-2701(03)00121-1.

[37] Ratheesh, S. and A. Kannan. Holdup and pressure drop studies in structured packings with catalysts. *Chem. Eng. J.* **104**, (2004), 45–54. DOI: 10.1016/j.cej.2004.08.004.

[38] Ellenberger, J. and R. Krishna. Counter-current operation of structured catalytically packed distillation columns: pressure drop, holdup and mixing. *Chem. Eng. Sci.* **54**, (1999), 1339–1345. DOI: 10.1016/S0009-2509(99)00055-X.

[39] Nentwich, F. Konstruktion eines Reaktors zur Direkthydratisierung von Olefinen zu Alkoholen. Thesis, Clausthal University of Technology, 2010.

5 Simulation of Reactive Extraction for Synthesis of *sec*-Alcohols

The simulations of the proposed process for the hydration of linear C_3- and C_4-alkenes provides estimates on the performance of the heterogeneous reactive extraction reactor and allows for comparison between the separation units of the old and the newly proposed process. It should be noted that the denotation *estimates* was used intentionally because there are still some remarkable uncertainties in the properties which, until now, could not be resolved neither by this work nor by other studies.

More detailed, these arguable properties are:

i) mass transfer coefficients for the mixtures and conditions (temperature, pressure, sub- or supercritical state, etc.) under consideration,

ii) flow patterns in structured packings at real process conditions,

iii) dispersion coefficients in structured packings at real process conditions, and

iv) boundary conditions for the reactor model with respect to the consideration of nonideal flow behavior.

The investigation of these items is recommended for further research in the field of heterogeneous reactive extraction, particularly for the hydration of linear C_3- and C_4-alkenes (cf. section 4.6.3).

Nevertheless, the simulation results will emphasize the tremendous potential of the heterogeneous reactive extraction to process intensification in the field under consideration.

5.1 Structured Packed Reactive Extraction Column

The proposed reactive extraction process is based on the application of OCFS which allow for separated flows of the immiscible liquid phases in separated sections within the packing cross section and which provide sufficiently large interface areas for proper mass transfer performance between the immiscible liquids.

The immiscible phases are supported by the two reactants alkenes and water. Hence, due to the two-fold purpose of alkenes and water as reactants and

solvents the conversion of both reactants is limited and unconverted fractions have to be recycled to the reactor. However, if additional solvents are used the effort for recycling of the solvents will almost be the same and there will be additional effort for the recovery of these solvents.

Therefore, the reactants serve also as solvents in this study, not least due to the excellent extraction potential of the alkenes for their corresponding alcohols. Furthermore, the alcohol content of the aqueous phase of the reactor effluent is low to such an extent that a product recovery from that phase is meaningless and the better way to process the aqueous phase is the direct recycling to the reactor inlet.

The organic reactor effluent is processed by a reboiled stripper which separates the relatively low boiling alkene from the main product alcohol, the by-product ether and water which is increasingly extracted with the alcohol during the course of the reaction. The recovered alkene is then recycled to the reactor inlet whereas proper actions (e. g. purging) must be considered in order to prevent from accumulation of accompanying saturated hydrocarbons. Figure 5.1 shows the described setup which is subject to the simulations described in this section.

For all reactor simulations co-current operation is considered although counter-current operation of the structured packed reactor is well imaginable. However, this was not considered here as the simulation of counter-current operation shifts the computationally less costly initial value problem (IVP) of the co-current plug flow tubular reactor (PFTR) model into a boundary value problem (BVP).

The modeling of temperature profiles in the reactor is abandoned as the maximum reactor diameter, at which the heat generation due to the formation of isopropyl alcohol and diisopropyl ether at 423 K exceeds the heat remove across the reactor wall, amounts to approximately 2.5 m assuming a heat flux through the reactor wall of only $10\,\mathrm{kW/m^2}$. Since this diameter is sufficiently large for production rates of up to 200 t/d and since the actual reaction rate is limited by intra-particle mass transfer resistances, which is characterized by a catalyst effectiveness factor of approximately 65 %, the generation and removal of heat can safely be neglected.

The simulations with respect to post-reactive separations (e. g. reboiled stripping, heteroazeotropic purification of product) are discussed separately providing a comparison between old and new process. The used model is presented in the last part of this section.

5.1.1 PFTR Model

The used one-dimensional PFTR model considers nonideal mass transfer between the immiscible liquid phases, in the Nernst layer surrounding the catalyst particles and simultaneously with the intrinsic reaction kinetics in the catalyst

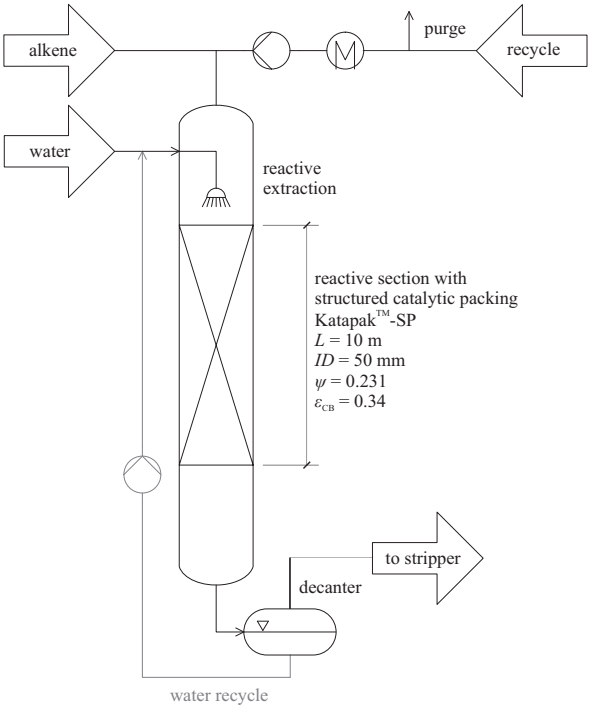

Figure 5.1: Schematic of a reactive extraction column as considered for simulations.

matrix. Hence, it is a full heterogeneous model which allows for analysis of the catalyst efficiency. This model can easily be adapted from common chemical engineering textbooks, e. g. Froment and Bischoff [1], pp. 467, 607-608.

Due to the reaction stoichiometric of the hydration reaction the number of moles changes with the extent of reaction. The utilization of molar flow rates in the component mass balances is, therefore, preferred. For each component two component mass balances are required – one for the organic fluid phase and one for the aqueous phase – which are written as

$$\frac{\mathrm{d}F_i'}{\mathrm{d}\xi} = V_\mathrm{R}\left(-a_\mathrm{SP}N_i^\mathrm{I}\right) \tag{5.1a}$$

for the organic phase and for the aqueous phase we have

$$\frac{\mathrm{d}F_i''}{\mathrm{d}\xi} = V_\mathrm{R}\left(a_\mathrm{SP}N_i^\mathrm{I} + \frac{\psi\,(1-\varepsilon_\mathrm{CB})}{V_\mathrm{CP}}\mathbb{N}_{i,\mathrm{CP}}\right) \tag{5.1b}$$

with

$$i = 1, 2, \ldots, n_\mathrm{c}\ . \tag{5.1c}$$

In eqs. (5.1a) and (5.1b), F_i', F_i'' denote the molar flow of component i in the organic and aqueous phase, respectively, and $\xi = \frac{z}{L_\mathrm{R}}$ is the dimensionless axial coordinate of the reactor. The first term on the right hand side of eqs. (5.1a) and (5.1b) accounts for nonequimolar mass transfer across the fluid interface, i. e. the component fluid interface fluxes N_i^I do not necessarily sum up to zero. A positive flux represents mass transfer from the organic to the aqueous phase and vice versa. It is further assumed that only the aqueous phase wets the catalyst whereby a mass transfer term with respect to the catalyst appears only in the aqueous mass balances (eq. (5.1b)). In contrast to the fluid interface fluxes, $\mathbb{N}_{i,\mathrm{CP}}$ is the mass transfer rate of component i with respect to a single catalyst particle.

Equations (5.1a) and (5.1b) form a $2n_\mathrm{c}$-dimensional set of ODE which are solved for the F_i. The fluid interface fluxes and catalyst mass transfer rates are obtained from the nonideal multicomponent mass transfer models as described in sections 2.3 and 3.4.3, respectively, and are updated at each integration step of the ODE-solver.

5.1.2 Nonequilibrium Separation Model

The so-called 2$^\mathrm{nd}$ generation nonequilibrium model (cf. Taylor et al. [2]) has been used in this work as basis for the simulations of separation columns.

Besides the interfacial transport of mass and heat the authors included the phenomena entrainment of liquid, occlusion of vapor and momentum transport into their model which has been neglected here. Furthermore, the authors equipped their model with a *design mode* which dynamically provides design calculations while solving the actual nonequilibrium model, e. g. calculation of the inner diameter of the column based on the minimum hydraulic diameter which is a requirement from feasibility criteria arising in the fluid dynamic model. However, in this work the design parameters were set manually rather than estimating these parameters dynamically.

The used nonequilibrium model is a steady state model based on algebraic balances which are repeatedly applied to the considered stages of the column. This treatment forms a sparse nonlinear algebraic equation system. Hence, the model equations represent a quasi-discretization of an according differential model whereas each finite volume element corresponds to a nonequilibrium stage (fig. 5.2).

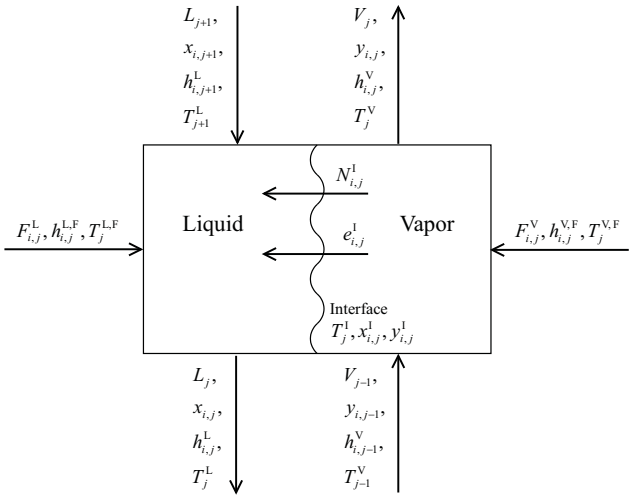

Figure 5.2: Schematic representation of a nonequilibrium separation stage as considered in this work.

As initially stated, neglecting entrainment of liquid, occlusion of vapor and side streams the component material balances for liquid and vapor phase at each stage j are written as

$$M^{\mathrm{L}}_{i,j} \equiv L_j x_{i,j} - L_{j+1} x_{i,j+1} - F^{\mathrm{L}}_{i,j} - \mathbb{N}^{\mathrm{L}}_{i,j} = 0 \tag{5.2a}$$

and

$$M_{i,j}^{\mathrm{V}} \equiv V_j y_{i,j} - V_{j-1} y_{i,j-1} - F_{i,j}^{\mathrm{V}} + \mathbb{N}_{i,j}^{\mathrm{V}} = 0 \tag{5.2b}$$

with

$$i = 1, 2, \ldots, n_{\mathrm{c}} \; , \tag{5.2c}$$

respectively. The total material balances for liquid and vapor phase are easily derived from eq. (5.2) by summing over the component index i

$$M_j^{\mathrm{L}} \equiv L_j - L_{j+1} - \sum_{i=1}^{n_{\mathrm{c}}} F_{i,j}^{\mathrm{L}} - \sum_{i=1}^{n_{\mathrm{c}}} \mathbb{N}_{i,j}^{\mathrm{L}} = 0 \tag{5.3a}$$

and

$$M_j^{\mathrm{V}} \equiv V_j - V_{j-1} - \sum_{i=1}^{n_{\mathrm{c}}} F_{i,j}^{\mathrm{V}} + \sum_{i=1}^{n_{\mathrm{c}}} \mathbb{N}_{i,j}^{\mathrm{V}} = 0 \; . \tag{5.3b}$$

In eqs. (5.2) and (5.3) $\mathbb{N}_{i,j}^{\mathrm{L}}$, $\mathbb{N}_{i,j}^{\mathrm{V}}$ are the mass transfer rates which are defined as

$$\mathbb{N}_{i,j}^{\mathrm{L}} \equiv \int N_{i,j}^{\mathrm{L}} \mathrm{d}a_j \tag{5.4a}$$

and

$$\mathbb{N}_{i,j}^{\mathrm{V}} \equiv \int N_{i,j}^{\mathrm{V}} \mathrm{d}a_j \tag{5.4b}$$

wherein $N_{i,j}^{\mathrm{L}}$, $N_{i,j}^{\mathrm{V}}$ are the molar component fluxes and a_j is the volume-specific interfacial area which is available for mass transfer between vapor and liquid. The energy balances for liquid and vapor phase are written as

$$E_j^{\mathrm{L}} \equiv \sum_{i=1}^{n_{\mathrm{c}}} h_{i,j}^{\mathrm{L}} L_j - \sum_{i=1}^{n_{\mathrm{c}}} h_{i,j+1}^{\mathrm{L}} L_{j+1} - \sum_{i=1}^{n_{\mathrm{c}}} h_{i,j}^{\mathrm{L,F}} F_{i,j}^{\mathrm{L}} - \mathbb{E}_j^{\mathrm{L}} = 0 \tag{5.5a}$$

and

$$E_j^{\mathrm{V}} \equiv \sum_{i=1}^{n_{\mathrm{c}}} h_{i,j}^{\mathrm{V}} V_j - \sum_{i=1}^{n_{\mathrm{c}}} h_{i,j-1}^{\mathrm{L}} V_{j-1} - \sum_{i=1}^{n_{\mathrm{c}}} h_{i,j}^{\mathrm{V,F}} F_{i,j}^{\mathrm{V}} + \mathbb{E}_j^{\mathrm{V}} = 0 \tag{5.5b}$$

where $\mathbb{E}_j^{\mathrm{L}}$, $\mathbb{E}_j^{\mathrm{V}}$ are the energy transfer rates defined by

$$\mathbb{E}_j^{\mathrm{L}} \equiv \int e_j^{\mathrm{L}} \mathrm{d}a_j \tag{5.6a}$$

and

$$\mathbb{E}_j^{\mathrm{V}} \equiv \int e_j^{\mathrm{V}} \mathrm{d}a_j \ . \tag{5.6b}$$

In eq. (5.6) e_j^{L} , e_j^{V} are the local energy fluxes for liquid and vapor phase. The mass transport relations are expressed as

$$R_{i,j}^{\mathrm{L}} \equiv \mathbb{N}_{i,j} - \mathbb{N}_{i,j}^{\mathrm{L}} = 0 \tag{5.7a}$$

and

$$R_{i,j}^{\mathrm{V}} \equiv \mathbb{N}_{i,j} - \mathbb{N}_{i,j}^{\mathrm{V}} = 0 \tag{5.7b}$$

with

$$i = 1, 2, \ldots, n_{\mathrm{c}} - 1 \tag{5.7c}$$

and the energy transport relation is written as

$$E_j^{\mathrm{I}} \equiv \mathbb{E}_j^{\mathrm{L}} - \mathbb{E}_j^{\mathrm{V}} = 0 \ . \tag{5.7d}$$

A detailed discussion on the computation of the nonideal multicomponent mass transfer rates $\mathbb{N}^{\mathrm{L}}$, $\mathbb{N}^{\mathrm{V}}$ is given by Krishnamurthy and Taylor [3]. A survey on the calculation of the energy transfer rates $\mathbb{E}^{\mathrm{L}}$, $\mathbb{E}^{\mathrm{V}}$ is given in Taylor and Krishna [4], p. 402. Thermodynamic equilibrium is only assumed to exist at the interface. The corresponding equilibrium relation is written as

$$Q_{i,j}^{\mathrm{I}} \equiv K_{i,j} x_{i,j}^{\mathrm{I}} - y_{i,j}^{\mathrm{I}} = 0 \tag{5.8}$$

wherein $K_{i,j}$ is the distribution coefficient calculated for pressure P_j, temperature T_j^{I} and liquid and vapor mole fractions $x_{i,j}^{\mathrm{I}}$, $y_{i,j}^{\mathrm{I}}$ which are locally present at the interface.

For evaporator, condenser and an optional decanter equilibrium balances are used which are described by Kovach and Seider [5]. As the heat duties of condenser and evaporator are usually not known in advance the energy balance is replaced by a sufficient specification equation. For the evaporator, the purity (mole fraction) or total molar effluent of the bottom product and for

the condenser, the reflux ratio is specified in the simulations conducted in this work. Beyond that, feed stage, feed quality, flow rate and composition, overall number of stages, inner column diameter, packing type, stage length, condenser pressure and pressure drop per stage need to be specified by the user.

The resulting nonlinear algebraic equation system, which is solved using a pre-conditioned conjugate gradient algorithm (belongs to the class of NEWTON-methods), requires an initial guess for all dependent variables. The initial guess is obtained from the solution of the much simpler corresponding equilibrium separation model of Naphtali and Sandholm [6] which was found to be a feasible estimation method in the work of Voelskow [7]. The equilibrium model is solved by differential arc-length homotopy continuation using the NEWTON-homotopy as described in Vickery and Taylor [8]. The homtopy is implemented as basic differential equations (BDE) (cf. Zangwill and Garcia [9], pp. 24-42) and solved by an ODE-solver, e. g. GEAR'S method. In turn, the initial guess for the equilibrium model is obtained by computing the stage flows of vapor and liquid assuming constant molal overflow (i. e. the stage flow shifting effect, which is caused by differences in the heat of vaporization of the components, is neglected). The feed composition is initially taken for the compositions of vapor and liquid on all stages.

The model is used to simulate on one hand P stripper and hetero-azeotropic IPA purification columns of the reactive extraction process and on the other IPA pre-concentration and hetero-azeotropic IPA purification columns of the trickle bed reactor process for comparison. The results are discussed in section 5.3.

5.2 PFTR Simulation Results

A general solution to the PFTR-model provides fig. 5.3 for a simulation of the reactive extraction column as defined in fig. 5.1. It incorporates the assumption that the reactor effluent is separated by a decanter and the aqueous fraction together with all other aqueous reverse flows is directly recycled to the reactor inlet. Water loss due to conversion is compensated by additionally feeding an accordant amount of water. The results are obtained for an isothermal and isobaric co-current operation of the reactive extraction column at 423 K and 9.5 MPa.

It can be seen that the purely fed propene extracts residual isopropyl alcohol from the aqueous recycle very rapidly until the concentration of isopropyl alcohol almost corresponds to its fluid phase equilibrium. Chemical reaction and mass transfer from the catalyst into the aqueous phase are obviously slower than mass transfer across the fluid interface. On the other hand, the concentration of propene in the aqueous phase correlates strongly with the aqueous concentration of isopropyl alcohol. A high aqueous propene concentration in combination with

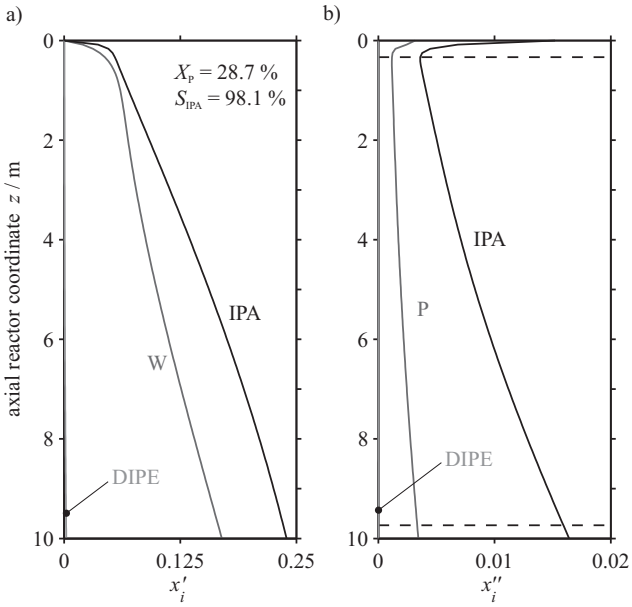

Figure 5.3: Axial mole fraction profiles in the reactive extraction column with recycling of water 423 K and 9.5 MPa, a) organic phase, b) aqueous phase. The dashed lines mark locations for mass transfer analysis (figs. 5.4 and 5.5).

a high aqueous isopropyl alcohol concentration has no accelerating effect on the formation of isopropyl alcohol, it rather decelerates the formation. This is due to the stronger influence of the IPA concentration on the dehydration (reverse reaction) rate than the influence of propene (P) on the hydration (forward reaction) rate.

The dashed horizontal lines in fig. 5.3 mark the axial positions at which mole fraction profiles in the diffusive mass transfer regions are gathered. The resulting profiles are given in figs. 5.4 and 5.5. For the sake of clarity, the mole fraction profiles of water are not included. It is noticeable that the mass transfer film (L1) between organic phase and fluid interface is much thicker than the other aqueous fluid films. This is due to the properties of a liquid-like supercritical phase and the low interstitial flow velocity of the organic phase which is approximately 6 mm/s.

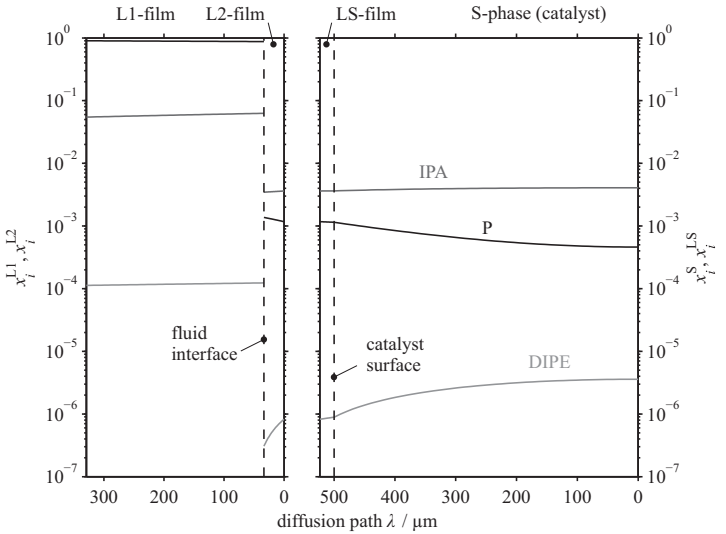

Figure 5.4: Mole fraction profiles along the diffusion paths: organic and aqueous films around the fluid interface (L1) and (L2), Nernst diffusion layer surrounding the catalyst particle (LS) and in the pore system of the catalyst (S). The location on the axial reactor coordinate is depicted by the upper dashed line in fig. 5.3.

The viscosity is rather gaseous while the density is rather in the range of organic liquids. Furthermore, the profiles in the organic film (L1) are relatively flat when compared to their aqueous counterparts (L2, LS) which can be explained by larger multicomponent diffusivities of the solutes propene,

isopropyl alcohol and diisopropyl ether in propene as solvent than in water. The mole fraction profiles at the end of the reactor fig. 5.5 are completely equalized in the organic film and that for isopropyl alcohol is equalized in the catalyst phase as well while the catalyst profiles for propene and diisopropyl ether are curvilinear.

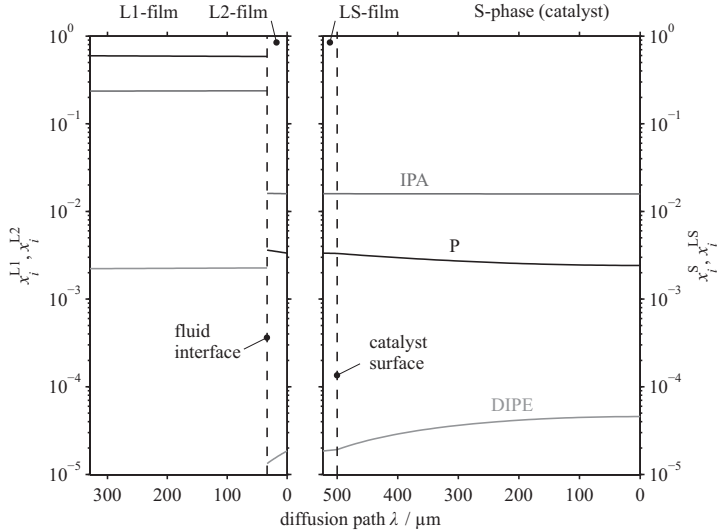

Figure 5.5: Mole fraction profiles along the diffusion paths: organic and aqueous films around the fluid interface (L1) and (L2), Nernst diffusion layer surrounding the catalyst particle (LS) and in the pore system of the catalyst (S). The location on the axial reactor coordinate is depicted by the lower dashed line in fig. 5.3.

5.2.1 Effect of Temperature and Pressure

Figures 5.6 and 5.7 illustrate the effect of temperature and pressure on conversion of propene and selectivity with respect to isopropyl alcohol, respectively. Conversion is increasing with temperature and pressure as is expected. This is due to the reaction rate which on one hand increases by the temperature-driven activation and on the other by the pressure-driven solubility of propene in water. But, it is also shown in fig. 5.6 that the pressure influence is limited. The increase in conversion of propene from 8 MPa to 9.5 MPa is much less than from 6.5 MPa to 8 MPa. Hence, using a pressure which is higher than

approximately 10 MPa is not beneficial. But, the pressure should not be set to a value below 8 MPa as the loss in conversion becomes more significant.

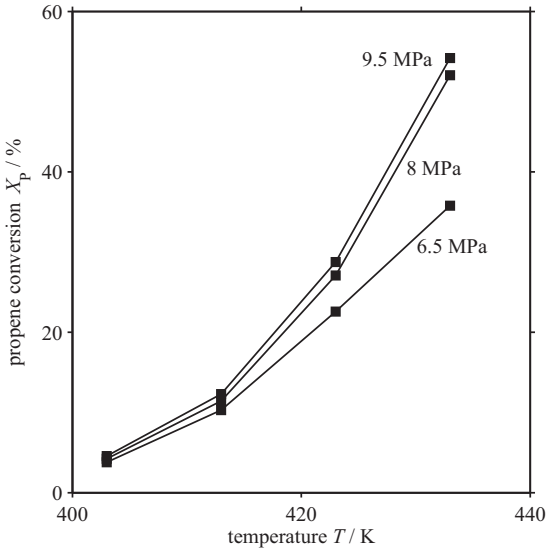

Figure 5.6: Effect of temperature and pressure on P conversion in a 10 m long reactive extraction column (ID 50 mm).

These recommendations are affirmed by the results for selectivity with respect to isopropyl alcohol. In fig. 5.7 it is shown that the selectivity drops with increasing temperature and decreasing pressure. There is practically no difference between the isobars for 8 MPa and 9.5 MPa, but a drastic selectivity drop is obtained at 6.5 MPa.

The temperature has an enhancing effect on conversion but an attenuating effect on selectivity. At a temperature of 423 K the conversion is five to six times the value corresponding to a temperature of 403 K. Accordingly, the selectivity decreases from 100 % to 98 %. But, at 433 K the selectivity declines to 94 %. As a result, temperatures above 423 K should not be employed for the hydration of propene with fresh (activated) catalyst. Further discussion on the recommended range of temperature will be given in the following subsection.

5.2.2 Reactor Efficiency and Performance

According to the simulation as depicted in fig. 5.3, figs. 5.8 and 5.9 illustrate the course of the catalyst effectiveness factors η_S and η_B along the axial reactor

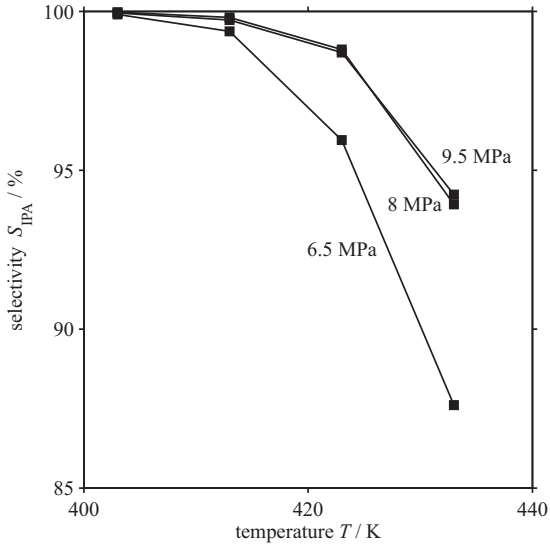

Figure 5.7: Effect of temperature and pressure on IPA selectivity in a 10 m long reactive extraction column (ID 50 mm).

coordinate z for the hydration of propene and the etherification of isopropyl alcohol, respectively. Comparing the mole fraction profile of isopropyl alcohol in the aqueous phase (fig. 5.3) with the catalyst efficiency profile for the hydration of propene the correlation of catalyst efficiency with isopropyl alcohol content in the aqueous phase becomes apparent. This is due to the acceleration of the rate of the reverse reaction (dehydration) with increasing isopropyl alcohol content.

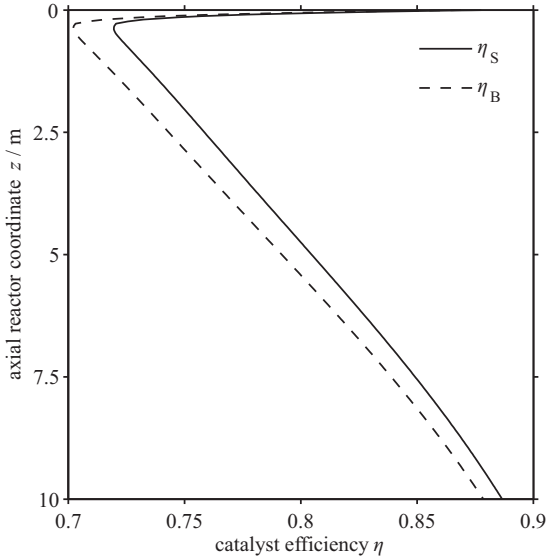

Figure 5.8: Catalyst efficiency profiles for the hydration of P along axial reactor coordinate at 423 K and 9.5 MPa with aqueous phase recycle.

The magnitude of the catalyst efficiency with respect to bulk conditions is in the range between approximately 0.7 for a reaction mixture containing 0.5 mol % isopropyl alcohol and 0.9 for an isopropyl alcohol content of 1.5 mol % at 423 K. The magnitude of the catalyst efficiency with respect to conditions at the catalyst surface takes its course close to that which is related to conditions in the bulk of the aqueous phase. Hence, the reaction rate is significantly affected by mass transfer limitations within the catalyst matrix. This holds also for the catalyst efficiency of the etherification of isopropyl alcohol. From fig. 5.9 it is seen that the catalyst efficiency exceeds unity which is the consequent result for a consecutively appearing side reaction.

But, in the second half of the reactor length the catalyst efficiency of the

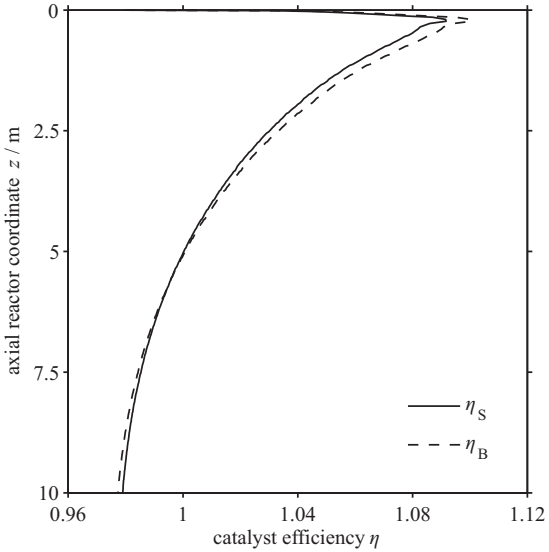

Figure 5.9: Catalyst efficiency profiles for the etherification of IPA along axial reactor coordinate at 423 K and 9.5 MPa with aqueous phase recycle.

etherification declines below unity which is caused by the acceleration of the etherification rate accompanied by the deceleration of the hydration rate due to an increased isopropyl alcohol content in the reaction mixture.

The effect of temperature on the more important catalyst efficiency of the hydration reaction presents fig. 5.10. A recycling of the aqueous reactor effluent has not been considered here. It is seen that the catalyst efficiency drops significantly with increasing temperature whereas the conversion, which is known to increase with temperature, leads to a compensation of the hydration rate by an accelerating reverse reaction rate.

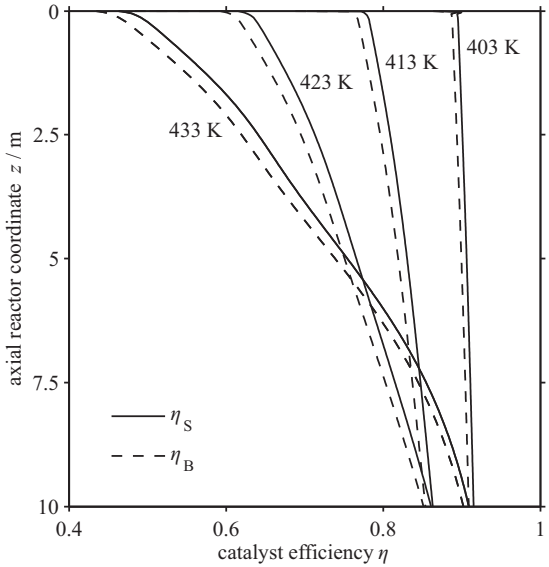

Figure 5.10: Effect of temperature on the catalyst efficiency profiles for the hydration of P at 9.5 MPa without aqueous phase recycle.

In view of the catalyst deactivation, see also section 3.1.2, which strongly enhances with temperature, and a significant drop in selectivity for temperatures above 423 K one should not exhaust the maximum temperature which the catalyst is able to withstand (433 K to 443 K). Furthermore, the drop of catalyst activity due to a loss of acid sites during the life cycle of the catalyst might be compensated by a continuous increase of reactor temperature. This leads – with respect to an optimal temperature – to an optimization problem between the life cycle period of the catalyst and the required reactor size (length) for which the desired extent of reaction is achieved.

Figure 5.11 shows the contributions of the four considered diffusive mass transfer regions:

i) the organic film at the fluid interface (L1),

ii) the aqueous film at the fluid interface (L2),

iii) the film surrounding the catalyst (LS), and

iv) the catalyst matrix (S),

to the overall mass transfer resistance of all components of the C_3-hydration system. The organic components have their respective main mass transfer resistance in the aqueous pore liquid of the catalyst (S). Only the transport of water is limited by the organic film (L1). Due to the relatively low propene flow in the reactive extraction column the main part of the remaining contributions to the overall mass transfer resistance is located in the organic film (L1) for the case of isopropyl alcohol and diisopropyl ether.

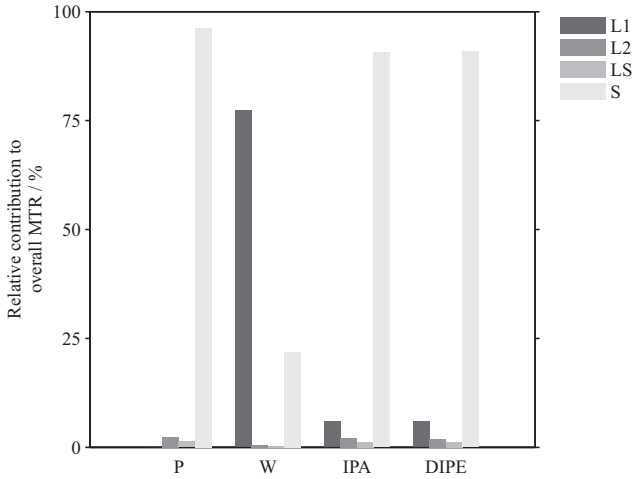

Figure 5.11: Relative contributions of the diffusive mass transfer regions to the overall component mass transfer resistances.

In fig. 5.12, the relative component mass transfer resistances within the four mass transfer regions are presented. The components propene and water do not contribute to the overall mass transfer resistance in those regions in which they are the solvent component. Otherwise, the contributions of the solutes are almost equal. There is only a weak dependence on the size of molecule.

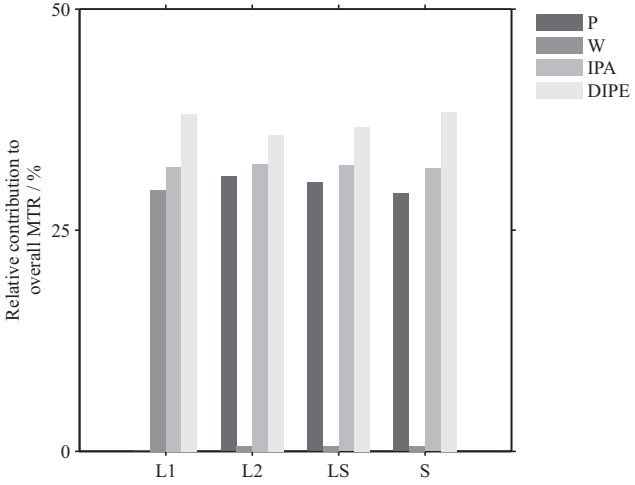

Figure 5.12: Relative component mass transfer resistances with respect to diffusive mass transfer regions.

5.2.3 Optimal Extent of Reaction

The effort for the recovery of the main-product isopropyl alcohol can generally be reduced when the proposed reactive extraction process is employed for the hydration of linear alkenes. In contrast to the trickle bed the reactive extraction allows recovering isopropyl alcohol from the organic extract phase. The unconverted propene can be removed from the organic reactor effluent by stripping which produces a bottom product mainly consisting of isopropyl alcohol, water and diisopropyl ether. The ratio of isopropyl alcohol to water in the bottom product is a key-parameter for a reduced energy demand. The required reflux ratio of a hetero-azeotropic distillation strongly increases with increasing water content.

Due to fluid phase equilibria, the ratio of isopropyl alcohol to water in the organic reactor effluent exhibits a maximum with increasing extent of reaction (fig. 5.13). A maximum ratio of 1.35 is found for a propene conversion of 25 %.

The dependence of selectivity with respect to isopropyl alcohol on propene conversion is illustrated in fig. 5.14. It can be seen that the selectivity is 98 % at a conversion of approximately 30 %. With further increase of conversion the selectivity drops more strongly and reaches a level of 94 % at 55 % conversion.

Taking into account the selectivity loss with respect to conversion and the minimum energy demand of the hetero-azeotropic purification of isopropyl

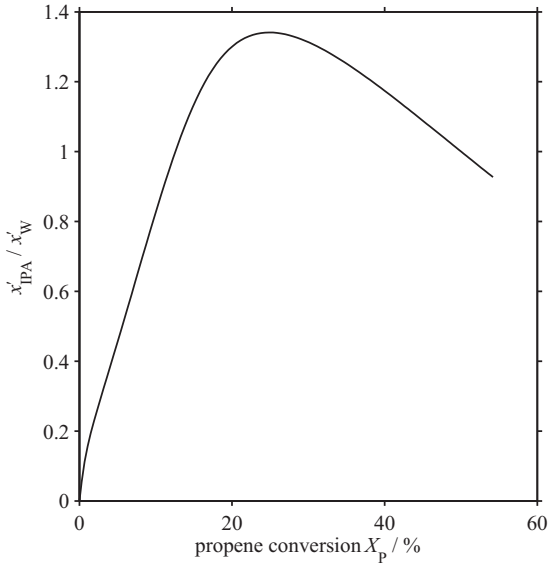

Figure 5.13: Ratio of IPA and W mole fractions in the organic phase $\frac{x'_{IPA}}{x'_W}$ as function of P conversion.

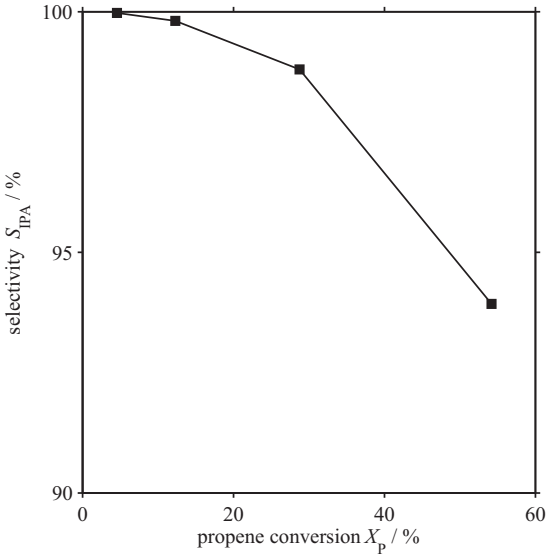

Figure 5.14: Effect of conversion on IPA selectivity at 423 K and 9.5 MPa.

alcohol at a maximum ratio of isopropyl alcohol to water in the feed of the hetero-azeotropic distillation, a conversion of 25 % propene is obviously optimal.

5.3 Separation Processes

The older trickle bed process produces an aqueous reactor effluent which contains due to the excessive water feed stream only approximately 7 mol % isopropyl alcohol. As is described in section 4.5, this reactor effluent is processed using an ordinary distillation for pre-concentration of isopropyl alcohol close to the azeotropic composition of the aqueous isopropyl alcohol ($x_{\mathrm{IPA}} = 60\,\mathrm{mol}\,\%$ to $70\,\mathrm{mol}\,\%$) and a hetero-azeotropic distillation for final purification of isopropyl alcohol. A simulation program of the pre-concentration column for the binary system isopropyl alcohol-water was previously developed in the work of Voelskow [7]. The proposed reactive extraction process produces an aqueous and an organic reactor effluent whereas the organic reactor effluent contains the main part of the formed isopropyl alcohol. The aqueous phase does not need a recovery process, it may be recycled directly to the reactor (see also section 5.1).

However, the organic phase can be separated with less effort when compared to the aqueous reactor effluent of the trickle bed process. Due to the relatively low boiling point of propene it can be separated by a reboiled stripper and recycled to the reactor inlet. The stripper column is less energy demanding than the pre-concentration column of the trickle bed process. The bottom product of the stripper is then processed by a hetero-azeotropic distillation tower, which is common with the trickle bed process.

The hetero-azeotropic distillation requires an entrainer component which forms a ternary hetero-azeotrop with isopropyl alcohol and water, i. e. the liquid phase is unstable at the azeotropic point, it separates into two or more immiscible liquid phases. The major by-product of the C_3-hydration is diisopropyl ether which forms such a ternary mixture together with isopropyl alcohol and water. The VLLE of this system is discussed in section 2.1.4.

Figure 5.15 shows a residue curve map of the ternary system diisopropyl ether-isopropyl alcohol-water. The thick black graphs represent distillation borders, i. e. a distillation trajectory or residue curve cannot cross these borders. The thinner grey lines are residue curves which are possible equilibrium distillation trajectories.

Figure 5.16 shows the VLLE diagram in the ternary composition space. Also here, the thick black lines are the distillation boundaries. The grey lines are tie lines connecting the compositions of the immiscible liquids. The thin black solid and dashed graph are distillation trajectories of liquid and vapor phase, respectively.

The vapor phase trajectory starts in the upper left corner at pure isopropyl alcohol and ends at a tie line. It is this split of the liquid phase into an aqueous and an organic liquid that allows for a breakthrough of the distillation boundary which separates the upper and lower distillation regions and thereby the feasible

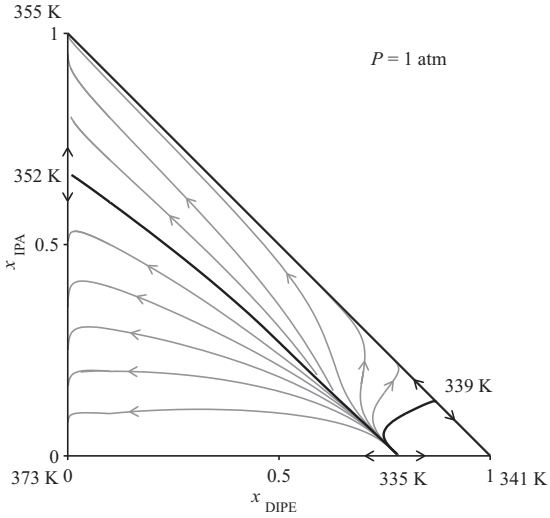

Figure 5.15: Residue curve map of the system DIPE-IPA-W showing distillation borders (thick black lines) and batch distillation trajectories (gray lines); the arrows mark directions of the trajectories.

product streams. The aqueous liquid phase is separated from the organic liquid phase in a decanter and recycled to the reactor inlet.

The organic liquid reflux initiates the liquid composition trajectory which then tends towards pure isopropyl alcohol. Due to mixing of the liquid from the rectifying section with the column feed there is a large step in the trajectory towards the long branch of the distillation boundary. The fronts in the composition trajectories are less steep when compared to the residue curves in fig. 5.15 because the trajectories are obtained from a mass transfer rate based simulation while the residue curves are computed assuming equilibrium between liquid and vapor phase.

It can be seen that the liquid phase trajectory never crosses the heterogeneous region while the vapor phase trajectory enters the heterogeneous region somewhat before being condensed. This situation reflects the optimal operational state of the column because on one hand there is no phase separation of the liquid in the column except in the condenser/decanter section and on the other the condensate being formed from the total liquefaction of the vapor leaving the column separates into an aqueous and an organic liquid phase which can be easily separated by decantation. As there is no liquid phase separation throughout the whole column, the column always operates with optimal effi-

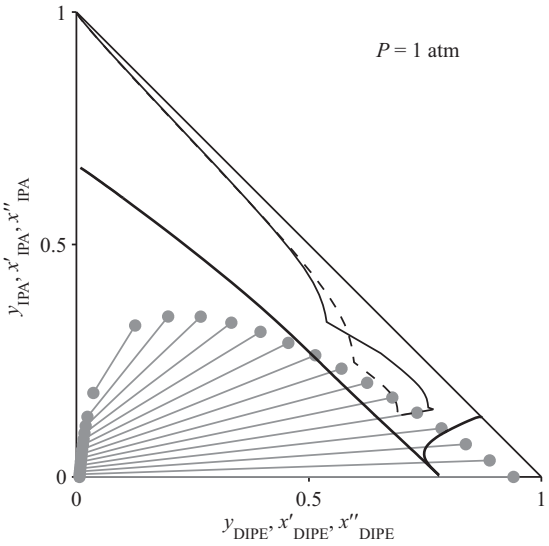

Figure 5.16: Column profiles for vapor (dashed black line) and liquid (solid black line) from a nonequilibrium simulation in the mole fraction phase plane for the system DIPE-IPA-W additionally showing the heterogeneous region (gray tie lines) and distillation borders (thick black solid lines).

ciency which would not be the case if the liquid phase would separate on one or several stages of the column. The prerequisite for such an efficient steady state is a sufficiently large reflux of the organic condensate and a sufficiently small reflux of the aqueous condensate from the decanter.

Resulting liquid phase mole fraction profiles for the hetero-azeotropic distillation column from the nonequilibrium simulation are shown in fig. 5.17. Numeric results and column configuration data are compiled in table 5.1. The heat duties in tables 5.1 to 5.4 are calculated as

$$Q = \sum_{i=1}^{n_c} V_{i,\mathrm{B}} \Delta h_i^{\mathrm{vap}} \tag{5.9}$$

wherein $V_{i,\mathrm{B}}$ is the vapor flow rate of component i leaving the evaporator and $\Delta h_i^{\mathrm{vap}}$ is the enthalpy of vaporization of the pure component i. Appendix E.1.4 provides a short outline on the computation of enthalpies which are required for the simulation of distillation and stripping equipment.

However, the influence of excess enthalpies is neglected, because the thermodynamic model only provides reliable excess enthalpies when experimental data for the excess enthalpies – at least of the binary pairs – are used for the fitting of interaction parameters in addition to phase equilibrium data (Ahlers and Gmehling [10]). Such data are only available for a few binaries.

The liquid phase mole fraction profiles for the pre-concentration of the trickle bed reactor effluent are illustrated in fig. 5.18 and numeric data of this simulation provides table 5.2.

Liquid phase mole fraction profiles in the stripping column for the recovery of unconverted propene from the organic reactor effluent of the reactive extraction process are given in fig. 5.19. Table 5.3 provides according numeric data.

A comparison of the required heat duties of both separation sequences, trickle bed and reactive extraction process, is presented in table 5.4.

It is found that the separation sequence of the reactive extraction process requires an overall evaporator heat duty of 11.3 MW which is approximately 38 % less than the sequence of the trickle bed process with an overall evaporator heat duty of 18.3 MW.

This noticeable reduction in heat demand of the separation sequences even is extended when considering the reduction of the water recycling stream. Of course, the recycling of propene, which comprises the steps condensation, repressurizing and heating, requires significant amounts of heat and electricity, but this is less than the energy demand of the exzessive water recycle stream of the trickle bed process.

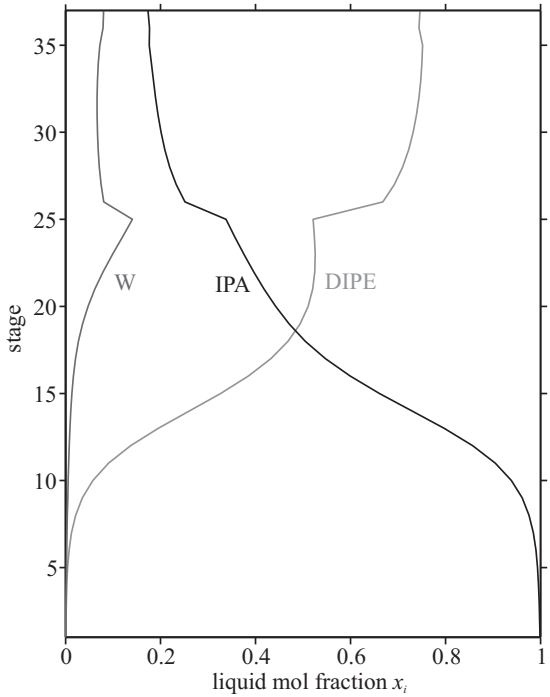

Figure 5.17: Liquid mole fraction profiles in heterogeneous azeotropic IPA purification of the reactive extraction process.

Table 5.1: Distillation column specifications and numeric simulation results for the heteroazeotropic purification of IPA.

Parameter	Unit	Value	Mole fraction		
			DIPE	IPA	W
Column					
Height, h_C	m	9.0			
Diameter, d_C	m	2.0			
Stages		35			
Reflux ratio, ν		20.0			
Heat duty, Q	MW	9.1			
Packing					
Type		Sulzer BX			
Feed					
Stage		25			
Temperature, T	K	330			
Pressure, P	kPa	160.0			
Flow, F	mol/s	59.3			
Composition, $x_{i,F}$	mol %		2.0	56.0	42.0
Makeup (DIPE), M	mol/s	6.0			
Distillate					
Temperature, T	K	296.8			
Pressure, P	kPa	141.0			
Org. Flow, D'	mol/s	9.1			
Org. Comp., $x'_{i,D}$	mol %		78.0	13.7	8.3
Aq. Flow, D''	mol/s	24.4			
Aq. Comp., $x''_{i,D}$	mol %		0.2	1.3	98.5
Raffinate					
Temperature, T	K	369.8			
Pressure, P	kPa	177.0			
Flow, R	mol/s	31.7			
Composition, $x_{i,R}$	mol %		0.0	99.9	0.1

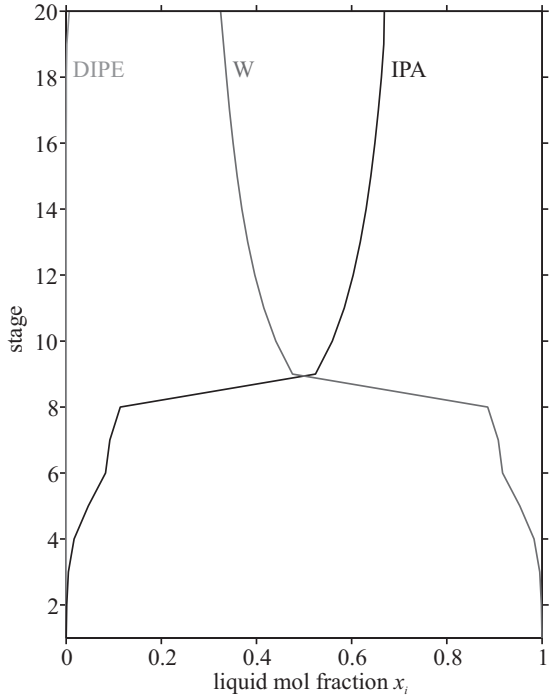

Figure 5.18: Liquid mole fraction profiles in distillation column for preconcentration of IPA of the trickle bed process.

Table 5.2: Distillation column specifications and numeric simulation results for the pre-concentration of IPA.

Parameter	Unit	Value	Mole fraction		
			DIPE	IPA	W
Column					
Height, h_C	m	5.0			
Diameter, d_C	m	3.0			
Stages		20			
Reflux ratio, ν		2.0			
Heat duty, Q	MW	9.2			
Packing					
Type		Sulzer BX			
Feed					
Stage		8			
Temperature, T	K	323.0			
Pressure, P	kPa	110.0			
Flow, F	mol/s	666.0			
Composition, $x_{i,F}$	mol %		0.1	5.0	94.9
Distillate					
Temperature, T	K	351.0			
Pressure, P	kPa	99.0			
Flow, D	mol/s	49.8			
Composition, $x_{i,D}$	mol %		0.7	66.7	32.6
Raffinate					
Temperature, T	K	379.7			
Pressure, P	kPa	120.0			
Flow, R	mol/s	616.2			
Composition, $x_{i,R}$	mol %		0.0	0.01	99.99

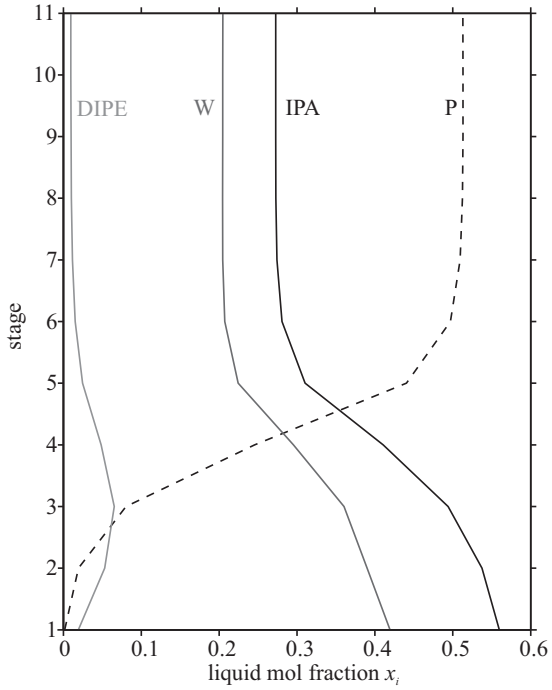

Figure 5.19: Liquid mole fraction profiles in stripper column for recovery of P of the reactive extraction process.

Table 5.3: Stripping column specifications and numeric simulation results for the recovery of P.

Parameter	Unit	Value	Mole fraction			
			P	DIPE	IPA	W
Column						
Height, h_C	m	3.0				
Diameter, d_C	m	1.2				
Stages		10				
Reflux ratio, ν		0				
Heat duty, Q	MW	2.2				
Packing						
Type		Sulzer BX				
Feed						
Stage		11				
Temp., T	K	290.0				
Pressure, P	kPa	1000				
Flow, F	mol/s	120.0				
Comp., $x_{i,F}$	mol %		50.5	1.0	27.7	20.8
Distillate						
Temp., T	K	290.7				
Pressure, P	kPa	989.0				
Flow, D	mol/s	60.7				
Comp., $y_{i,D}$	mol %		99.5	0.1	0.2	0.2
Raffinate						
Temp., T	K	417.1				
Pressure, P	kPa	1000				
Flow, R	mol/s	59.3				
Comp., $x_{i,R}$	mol %		0.2	1.9	56.0	41.9

Table 5.4: Comparison of evaporator heat duties between trickle bed and reactive extraction process.

Separation unit	Evaporator heat duty, MW		Energy saving, %
	Trickle bed	Reactive extraction	
	Q_{TB}	Q_{RE}	$\frac{Q_{\mathrm{TB}}-Q_{\mathrm{RE}}}{Q_{\mathrm{TB}}}$
Stripping	-	2.2	-
Pre-concentration	9.2	-	-
Purification	9.1	9.1	-
$\sum$	18.3	11.3	38.3

5.4 Conclusions

The results with respect to the simulation of the reactive extraction column affirm once more the importance of an *in situ* product separation. By efficient *in situ* product extraction it is possible to enhance the efficiencies of reactor and downstream processing sequence.

The reduced heat duty demand of the separation sequence of 38 % is an astonishing result. It clearly confirms the high potential of integrated reaction and separation processes for process intensification.

Only results for the C_3-hydration system are presented, but they hold also for the C_4-hydration system, at least qualitatively.

Nevertheless, at least the reactive extraction model needs a carefully conducted experimental validation for both hydration systems, C_3 and C_4.

Although the hydration of linear alkenes is an extraordinary system it might be a promising approach applying the concept of heterogeneous reactive extraction to other systems for which a reactive (catalytic) distillation process is infeasible either caused by a too wide spreading of the boiling points of the reactants or by temperature and/or pressure limits due to requirements of the reaction.

References

[1] Froment, G. F. and K. B. Bischoff. *Chemical reactor analysis and design*, 2nd. Wiley, New York, 1990.

[2] Taylor, R., H. A. Kooijman, and J.-S. Hung. A second generation nonequilibrium model for computer simulation of multicomponent separation processes. *Comput. Chem. Eng.* **18**, (1994), 205–217. DOI: 10.1016/0098-1354(94)85009-7.

[3] Krishnamurthy, R. and R. Taylor. A nonequilibrium stage model of multicomponent separation processes. Part I: Model description and method of solution. *AIChE J.* **31**, (1985), 449–456. DOI: 10.1002/aic.690310312.

[4] Taylor, R. and R. Krishna. *Multicomponent mass transfer*. Wiley, New York, 1993.

[5] Kovach, J. W. and W. D. Seider. Heterogeneous azeotropic distillation: Experimental and simulation results. *AIChE J.* **33**, (1987), 1300–1314. DOI: 10.1002/aic.690330807.

[6] Naphtali, L. M. and D. P. Sandholm. Multicomponent Separation Calculations by Linearization. *AIChE J.* **17**, (1971), 148–153. DOI: 10.1002/aic.690170130.

[7] Voelskow, K. Kinetische Simulation der Destillation nicht-idealer Mischungen. Diploma Thesis, Clausthal University of Technology, 2008.

[8] Vickery, D. J. and R. Taylor. Path-following approaches to the solution of multicomponent, multistage separation process problems. *AIChE J.* **32**, (1986), 547–556. DOI: 10.1002/aic.690320404.

[9] Zangwill, W. I. and C. B. Garcia. *Pathways to solutions, fixed points, and equilibria*. Prentice-Hall, Englewood Cliffs, 1981.

[10] Ahlers, J. and J. Gmehling. Development of a Universal Group Contribution Equation of State III. Prediction of Vapor-Liquid Equilibria, Excess Enthalpies, and Activity Coefficients at Infinite Dilution with the VTPR Model. *Ind. Eng. Chem. Res.* **41**, (2002), 5890–5899. DOI: 10.1021/ie0203734.

6 Summary

6.1 Conclusions

A new concept for process intensification in the field of acid ion exchange resin catalyzed liquid phase hydration of linear C_3- and C_4-alkenes to their corresponding alcohols isopropyl alcohol and *sec*-butyl alcohol has been developed within this work. The tremendous advantage of a reactive extraction reactor is clearly demonstrated, at least on a theoretical level. The underlying work comprises experimental as well as theoretical and simulation work, respectively, on fundamental aspects of the liquid phase hydration of C_3- and C_4-alkenes.

Using a modern cubic equation of state which employs well-proven activity coefficient models for the mixing rule the important fluid phase equilibria of these systems – involving supercritical components – could be modeled and validated with the help of experimental data with good accuracy. Besides the high pressure liquid-liquid equilibria, vapor-liquid equilibria, chemical equilibria and the nonideal multicomponent mass transfer were simulated and partially validated to experimental data.

The experimental results for micro- and macrokinetics of these reversible reaction systems confirm the few earlier studies which can be found in the literature on a qualitative level. The experiments were conducted in a novel continuously stirred multiphase tank reactor setup which was developed during this work. The reactor and its peripheral systems allow an independent control of hold-up and residence time for each phase individually. To the authors knowledge, a similar liquid-liquid reactor concept for the use of solid catalysts is not yet available in literature. The range of operating conditions at which the reaction rates are not being affected by mass transfer limitations could well be identified. Results which were obtained in the makrokinetic regime can be reproduced fairly well by the developed intrinsic rate model which is embedded in a nonideal mass transfer model.

The issues of the trickle bed reactor which is used for the hydration of propene on an industrial scale are analyzed. The accordant results serve as starting point for the development of a new reactor concept. It is found that this reaction system has some analogies to other systems for which an integrated process, e. g. reactive distillation, is a promising option for manufacture. The simultaneous removal of the product from the catalyst wetting aqueous phase is beneficial with respect to space time yield and selectivity. Due to the special

fluid phase behavior of the C_3- and C_4-hydration systems, heterogeneously catalyzed reactive extraction turned out to be a sufficient concept for hydration.

Improvements are not only achieved in the reactor, but also within the post-reactive separation sequence for the purification of the alcohol. For the case of the hydration of propene it is demonstrated by nonequilibrium separation simulations that energy savings for required evaporator heat duties of distillation and stripping columns of almost 40 % are possible. Such an enormous improvement is only accessible by a substantial revision of the existing process. Using a structured catalytic packing in the reactor two immiscible liquid phases are obtained of which the organic phase extracts the product alcohol from the catalyst wetting aqueous phase. Forming this alcohol-rich extract phase in the reactor is the key for the opportunity of redesigning the separation sequence.

In addition, the recycling of an excess of 15 : 1 parts water over alkene can considerably be reduced and the reactor performance can be enhanced. The simulations of the reactive extraction process in a structured catalytic packing are based on the fundamental experimental and theoretical results of this work.

Finally, some preliminary reaction experiments and fluid dynamic experiments at ambient conditions in a model system are presented. The experiments on fluid dynamics of two immiscible liquid phases in a structured catalytic packing were conducted to provide an estimate on important design parameters for a lab-scale reactive extraction plant.

6.2 Future Work

The novel concept of heterogeneous reactive extraction, which has been developed for the particular hydration of linear C_3- and C_4-alkenes by this work, might be a promising process option also for other reaction systems. The limitations on process conditions being subject in (heterogeneous) reactive distillation processes can be circumvented by making use of (heterogeneous) reactive extraction. For reaction systems that are limited in conversion due to chemical equilibrium and/or selectivity issues and which cannot be processed in reactive distillation systems because of limited process conditions, (heterogeneous) reactive extraction might enable an access for such processes to process intensification. As a conclusion, the concept of heterogeneous reactive extraction has the potential being further developed.

As the heterogeneous reactive extraction for the hydration of linear C_3- and C_4-alkenes has yet been investigated only by simulation attempts it is necessary to study this concept experimentally and to validate or modify – when indicated – the proposed model.

A general proposal for the lab-scale reactive extraction column is provided. It considers a high pressure reactive extraction apparatus with separated recycles

for organic and aqueous phase which allow for a CSTR-like operation mode and co- as well as counter-current flow of the immiscible phases in the structured packing of the reactive extraction column. The peripheral equipment which has been used for the kinetic investigations of this work can also be employed to the reactive extraction column.

With this lab-scale reactive extraction column the interface mass transfer in the systems under consideration should be investigated for which accordant coefficients are not yet available. In addition to that, the fluid dynamics, i. e. hold-up, pressure drop, load point, wetting performance and interfacial area, at relevant operating conditions should be studied.

Furthermore, the low flow rate of the organic phase as being considered for the PFTR-simulations of the reactive extraction column gives rise to the question if axial dispersion affects the mole fraction profiles in the reactive extraction column. Hence, appropriate measurements of the residence time distribution behavior at relevant process conditions need to be performed. Finally, it needs to be studied if the flow rate of the organic phase at such an order of magnitude limits the overall mass transfer performance.

Using the findings of this work and following the recommendations on further research in the field of heterogeneous reactive extraction for the hydration of linear C_3- and C_4-alkenes or any other suitable reaction system, as given above, it should be possible to derive guidelines for the design of a pilot-scale heterogeneous reactive extraction process.

Appendix A

Gas Chromatographic Methods

The determination of the compositions of both liquid phases requires a two-way sampling and analysis system. Furthermore, due to the strong volatility of the alkenes the sampling must be conducted at system pressure and temperature by a high-pressure online sampling system, i. e. the samples are to be taken under system pressure and temperature directly injecting the sample into the low pressure carrier gas supply line of the gas chromatograph. This sampling strategy was achieved by employment of the rapid online sample injector (ROLSI).

The ROLSI-system is a superheated capillary needle valve which allows for the direct injection of a fluidic sample in the µl-domain from a high pressure system into a gas stream at low pressure. With *superheated* it is meant that the valve body is heated to such an extent that the sample is instantaneously evaporated and no adsorption of sample components occurs on the inner surfaces of the valve body.

However, in contrast to common sample-loop injection valves, using ROLSI the absolute sample quantity is practically unknown. Thus, it is necessary to detect all components in the sample and to use a quasi-internal standard for quantification purposes. With *quasi-internal* it is meant that test-mixtures with well known compositions are used instead of absolute sample quantity in order to relate component mole fractions to peak area fractions rather than the number of moles for a respective component to their absolute peak area of the detector signal. By using a thermal conductivity detector (TCD) the detection of all components can be ensured.

Due to the rigorous detection and evaluation of all components the mole fractions of solvent and solutes differ significantly. This requires toggling the detector sensitivity. The detector sensitivity of the TCD of the HEWLETT-PACKARD 5890™ gas chromatograph allows two settings, low and high sensitivity whereas the setting *high sensitivity* is as high as 32-times the *low sensitivity*. The toggling of the detector sensitivity is highlighted in the exemplary chromatograms figs. A.2 to A.5.

The injected samples are transferred from the ROLSI to the gas chromatograph by the carrier gas which is drawn to the injector of the gas chromatograph. An evaporation does not occur in the injector as the sample already evaporates

in the sampling valve. Only the sample splitting capabilities of the injector are used to reduce the sample quantity appropriately for capillary gas chromatography columns. The used online gas chromatography system is illustrated in fig. A.1.

Tables compiling system-specific method data and exemplary chromatograms are provided in the next sections.

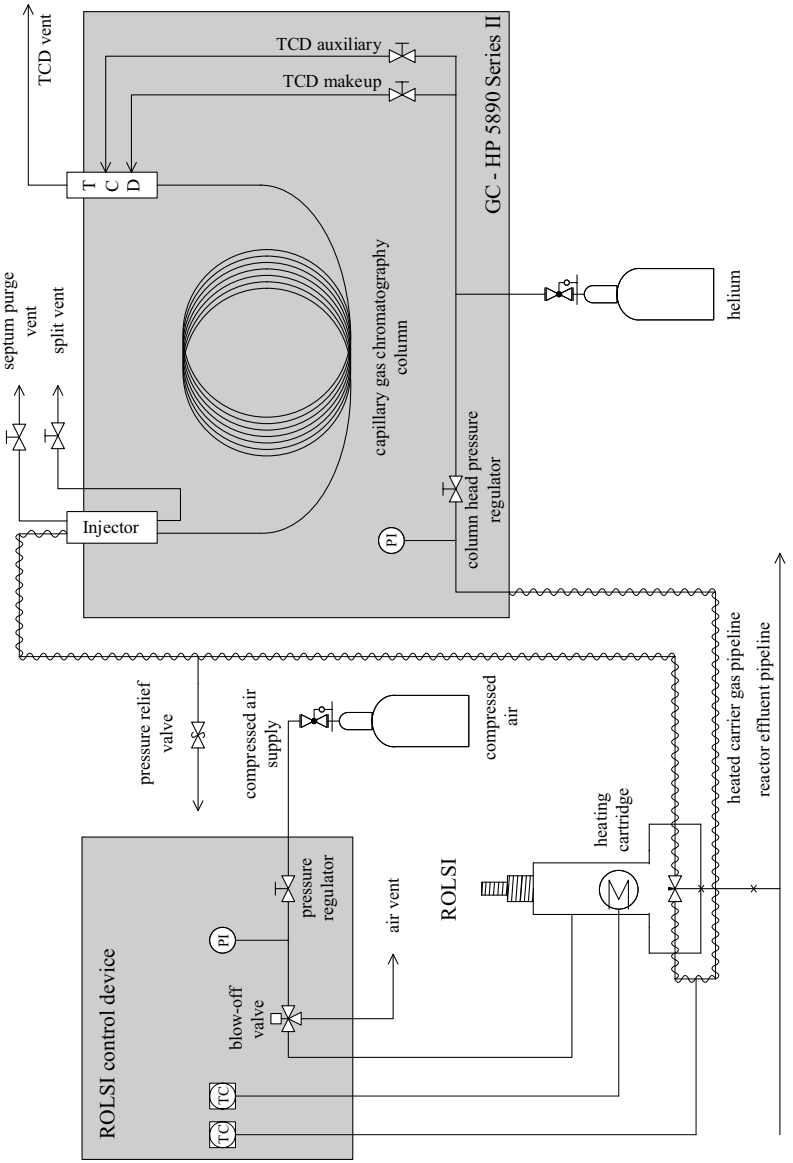

Figure A.1: Flow chart of the online sampling gas chromatography system.

A.1 C_3-Hydration System

Table A.1: Parameters of gas chromatography method for the C_3-system.

Parameter	DET A (aqueous phase)	DET B (organic phase)
Column		
Dimensions	30 m x 0.53 mm x 2 µm	30 m x 0.53 mm x 2 µm
Stationary phase	poly(ethylene glycol)	poly(ethylene glycol)
Carrier gas flow	20 cm/s helium	20 cm/s helium
Split ratio	25:1	25:1
Detector	TCD	TCD
Temperatures		
Injector	200 °C	200 °C
Detector	170 °C	170 °C
Oven		
Start temperature	5 min @ 80 °C	
Ramp	20 °C/min	
End temperature	1.5 min @ 150 °C	

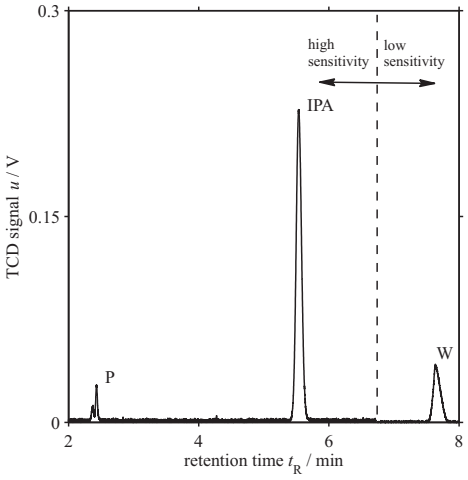

Figure A.2: Gas chromatogram from an aqueous phase sample of the C_3-system.

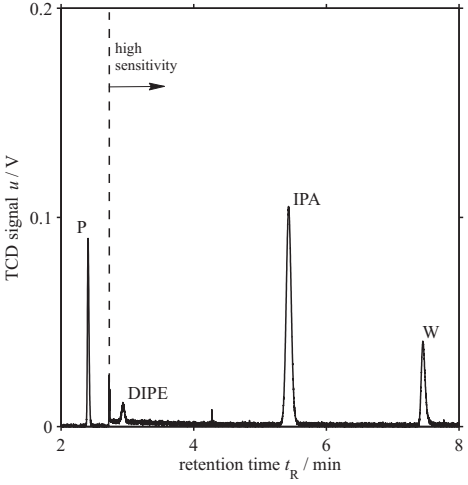

Figure A.3: Gas chromatogram from an organic phase sample of the C_3-system.

A.2 C_4-Hydration System

Table A.2: Parameters of gas chromatography method for the C_4-system.

Parameter	DET A (aqueous phase)	DET B (organic phase)
Column		
Dimensions	60 m x 0.53 mm x 5 µm	60 m x 0.53 mm x 5 µm
Stationary phase	poly(dimethyl siloxane)	poly(dimethyl siloxane)
Carrier gas flow	20 cm/s helium	20 cm/s helium
Split ratio	25:1	25:1
Detector	TCD	TCD
Temperatures		
Injector	250 °C	250 °C
Detector	250 °C	250 °C
Oven		
Start temperature	5 min @ 120 °C	
Ramp	20 °C/min	
End temperature	2 min @ 180 °C	

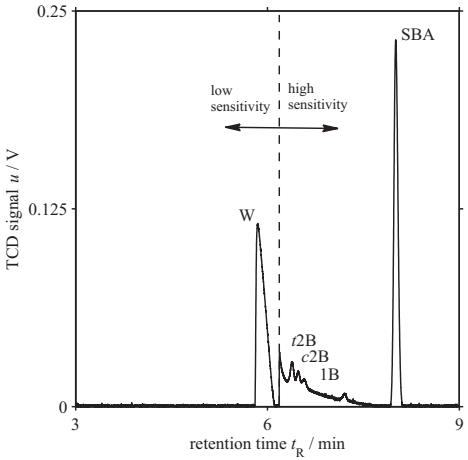

Figure A.4: Gas chromatogram from an aqueous phase sample of the C_4-system.

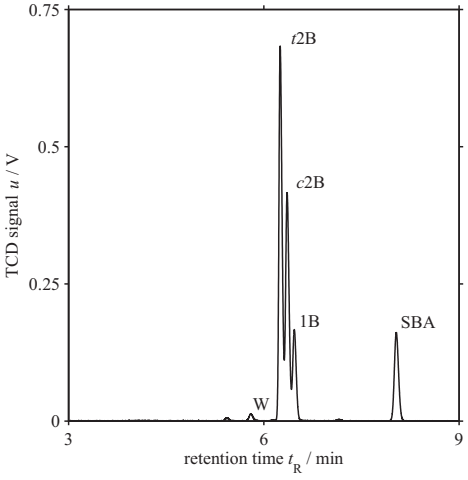

Figure A.5: Gas chromatogram from an organic phase sample of the C_4-system.

Appendix B

Flow Chart of Miniplant for Kinetic Investigations

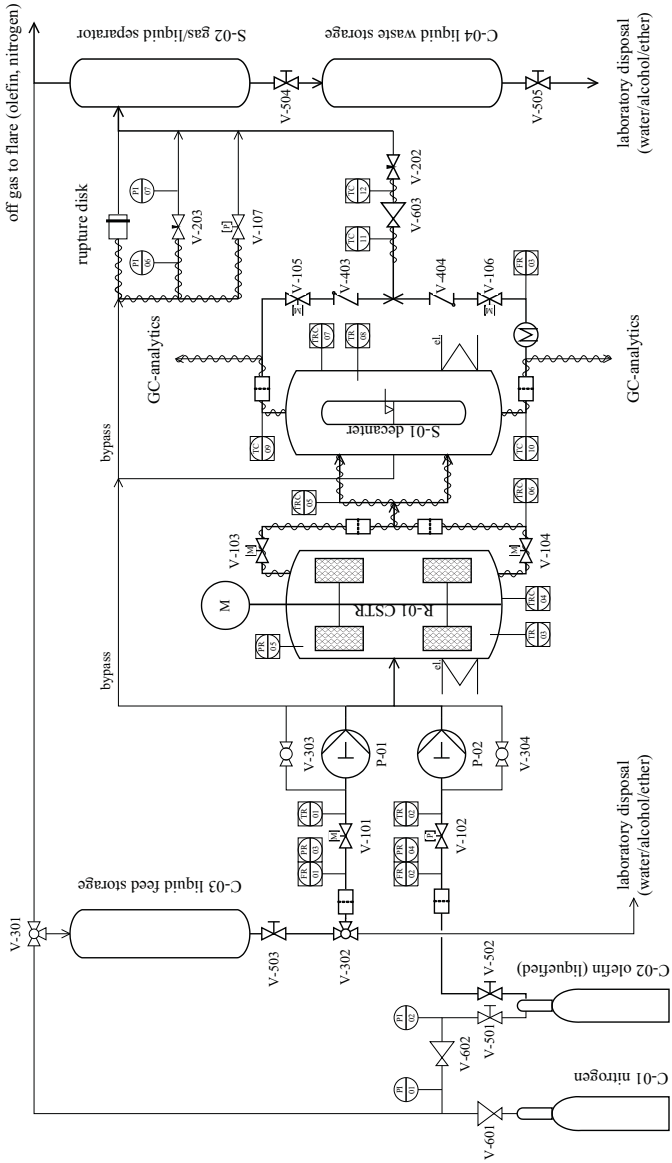

Figure B.1: Flow chart of the lab-scale plant for kinetic experiments.

Appendix C

Experimental Results

C.1 Kinetic Experiments C_3-Hydration System

Table C.1: Experimental data and reaction conditions used for rate model parameter fitting calculations for the C_3-hydration system.

No.	T	P	Feed[a]			Mole fraction at reactor exit[b]					X	r_{obs}	
	°C	MPa	mol/h			mol %					%	mmol/(eq s)	
						x'_i			x''_i[c]				
			P	W	IPA	P	IPA	DIPE	P	IPA		IPA	DIPE
1	125.2	8.1	0.366	1.657	0.0	98.69	0.45	0.0	0.21	0.22	3.37	0.235	0.0
2	129.8	8.2	0.367	1.658	0.0	98.56	0.58	0.0	0.22	0.28	3.8	0.302	0.0
3[d]	139.7	8.1	0.368	1.659	0.0	97.17	1.42	0.04	0.23	0.58	6.17	0.665	0.007
4	157.7	8.1	0.366	1.657	0.0	94.19	3.86	0.29	0.31	1.58	13.96	1.819	0.043
5	154.7	8.1	0.366	1.657	0.0	94.86	3.35	0.22	0.29	1.39	12.42	1.59	0.033
6	150.8	8.1	0.366	1.658	0.0	95.57	2.86	0.12	0.27	1.11	10.34	1.285	0.018
7	144.7	8.1	0.366	1.657	0.0	96.54	2.05	0.09	0.25	0.83	8.11	0.951	0.014
8[d]	139.8	8.2	0.366	1.657	0.0	97.17	1.48	0.05	0.23	0.58	6.26	0.673	0.007
9	130.3	8.3	0.366	1.628	0.016	96.64	1.76	0.04	0.25	0.86	3.44	0.193	0.006
10	150.1	8.4	0.366	1.629	0.016	94.92	3.04	0.17	0.3	1.56	8.46	0.932	0.027
11	120.1	8.2	0.176	0.782	0.008	96.61	1.88	0.05	0.25	0.82	3.41	0.092	0.004
12	160.1	7.9	1.106	1.517	0.08	92.78	4.03	0.29	0.45	3.06	3.08	0.896	0.148
13	155.1	7.9	1.109	1.518	0.08	92.74	3.66	0.19	0.45	2.99	2.39	0.577	0.098
14	150.6	8.0	1.109	1.518	0.08	92.91	3.5	0.14	0.44	2.97	2.1	0.434	0.075

continued on next page

Table C.1: Experimental data and reaction conditions used for rate model parameter fitting calculations for the C_3-hydration system (*continued*).

No.	T	P	Feed[a]			Mole fraction at reactor exit[b]					X	r_{obs}	
	°C	MPa	mol/h			mol %					%	mmol/(eq s)	
						x'_i			x''^{c}_i				
			P	W	IPA	P	IPA	DIPE	P	IPA		IPA	DIPE
15	145.6	8.0	1.112	1.519	0.08	93.27	3.24	0.08	0.44	2.95	1.69	0.236	0.044
16[d]	140.2	8.0	1.111	1.52	0.08	93.26	3.13	0.05	0.44	2.93	1.47	0.133	0.028
17[d]	140.2	8.0	1.111	1.576	0.049	94.08	2.18	0.04	0.32	1.81	1.43	0.26	0.019
18	145.1	8.0	1.109	1.576	0.049	94.44	2.34	0.05	0.33	1.85	1.69	0.374	0.024
19	150.0	7.9	1.111	1.576	0.049	92.27	2.56	0.08	0.35	2.1	2.38	0.699	0.044
20	160.6	8.0	1.108	1.576	0.049	91.66	2.95	0.24	0.39	2.48	3.72	1.305	0.124
21	159.9	8.0	1.111	1.384	0.154	88.36	5.79	0.44	0.81	5.22	2.25	0.1	0.241
22	155.3	8.0	1.109	1.382	0.154	88.47	5.84	0.31	0.88	5.51	2.55	0.163	0.171
23	130.1	8.0	1.103	1.631	0.016	95.65	0.83	0.01	0.24	0.73	1.14	0.215	0.004
24	134.8	8.0	1.102	1.63	0.016	95.62	0.89	0.01	0.25	0.8	1.33	0.302	0.007
25[d]	139.7	8.0	1.102	1.63	0.016	95.52	0.99	0.02	0.26	0.97	1.73	0.481	0.01
26	144.4	8.0	1.103	1.63	0.016	95.08	1.13	0.02	0.27	1.14	2.16	0.673	0.011
27	149.5	8.0	1.102	1.63	0.016	95.13	1.34	0.04	0.29	1.33	2.72	0.926	0.022
28	154.7	7.9	1.102	1.63	0.016	94.86	1.55	0.08	0.31	1.67	3.56	1.301	0.042

continued on next page

Table C.1: Experimental data and reaction conditions used for rate model parameter fitting calculations for the C_3-hydration system (*continued*).

No.	T	P	Feed[a]			Mole fraction at reactor exit[b]					X	r_{obs}	
	°C	MPa	mol/h			mol %					%	mmol/(eq s)	
						x_i'			x_i''[c]				
			P	W	IPA	P	IPA	DIPE	P	IPA		IPA	DIPE
29	160.3	7.9	1.104	1.63	0.016	94.06	1.81	0.17	0.34	2.02	4.58	1.758	0.083
30	160.6	8.0	1.105	1.125	0.281	80.57	13.59	0.53	1.33	6.98	2.6	−0.086	0.319
31	155.2	8.0	1.105	1.125	0.281	80.96	13.52	0.35	1.7	7.92	3.78	0.084	0.209
32	150.4	8.0	1.103	1.124	0.281	80.93	13.16	0.23	2.14	8.75	4.82	0.121	0.133
33	145.2	8.0	1.104	1.013	0.253	82.69	11.73	0.15	2.52	9.34	5.14	0.125	0.085
34	140.4	8.0	1.104	1.013	0.253	82.47	12.03	0.1	2.28	8.97	4.53	0.079	0.057
35	135.5	8.0	1.104	1.012	0.253	82.3	12.19	0.07	2.21	8.84	4.41	0.084	0.038
36	130.1	8.0	1.103	1.013	0.253	82.27	11.74	0.04	2.59	9.38	5.05	0.04	0.023

[a] no DIPE was used as feed stock in any experiment
[b] $x_W = 1 - x_P - x_{IPA} - x_{DIPE}$
[c] DIPE could never be observed in the aqueous phase
[d] data points illustrated in fig. 3.17

C.2 Kinetic Experiments C_4-Hydration System

Table C.2: Experimental data and reaction conditions used for rate model parameter fitting calculations for the C_4-hydration system.

No.	T	P	Feed			Mole fraction at reactor exit[a]				X	r_{obs}
	°C	MPa	mol/h			mol %				%	mmol/(eq s)
						x_i'		x_i''			
			SBA	B	W	SBA	B	SBA	B		SBA
1	131.5	8.0	0.64	3.318	0.0	97.71	0.45	0.07	0.0	0.45	0.172
2	129.6	5.8	0.64	3.319	0.0	97.74	0.33	0.06	0.0	0.33	0.126
3	124.3	6.0	0.64	3.321	0.0	98.02	0.24	0.06	0.0	0.24	0.09
4	124.3	8.0	0.64	3.321	0.0	98.03	0.25	0.07	0.0	0.26	0.096
5	124.9	8.0	0.317	1.543	0.024	93.66	4.85	0.07	0.56	0.44	0.069
6	135.0	7.9	0.317	1.545	0.024	93.62	4.91	0.07	0.59	0.65	0.102
7[b]	145.2	7.9	0.318	1.546	0.024	93.30	5.21	0.07	0.61	1.08	0.17
8[b]	145.3	7.9	0.318	1.546	0.024	93.26	5.23	0.07	0.61	1.09	0.172
9	143.9	6.0	0.317	1.545	0.024	93.36	5.14	0.06	0.64	1.13	0.177
10	134.9	6.0	0.317	1.546	0.024	93.63	4.93	0.06	0.6	0.73	0.116
11	124.7	6.0	0.317	1.544	0.024	93.86	4.72	0.06	0.59	0.46	0.072
12	124.7	6.0	0.317	1.619	0.008	96.97	1.97	0.06	0.19	0.41	0.065
13	135.1	6.0	0.317	1.620	0.008	96.6	2.26	0.06	0.22	0.87	0.137
14	144.9	6.1	0.317	1.619	0.008	96.01	2.82	0.06	0.31	1.86	0.292

continued on next page

Table C.2: Experimental data and reaction conditions used for rate model parameter fitting calculations for the C_4-hydration system (*continued*).

No.	T	P	Feed			Mole fraction at reactor exit[a]				X	r_{obs}
	°C	MPa	mol/h			mol %				%	mmol/(eq s)
						x_i'		x_i''			
			B	W	SBA	B	SBA	B	SBA		SBA
15[b]	145.0	7.9	0.317	1.619	0.008	96.29	2.54	0.07	0.41	2.1	0.329
16	134.9	7.9	0.317	1.620	0.008	96.69	2.21	0.07	0.28	1.11	0.174
17	125.0	7.9	0.317	1.620	0.008	97.12	1.88	0.07	0.25	0.64	0.1
18	130.0	7.9	0.317	1.619	0.008	96.98	1.96	0.07	0.26	0.74	0.116
19	139.9	7.9	0.317	1.658	0.0	97.75	1.17	0.07	0.17	2.04	0.321
20[b]	144.9	7.9	0.316	1.657	0.0	97.34	1.66	0.07	0.24	2.9	0.454
21[c]	155.1	7.9	0.316	1.657	0.0	96.6	2.36	0.07	0.37	4.27	0.669
22[c]	150.0	7.9	0.317	1.658	0.0	97.14	1.87	0.07	0.32	3.51	0.551
23	135.0	7.9	0.316	1.657	0.0	98.26	0.85	0.07	0.12	1.49	0.233
24[c]	160.1	8.0	0.317	1.658	0.0	95.95	2.89	0.07	0.52	5.52	0.866
25	124.7	7.9	0.637	2.761	0.115	86.2	10.69	0.07	1.28	−0.09	−0.03
26	134.8	7.8	0.637	2.760	0.115	85.9	10.74	0.07	1.24	−0.2	−0.061
27	144.8	7.9	0.637	2.760	0.115	86.16	10.64	0.07	1.18	−0.55	−0.173

[a] $x_W = 1 - x_B - x_{SBA}$
[b] data points illustrated in fig. 3.25
[c] affected by internal mass transfer, not used for fitting calculations

C.3 Fluid Dynamic Experiments Katapak™-SP

Table C.3: Experimental data of fluid dynamic experiments in laboratory packing of KATAPAK™-SP.

No.	Aq. load u_L $m^3/(m^2\,h)$	Org. load u_G $m^3/(m^2\,h)$	Pressure drop $\frac{\Delta P}{\Delta z}$ Pa/m	Aq. hold-up h_L vol%
1	1.5	21.4	13.0	5.64
2	3.2	21.4	14.0	6.78
3	4.1	21.4	13.3	7.37
4	5.0	21.4	13.3	7.88
5	6.7	21.4	15.0	8.48
6	8.9	21.4	22.0	9.42
7	1.5	33.6	28.7	5.46
8	3.2	33.6	27.7	6.85
9	4.1	33.6	29.3	7.41
10	5.0	33.6	30.0	7.79
11	6.7	33.6	37.0	8.37
12	8.9	33.6	50.0	9.47
13	1.5	38.2	34.3	5.46
14	3.2	38.2	34.7	6.8
15	4.1	38.2	34.7	7.37
16	5.0	38.2	35.3	7.7
17	6.7	38.2	47.3	8.35
18	8.9	38.2	60.7	9.39

Appendix D

Fluid Dynamic Model for OCFS

The entire fluid dynamic model which is presented in the following paragraphs is based on the model of Stichlmair et al. [1]. Their approach has been used by several authors as basis for the development of models describing fluid dynamics in OCFS (cf. Moritz and Hasse [2], Hoffmann et al. [3], Ellenberger and Krishna [4], Ratheesh and Kannan [5]). Although these models were developed to describe counter-current flow of gas and liquid a model for the here considered case of two co-currently flowing immiscible liquids can be derived.

D.1 Load Point

First of all, for the description of fluid dynamics in OCFS it is important to determine the maximum possible liquid load with respect to the catalyst basket of the OCFS also referred to as load point. According to Moritz and Hasse [2] the load point can be determined from a Bernoulli balance around a longitudinal section of the fixed bed inside the catalyst basket. The resulting equations are:

$$u_{\mathrm{max,L}}^2 = \frac{\varepsilon_{\mathrm{CB}}^3}{1-\varepsilon_{\mathrm{CB}}} \frac{g d_{\mathrm{CP}}}{\xi_{\mathrm{CB}}} \tag{D.1a}$$

with the friction factor ξ_{CB}

$$\xi_{\mathrm{CB}} = \frac{160}{Re_{\mathrm{LP}}} + \frac{3.1}{Re_{\mathrm{LP}}^{0.1}} \,. \tag{D.1b}$$

The Reynolds number at the load point Re_{LP} is calculated from

$$Re_{\mathrm{LP}} = \frac{u_{\mathrm{max,L}} d_{\mathrm{CP}} \rho_{\mathrm{L}}}{(1-\varepsilon_{\mathrm{CB}})\eta_{\mathrm{L}}} \,. \tag{D.1c}$$

Equations (D.1a) to (D.1c) are solved implicitly for the maximum liquid load in the catalyst baskets $u_{\mathrm{max,L}}^2$. As is explained in section 4.6.2 the load point

marks an important fluid dynamic state of an OCFS. Besides the importance of operating the OCFS at least at or above the load point, respectively, for a most effectively utilization of the catalyst, the load point also marks discontinuities in the courses of hold-up and pressure drop.

D.2 Pressure Drop

Figure 4.17 shows that the pressure drop is completely independent of the liquid load below the load point but not above. As the continuous phase – usually the gas phase, here the liquid or supercritical organic phase – does not flow through the catalyst baskets but within the *open channels* of the OCFS the increasing load of the disperse phase, exclusively flowing inside the catalytic compartment, has no impact on the pressure drop up to the load point. If the dispersive phase load exceeds the load point excessive dispersive phase will flow on the packing surfaces which enclose the *open channels*, thereby reducing the available cross section for the continuous phase flow.

Due to the discontinuity in the pressure drop as function of the dispersive phase load the pressure drop in the sub-load point situation is described independently from the super-load point situation as *dry* pressure drop which can be expressed as (cf. Ellenberger and Krishna [4]):

$$\frac{\Delta P_{\mathrm{dry}}}{\Delta z} = \xi_{\mathrm{OC}} \frac{1}{d_{\mathrm{h}}} \rho_{\mathrm{G}} u_{\mathrm{G}}^2 \tag{D.2a}$$

where ξ_{OC} is the friction factor and d_{h} is the hydraulic diameter of the *open channels*, defined by

$$d_{\mathrm{h}} = \frac{4\varepsilon_{\mathrm{OC}}}{a_{\mathrm{SP}}} \,. \tag{D.2b}$$

The gas velocity u_{G} is obtained from the superficial gas load w_{G}, the volume fraction of the *open channels* $\varepsilon_{\mathrm{OC}}$, and the inclination angle θ

$$u_{\mathrm{G}} = \frac{w_{\mathrm{G}}}{\varepsilon_{\mathrm{OC}} \sin\theta} \,. \tag{D.2c}$$

The correlation of the friction factor was found, fitting it to experimental pressure drop data, to be

$$\xi_{\mathrm{OC}} = \frac{10.75}{Re_{\mathrm{G}}^{0.34}} = 10.75 \left(\frac{\rho_{\mathrm{G}} u_{\mathrm{G}} d_{\mathrm{h}}}{\eta_{\mathrm{G}}} \right)^{-0.34} \,. \tag{D.2d}$$

The *irrigated* pressure drop, i. e. the pressure drop which is additionally

affected by the cross section reducing liquid flow in the *open channels*, can be expressed as an enhancement to the *dry* pressure drop

$$\frac{\Delta P}{\Delta z} = \frac{\Delta P_{\mathrm{dry}}}{\Delta z} 20 \sqrt{Fr_{\mathrm{L,OC}}} \; . \tag{D.3}$$

wherein $Fr_{\mathrm{L,OC}}$ is the FROUDE number of the gravity driven liquid flow in the *open channels*. Equation (D.3) has been somewhat simplified over that which was originally proposed by Ellenberger and Krishna [4], but expresses essentially the same. Pre-factor and exponent were correlated to the experimental pressure drop data. The FROUDE number is calculated from

$$Fr_{\mathrm{L,OC}} = \frac{u_{\mathrm{L,OC}}}{\sqrt{g d_{\mathrm{h}}}} \tag{D.4a}$$

with the liquid velocity in the *open channels* $u_{\mathrm{L,OC}}$ defined by

$$u_{\mathrm{L,OC}} = \frac{w_{\mathrm{L,OC}}}{\varepsilon_{\mathrm{OC}} \sin\theta} = \frac{w_{\mathrm{L}} - w_{\mathrm{LP}}}{\varepsilon_{\mathrm{OC}} \sin\theta} \; . \tag{D.4b}$$

The liquid load at the load point w_{LP} is related to the maximum possible liquid flow velocity in the catalyst baskets $u_{\mathrm{max,L}}$

$$w_{\mathrm{LP}} = u_{\mathrm{max,L}} \psi \left(\gamma + 1\right) \tag{D.4c}$$

where ψ is the volume fraction of the catalyst baskets and γ accounts for the distribution of the liquid load between catalyst baskets and *open channels*. According to Ratheesh and Kannan [5] we have

$$\gamma = \frac{\varepsilon_{\mathrm{OC}} u_{\mathrm{L,OC}}}{\psi u_{\mathrm{L,CB}}} \; . \tag{D.4d}$$

In this work the liquid load distribution is set to $\gamma = 0.5$. This value is chosen due to the ratio of jets of the dispersive phase distributor directed to the *open channels* to those directed to the catalyst baskets which is $3 : 6$.

D.3 Hold-up

The dispersive phase hold-up consists of two contributions – hold-up within the catalyst baskets and hold-up in the *open channels*

$$h_{\mathrm{L}} = h_{\mathrm{L,CB}} + h_{\mathrm{L,OC}} \; . \tag{D.5}$$

Following the approach of Ratheesh and Kannan [5] the hold-up in the *open channels* $h_{\mathrm{L,OC}}$ is described by a correlation with respect to the FROUDE

number in the *open channels* $Fr_{\mathrm{L,OC}}$. For the experimental data the following correlation is derived

$$h_{\mathrm{L,OC}} = 96.3 Fr_{\mathrm{L,OC}}^{1.785} \tag{D.6a}$$

and for the hold-up in the catalyst baskets $h_{\mathrm{L,CB}}$ we have

$$h_{\mathrm{L,CB}} = \psi \varepsilon_{\mathrm{CB}} \left(\frac{u_{\mathrm{L,CB}}}{u_{\mathrm{L,max}}} \right)^{0.295} . \tag{D.6b}$$

Equations (D.6a) and (D.6b) can be applied to the whole range of liquid flow patterns in the OCFS. In contrast to the fluid dynamic models for gas-liquid counter-current flow in OCFS, here no term considering an impact of the gas flow on the liquid hold-up in the *open channels* is necessary due to the co-current liquid-liquid flow which was employed in the fluid dynamic experiments of this work.

References

[1] Stichlmair, J., J. R. Fair, and J. L. Bravo. General model for prediction of pressure drop and capacity of countercurrent gas/liquid packed columns. *Gas Sep. Pur.* **3**, (1989), 19–28. DOI: 10.1016/0950-4214(89)80016-7.

[2] Moritz, P. and H. Hasse. Fluid dynamics in reactive distillation packing Katapak-S™. *Chem. Eng. Sci.* **54**, (1999), 1367–1374. DOI: 10.1016/S0009-2509(99)00078-0.

[3] Hoffmann, A., C. Noeres, and A. Górak. Scale-up of reactive distillation columns with catalytic packings. *Chem. Eng. Process.* **43**, (2004), 383–395. DOI: 10.1016/s0255-2701(03)00121-1.

[4] Ellenberger, J. and R. Krishna. Counter-current operation of structured catalytically packed distillation columns: pressure drop, holdup and mixing. *Chem. Eng. Sci.* **54**, (1999), 1339–1345. DOI: 10.1016/S0009-2509(99)00055-X.

[5] Ratheesh, S. and A. Kannan. Holdup and pressure drop studies in structured packings with catalysts. *Chem. Eng. J.* **104**, (2004), 45–54. DOI: 10.1016/j.cej.2004.08.004.

Appendix E

Property Methods and Mass Transfer Coefficients

E.1 Property Methods

This section deals with the property methods which have been used in this work. The according parameters are needed for the simulation of the reaction and separation processes.

The important modeling of fluid phase equilibria and chemical equilibria of the C_3- and the C_4-hydration system is discussed in detail in chapter 2. Therefore, fluid phase equilibria are no subject of this appendix. However, a derivation of the analytic expression for the partial molar fugacity coefficient eq. (2.9a), which is essential for the computation of fluid phase equilibria, is provided here.

Additionally needed properties are:

i) viscosity,

ii) diffusivity,

iii) enthalpy, and

iv) mass transfer coefficients.

The latter will be discussed in appendix E.2.

E.1.1 Partial Molar Fugacity Coefficient

An explicit expression for the partial molar fugacity coefficient $\bar{\varphi}_i$ of a component i can be derived analytically from the following expression (cf. Poling et al. [1], eq. 6-7.7, p. 6.27):

$$\ln \bar{\varphi}_i = \int_V^\infty \left[\left(\frac{\partial \left(PV/\left(RT\right)\right)}{\partial n_i} \right)_{T,V,n_{j\neq i}} - 1 \right] \frac{\mathrm{d}V}{V} - \ln Z \,. \tag{E.1}$$

According to Poling et al. [1], the derivative in eq. (E.1) can be taken before carrying out the integration. As the task here is to derive the partial molar fugacity coefficient of the VTPR-EoS, but neglecting the volume correction c (cf. section 2.1.1), it is the PENG-ROBINSON equation of state (PR-EoS) which needs to be used here for the derivation of the partial molar fugacity coefficient.

Starting from the PR-EoS in the compressibility explicit form expressed in total volume V:

$$\frac{PV}{RT} = \frac{nV}{V - nb} - \frac{n^2 a(T) V}{RT\left(V^2 + 2nbV - n^2 b^2\right)} , \tag{E.2}$$

and the partial molar parameters $\bar{a}_i$ and $\bar{b}_i$ (eqs. (2.9c) and (2.9e))

$$\bar{a}_i = \frac{\partial\,(na)}{\partial n_i} , \qquad \bar{b}_i = \frac{\partial\,(nb)}{\partial n_i} ,$$

for the derivative of the first term of the r. h. s. of eq. (E.2) follows

$$\frac{\partial\left(nV/\left(V - nb\right)\right)}{\partial n_i} = \frac{V\left(V - nb\right) + nV\bar{b}_i}{\left(V - nb\right)^2} , \tag{E.3}$$

and for the second term

$$\begin{aligned} &\frac{1}{RT}\frac{\partial\left(naV/\left(V^2 + 2nbV - n^2 b^2\right)\right)}{\partial n_i} \\ &\quad = \frac{nV\left(a + \bar{a}_i\right)\left(V^2 + 2nbV - n^2 b^2\right) - n^2 aV\left(2\bar{b}_i V - 2n\bar{b}_i b\right)}{RT\left(V^2 + 2nbV - n^2 b^2\right)^2} . \end{aligned} \tag{E.4}$$

Introducing eqs. (E.3) and (E.4) into eq. (E.1) the integrand becomes

$$\begin{aligned} &\int_V^\infty \left[\left(\frac{\partial\left(PV/\left(RT\right)\right)}{\partial n_i}\right)_{T,V,n_{j\neq i}} - 1\right]\frac{\mathrm{d}V}{V} \\ &\quad = \int_V^\infty \left(\frac{1}{V - nb} - \frac{1}{V} + \frac{n\bar{b}_i}{\left(V - nb\right)^2}\right. \\ &\quad\quad \left. - \frac{n\left(a + \bar{a}_i\right)\left(V^2 + 2nbV - n^2 b^2\right) - 2n^2 a\bar{b}_i\left(V - nb\right)}{RT\left(V^2 + 2nbV - n^2 b^2\right)^2}\right)\mathrm{d}V . \end{aligned} \tag{E.5}$$

Integrating the individual terms of the integrand, we obtain for the first two terms

$$\int_V^\infty \left(\frac{1}{V-nb} - \frac{1}{V}\right) \mathrm{d}V = \ln\left(V-nb\right) - \ln V\Big|_V^\infty = -\ln\frac{V-nb}{V}\,, \tag{E.6a}$$

for the third term

$$\int_V^\infty \frac{n\bar{b}_i}{\left(V-nb\right)^2}\,\mathrm{d}V = -\frac{n\bar{b}_i}{V-nb}\bigg|_V^\infty = \frac{n\bar{b}_i}{V-nb} \tag{E.6b}$$

and for the fourth term

$$\begin{aligned}
&\int_V^\infty \left(-\frac{n\left(a+\bar{a}_i\right)\left(V^2+2nbV-n^2b^2\right)-2n^2a\bar{b}_i\left(V-nb\right)}{RT\left(V^2+2nbV-n^2b^2\right)^2}\right)\mathrm{d}V \\
&\quad= \frac{\bar{b}_i}{b}\frac{naV}{RT\left(V^2+2nbV-n^2b^2\right)} \\
&\qquad -\frac{a}{2\sqrt{2}bRT}\left(\frac{\bar{a}_i}{a}+1-\frac{\bar{b}_i}{b}\right)\ln\frac{2\left(V+nb-nb\sqrt{2}\right)}{2\left(V+nb+nb\sqrt{2}\right)}\bigg|_V^\infty \\
&\quad= -\frac{\bar{b}_i}{b}\frac{naV}{RT\left(V^2+2nbV-n^2b^2\right)} \\
&\qquad -\frac{a}{2\sqrt{2}bRT}\left(\frac{\bar{a}_i}{a}+1-\frac{\bar{b}_i}{b}\right)\ln\frac{V+nb+nb\sqrt{2}}{V+nb-nb\sqrt{2}}\,.
\end{aligned} \tag{E.6c}$$

Introducing the integration result eq. (E.6) back into eq. (E.1) and substituting the molar volume by $V = vn$ we obtain

$$\begin{aligned}
\ln\bar{\varphi}_i = {}& \frac{\bar{b}_i}{b}\left(\frac{Pv}{RT}-\frac{v}{v-b}\right)+\frac{\bar{b}_i}{v-b}-\ln\frac{v-b}{v}-\ln Z \\
& -\frac{a}{2\sqrt{2}bRT}\left(\frac{\bar{a}_i}{a}+1-\frac{\bar{b}_i}{b}\right)\ln\frac{v+b\left(1+\sqrt{2}\right)}{v+b\left(1-\sqrt{2}\right)}\,.
\end{aligned} \tag{E.7}$$

The final result is found by replacing the compressibility with $Z = \frac{Pv}{RT}$ and

some algebraic manipulations

$$\ln \bar{\varphi}_i = \frac{\bar{b}_i}{b}\left(\frac{Pv}{RT} - 1\right) - \ln \frac{P(v-b)}{RT} - \frac{a}{2\sqrt{2}bRT}\left(\frac{\bar{a}_i}{a} + 1 - \frac{\bar{b}_i}{b}\right) \ln \frac{v + b\left(1+\sqrt{2}\right)}{v + b\left(1-\sqrt{2}\right)} \tag{E.8}$$

E.1.2 Viscosity

Dynamic liquid viscosities of the pure components are calculated with the correlation of the DIPPR Project (Rowley et al. [2]). The temperature-dependent correlation is written as

$$\frac{\eta}{\mathrm{Pa\,s}} = \exp\left(a_0 + \frac{a_1}{T} + a_2 \ln T + a_3 T^{a_4}\right) \tag{E.9}$$

whereas the temperature T is in K. The coefficients a_0-a_4 in eq. (E.9) are listed in Rowley et al. [2] for a variety of components. Coefficients for the C_3-hydration system are compiled in table E.1.

Table E.1: Coefficients for temperature correlation of pure component liquid viscosity [2].

Comp.	Coefficients				
	a_0	a_1	a_2	a_3	a_4
P	−9.1477	500.87	−0.317 45	–	–
W	−52.843	3703.6	5.866	-5.879×10^{-29}	10
IPA	−8.23	2282.2	−0.984 95	–	–
DIPE	−11.5	993.0	0.022	–	–

Viscosities for liquid mixtures are computed from composition and pure component viscosities by the Grunberg-Nissan mixing rule

$$\ln \eta = \sum_i x_i \ln \eta_i \tag{E.10}$$

which has been critically analyzed in Poling et al. [1]. The original method includes an interaction term which has been skipped from eq. (E.10) for simplicity.

E.1.3 Diffusivity

For the bulk phase diffusivities two methods are employed depending on the state of the phase under consideration. For vapor phases diffusivities the method of Fuller and for liquid diffusivities at infinite dilution that of Tyn and Calus are used. Both methods are intensively discussed in Poling et al. [1]. For diffusivities in high pressure supercritical phases the method for liquids is used.

The correlation of Fuller is written as

$$D_{\mathrm{AB}} = \frac{0.00143 T^{1.75}}{P\sqrt{M_{\mathrm{AB}}}\left(\sqrt[3]{(\Sigma_v)_{\mathrm{A}}} + \sqrt[3]{(\Sigma_v)_{\mathrm{B}}}\right)^2} \tag{E.11}$$

whereas D_{AB} is the diffusivity of solute A in solvent B in cm^2/s, T is in K, P is in bar, M_{AB} in g/mol is obtained from the molecular weights of A and B as $2\left(\frac{1}{M_{\mathrm{A}}} + \frac{1}{M_{\mathrm{B}}}\right)^{-1}$, and Σ_v is found by summing atomic diffusion volumes (cf. table E.2) for each component individually.

Table E.2: Atomic diffusion volumes of Fuller-method for gas phase diffusivities [1], p. 11.11.

Atom/group	Diffusion volume
C	15.9
H	2.31
O	6.11
H_2O	13.1

The method for estimation of liquid phase diffusivities at infinite dilution $Đ^{\circ}_{\mathrm{AB}}$ of Tyn and Calus uses the following relation

$$Đ^{\circ}_{\mathrm{AB}} = 8.93 \times 10^{-8} \left(\frac{v_{\mathrm{A}}^{\mathrm{NBP}}}{\left(v_{\mathrm{B}}^{\mathrm{NBP}}\right)^2}\right)^{\frac{1}{6}} \left(\frac{\mathbf{P}_{\mathrm{B}}}{\mathbf{P}_{\mathrm{A}}}\right)^{0.6} \frac{T}{\eta_{\mathrm{B}}} \,. \tag{E.12}$$

In eq. (E.12), $Đ^{\circ}_{\mathrm{AB}}$ is in cm^2/s, v^{NBP} is the molar volume of the liquid at normal boiling point in $\mathrm{cm}^3/\mathrm{mol}$ of solute A or solvent B, respectively, $\mathbf{P}$ is the dimensionless parachor, T is in K, and η_B is the dynamic viscosity of the pure solvent in cP ($10^{-3}\,\mathrm{Pa\,s}$).

Parachors for the components that are involved in this work are provided in table E.3.

Table E.3: Parachors for eq. (E.12) [3].

Component	Parachor
P	139.1
B	179.1
IPA	164.4
SBA	201.9
DIPE	288.9
W	45.3

Equation (E.12) is subject to the following restrictions according to Poling et al. [1], pp. 11.23-11.25:

i) the method should not be used for diffusion in viscous solvents. Values of η_B above about 20 cP to 30 cP would classify the solvent as viscous,

ii) if the solute is water, a dimer value of v_A and $\mathbf{P}_A$ should be used,

iii) if the solute is an organic acid and the solvent is other than water, methyl alcohol, or butyl alcohol, the acid should be considered a dimer with twice the expected values of v_A and $\mathbf{P}_A$, and

iv) for nonpolar solutes diffusing into monohydroxy alcohols, the values of v_B and $\mathbf{P}_B$ should be multiplied by a factor equal to $8\eta_B$.

For the dependency of liquid phase diffusivities on composition the generalized multicomponent Darken-relation is used, (Krishna and Baten [4, 5]), which relates the binary Maxwell-Stefan-diffusivity to self-diffusivities

$$Đ_{AB} = \frac{x_B}{x_A + x_B} D_{A,self} + \frac{x_A}{x_A + x_B} D_{A,self} \tag{E.13a}$$

with the self-diffusivities obtained from

$$D_{i,self} = \sum_{j=1}^{n_c} \omega_j Đ^{\circ}_{i,j} \ . \tag{E.13b}$$

In eq. (E.13b), ω_i is the mass fraction of component i. The linear dependence of the self-diffusivities on mass fractions has been justified by Krishna and Baten [4] for a variety of ternary and quaternary aliphatic alkane systems.

E.1.4 Enthalpy and free (Gibbs) energy

Enthalpies of liquid and gaseous components for given temperature and pressure are obtained from

$$h(T,P) = h(T,P^0) - RT^2 \frac{\mathrm{d}\varphi}{\mathrm{d}T} \tag{E.14a}$$

with the temperature dependent enthalpy at reference state

$$h(T,P^0) = h^{\mathrm{ref}} + \int_{T^{\mathrm{ref}}}^{T} c_P^{\mathrm{IG}}(T)\,\mathrm{d}T\ . \tag{E.14b}$$

The type of state (liquid or gas) of enthalpy is determined by an appropriate choice for the pure component fugacity coefficient φ computed with the thermodynamic model which is described in section 2.1.1. The temperature derivatives $\frac{\mathrm{d}\varphi}{\mathrm{d}T}$ are computed using finite difference approximations. A temperature correlation for c_P^{IG} and enthalpies at ideal gas reference state h^{ref} are provided in table 2.6.

Figure E.1 shows exemplary graphs for liquid and vapor enthalpies of isopropyl alcohol along the vapor pressure curve.

The temperature dependent pure component free (Gibbs) energy or chemical potential, respectively, at reference state can be computed from

$$\frac{\mu(T,P^0)}{T} = \frac{\mu^{\mathrm{ref}}}{T^{\mathrm{ref}}} - \int_{T^{\mathrm{ref}}}^{T} \frac{h(T,P^0)}{T^2}\,\mathrm{d}T \tag{E.15}$$

whereas chemical potentials at reference state μ^{ref} are given in table 2.6.

E.2 Mass Transfer Coefficients

The simulation of diffusive mass transfer in fluid zones at fluid phase interfaces requires the computation of mass transfer coefficients which incorporate the influence of fluid dynamics into molecular interactions. Thus, the mass transfer coefficients and models for their computation depend on the actual mass transfer process and phase contacting equipment.

E.2.1 External catalyst mass transfer

The mass transfer coefficient for the Nernst diffusion layer which surrounds the catalyst particle is calculated from the Sherwood function of Krevelen and Krekels [6] as

$$Sh_{\mathrm{LS}} = 1.8 Re_{\mathrm{LS}}^{0.5} Sc_{\mathrm{LS}}^{0.33}\ . \tag{E.16}$$

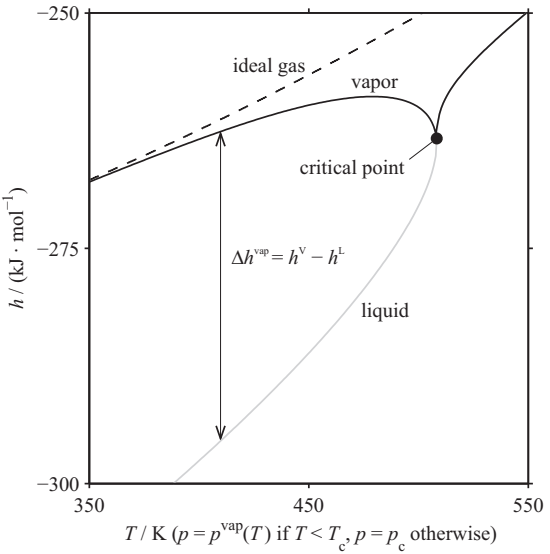

Figure E.1: Liquid, vapor, and ideal gas phase enthalpy of IPA as function of boiling temperature up to the critical point and beyond; pressure is set to vapor pressure below critical temperature and to the critical pressure above.

E.2.2 Reactive extraction

For the aqueous phase, the liquid phase mass transfer coefficients of Hoffmann et al. [7] are used. For the supercritical organic phase which flows through the *open channels* of the structured packing the correlation of Ruivo et al. [8], which was found for an extraction process with supercritical carbon dioxide, is used. Both models are derived from the mass transfer model of Rocha et al. [9] for distillation in structured packing, e. g. SULZER BX™.

The supercritical phase mass transfer coefficient can be computed from the SHERWOOD function

$$Sh_{\mathrm{SC}} = 4.68 \times 10^{-3} Re_{\mathrm{SC}}^{0.8} Sc_{\mathrm{SC}}^{0.33} \ . \tag{E.17}$$

The liquid phase mass transfer coefficient is expressed as

$$\kappa_{\mathrm{L}} = 2\sqrt{\frac{D u_{\mathrm{L,OC}}}{\pi S}} \tag{E.18}$$

with the effective liquid velocity in the *open channels* defined in eq. (D.4b). S is the corrugation side of the OCFS forming the *open channels*.

Equations (E.17) and (E.18) do not exactly represent the situation under consideration. Therefore, the used models are subject to future validation in the envisaged experimental study of reactive extraction (cf. section 4.6.3).

E.2.3 Distillation

The model for mass transfer coefficients for distillation processes in structured packings of Rocha et al. [9] is used in this work.

The liquid phase mass transfer coefficient is obtained from eq. (E.18) whereas the gas phase mass transfer coefficient is calculated from the SHERWOOD function

$$Sh_{\mathrm{G}} = 5.4 \times 10^{-2} Re_{\mathrm{G}}^{0.8} Sc_{\mathrm{G}}^{0.33} \tag{E.19a}$$

whereas the gas phase REYNOLDS number is expressed as

$$Re_{\mathrm{G}} = \frac{(u_{\mathrm{GE}} + u_{\mathrm{LE}})\, \rho_{\mathrm{G}} S}{\eta_{\mathrm{G}}} \tag{E.19b}$$

with the effective gas and liquid flow rates defined by

$$u_{\mathrm{GE}} = \frac{u_{\mathrm{GS}}}{\varepsilon\,(1 - h_{\mathrm{L}})\sin\theta} \tag{E.19c}$$

and

$$u_{\mathrm{LE}} = \frac{u_{\mathrm{LS}}}{\varepsilon h_{\mathrm{L}} \sin\theta} \ . \tag{E.19d}$$

References

[1] Poling, B. E., J. M. Prausnitz, and J. P. O'Connell. *The Properties of Gases and Liquids*, 5th. McGraw-Hill, New York, 2001.

[2] Rowley, R. L., W. V. Wilding, J. L. Oscarson, Y. Yang, and N. F. Giles. *DIPPR™Data Compilation of Pure Chemical Properties*, http://dippr.byu.edu.

[3] Quayle, O. R. The Parachors of Organic Compounds. An Interpretation and Catalogue. *Chem. Rev.* **53**, (1953), 439–589. DOI: 10.1021/cr60166a003.

[4] Krishna, R. and J. M. van Baten. The darken relation for multicomponent diffusion in liquid mixtures of linear alkanes: An investigation using molecular dynamics (MD) simulations. *Ind. Eng. Chem. Res.* **44**, (2005), 6939–6947. DOI: 10.1021/ie050146c.

[5] Krishna, R. and J. M. van Baten. MD simulations of diffusivities in methanol-n-hexane mixtures near the liquid-liquid phase splitting region. *Chem. Eng. Technol.* **29**, (2006), 516–519. DOI: 10.1002/ceat.200500376.

[6] Krevelen, D. W. van and J. T. C. Krekels. Rate of dissolution of solid substances. *Recl. Trav. Chim. Pays-Bas* **67**, (1948), 512.

[7] Hoffmann, A., C. Noeres, and A. Górak. Scale-up of reactive distillation columns with catalytic packings. *Chem. Eng. Process.* **43**, (2004), 383–395. DOI: 10.1016/s0255-2701(03)00121-1.

[8] Ruivo, R., M. J. Cebola, P. C. Simoes, and M. N. da Ponte. Fractionation of edible oil model mixtures by supercritical carbon dioxide in a packed column. 2. A mass-transfer study. *Ind. Eng. Chem. Res.* **41**, (2002), 2305–2315. DOI: 10.1021/ie0106579.

[9] Rocha, J. A., J. L. Bravo, and J. R. Fair. Distillation Columns Containing Structured Packings: A Comprehensive Model for Their Performance. 2. Mass-Transfer Model. *Ind. Eng. Chem. Res.* **35**, (1996), 1660–1667. DOI: 10.1021/ie940406i.

Symbols

Dimensionless Numbers

Fr	FROUDE number
Re	REYNOLDS number
Sc	SCHMIDT number
Sh	SHERWOOD number

Greek Letters

Γ		thermodynamic factor
Θ		dimensionless time
$\alpha(T)$		temperature correction function of the cohesive energy parameter of the VTPR-EoS
β		fraction of moles light phase in a flash split ($\beta = \frac{n'}{n'+n''}$)
δ	m	film thickness
δ		KRONECKER delta
ε	mol	extent of reaction
ε_{cat}		catalyst porosity
ε_{abs}	mmol/(eq s)	absolute fitting error (residual)
ε_{CB}		void fraction catalyst bed
ε		iteration stop criterion
ε_{OC}		void fraction *open channels*
η	Pa s	dynamic viscosity
η		catalyst efficiency
γ		activity coefficient
γ		distribution coefficient of disperse phase in OCFS
κ	m s	mass transfer coefficient

λ		dimensionless length coordinate
μ	kJ/mol	chemical potential
ν		reflux ratio
ν		stoichiometric coefficient
ω		acentric factor
ω		mass fraction
ψ		volume fraction of catalyst baskets in structured packing
ρ	kg/m^3	density
ρ_{H^+}	eq/kg	weight specific acid site concentration
τ_{cat}		tortuosity of catalyst pore structure
θ		inclination angle of structured packing
φ		fugacity coefficient
ξ		friction factor
ξ		dimensionless length coordinate

Latin Letters

A	m^2	area
D	m^2/s	FICK diffusivity
$Đ$	m^2/s	MAXWELL-STEFAN diffusivity
$Đ^\circ$	m^2/s	diffusivity at infinite dilution
D_{ax}	m^2/s	dispersion coefficient
D	mol/s	distillate stream
D_{self}	m^2/s	self diffusivity
E	mol/s	exit stream
E_a	kJ/mol	activation energy
E	kJ/s	energy balance residual
$\mathbb{E}$	kJ/s	energy transfer rate
F	mol/s	feed stream
F	mol/s	general flow
ID	m	internal diameter
K		distribution coefficient
K_a		chemical equilibrium constant based on activities

K_a^{398}		reference value of the equilibrium constant at 398 K
L	m	geometrical length
L	mol/s	molar liquid flow rate
M	mol/s	entrainer make up
M	mol/s	mass balance residual
N	mol/(m^2 s)	molar flux
$\mathbb{N}$	mol/s	mass transfer rate
N_{samples}		number of samples
P	MPa	pressure
$\mathbf{P}$		parachor
ΔP	Pa	pressure drop
P^{sat}	MPa	vapor pressure
Q	MW	heat duty
Q		equilibrium balance residual
R	mol/s	raffinate stream
R	mol/s	rate balance residual
R	J/(mol K)	gas constant
S	%	selectivity
S	mm	corrugation side of structured packing
$SMFV$	kg/(m^2 s)	superficial mass flow velocity
STY	mol/(m^3 s)	space time yield
T	K	temperature
TOS	h	time on stream
V	m^3	volume
V	mol/s	molar vapor flow rate
X	%	conversion
a	Pa(m^3)^2/mol^2	cohesive energy parameter of the VTPR-EoS
a		activity
a	K	first UNIQUAC interaction parameter
a	m^2/m^3	volume-specific surface area
b	m^3/mol	co-volume parameter of the VTPR-EoS
b		second UNIQUAC interaction parameter
c	m^3/mol	volume correction parameter of the VTPR-EoS

c	$\mathrm{mol/m^3}$	concentration
$c_{\mathrm{H^+}}$	$\mathrm{eq/m^3}$	volume specific acid site concentration
c	1/K	third UNIQUAC interaction parameter
c_P	$\mathrm{J/(mol\,K)}$	molar heat capacity at constant pressure
d	m	diameter
d_c	m	column diameter
e	$\mathrm{kJ/(m^2\,s)}$	energy flux
f	MPa	fugacity
g	kJ/mol	free (GIBBS') energy
g	$\mathrm{m^2/s}$	acceleration due to gravity
h	kJ/mol	enthalpy
Δh_r	kJ/mol	heat of reaction
h	m	height
h		hold-up
Δh^vap	kJ/mol	enthalpy of vaporization
k_+	$\mathrm{mmol/(eq\,s)}$	reaction rate constant of the forward reaction
k_+^0	$\mathrm{mmol/(eq\,s)}$	pre-exponential factor of the rate constant
n	mol	number of moles
n	1/min	rotational frequency
n_c		number of components
q'		additional parameter of the UNIQUAC-q'-model for alcohols and water
q		VAN DER WAALS surface parameter of the UNIQUAC-model
r	$\mathrm{mmol/(eq\,s)}$	reaction rate (mol/s in eq. (3.2b))
r_0	$\mathrm{mmol/(eq\,s)}$	initial reaction rate
r	m	radius
r		VAN DER WAALS volume parameter of the UNIQUAC-model
s	$\mathrm{m^2}$	surface area
t	s	time
u	m/s	interstitial flow velocity
u	V	voltage
v	$\mathrm{m^3/mol}$	molar volume
w	m/s	superficial flow velocity (load)
x		liquid phase mole fraction

y		vapor phase mole fraction
z		overall (feed) mole fraction
z		compressibility factor
z	m	length coordinate

Superscripts

0	reference state
$'$	light liquid phase
$''$	heavy liquid phase
$^-$	partial molar quantity
F	feed
I	identifier of fluid interface
L1	identifier of organic film layer
L2	identifier of aqueous film layer
L2S	identifier of catalyst surrounding film layer
S	identifier of catalyst body
E	excess
e	effective
G	gas
IG	ideal gas
iso	isomerization equilibrium
L	liquid
NBP	normal boiling point
ref	reference state
rev	reversible
V	vapor
α	phase identifier
β	phase identifier
ζ	phase identifier

Subscripts

1B	1-butene
B	*n*-butenes

B	bottom or bulk
*c*2B	*cis*-2-butene
CB	catalyst bed
C	column
CP	catalyst particle
DIPE	diisopropyl ether
G	gas (continuous phase)
H	upper boundary
IPA	isopropyl alcohol
L	liquid
L	lower boundary
L	liquid (dispersive phase)
LP	load point
LS	liquid-solid
OC	*open channels* in structured packing
P	propene
R	retention or reactor
RE	reactive extraction
S	surface
SBA	*sec* butyl alcohol
SC	supercritical
SP	structured packing
*t*2B	*trans*-2-butene
TB	trickle bed
vap	saturated (vapor)
W	water
calc	calculated quantity
cat	catalyst
c	parameter value at critical point
dry	dry packing
exp	experimentally determined quantity
h	hydraulic
i	index
input	value at reactor inlet
j	index

k	index
max	maximum
obs	observed quantity
output	value at reactor outlet
r	reaction or reduced parameter
res	residual
rev	reversible
t	total
tracer	value with respect to the tracer used for RTD analysis
wet	ion exchange resin saturated with solvent

Vector and Matrix Notation

[ ]	matrix
( )	vector
$\underline{\quad}$	vector

Abbreviations

*c*2B	*cis*-2-butene
*t*2B	*trans*-2-butene
1B	1-butene
A_E2	second order electrophilic addition mechanism
B	*n*-butenes
BDE	basic differential equation
BVP	boundary value problem
CSTR	continuously stirred tank reactor
DIPE	diisopropyl ether
DSBE	di-*sec*-butyl ether
E1	first order elimination mechanism
ETBE	ethyl *tert*-butyl ether
FTIR-ATR	Fourier transform infrared - attenuated total reflection
GMS	generalized Maxwell-Stefan equations
HP-LLE	high pressure liquid-liquid equilibrium
IPA	isopropyl alcohol
IVP	initial value problem
LLE	liquid-liquid equilibrium

MEK	methyl ethyl ketone
MTBE	methyl *tert*-butyl ether
NRTL	non-random two liquid
OCFS	open cross-flow structured catalytic packing
ODE	ordinary differential equation
P	propene
PDE	partial differential equation
PFTR	plug flow tubular reactor
ROLSI	rapid online sample injector
RTD	residence time distribution
S_N1	first order nucleophilic substitution mechanism
SBA	*sec*-butyl alcohol
SMFV	superficial mass flow velocity
STY	space time yield
TAME	*tert*-amyl methyl ether
TCD	thermal conductivity detector
TOS	time on stream
UNIFAC	universal functional activity coefficient
UNIQUAC	universal quasi-chemical
UNIQUAC-q'	modified universal quasi-chemical
VLE	vapor-liquid equilibrium
VLLE	vapor-liquid-liquid equilibrium
VTPR-EoS	volume translated PENG-ROBINSON equation of state
VTPR-UNIFAC	volume translated PENG-ROBINSON equation of state - universal functional activity coefficient

VTPR-UNIQUAC	volume translated PENG-ROBINSON equation of state - universal quasi-chemical
W	water

Publications in the course of this work

Publications

2006 Petre, D., Pfeuffer, B., Kunz, U., Hoffmann, U., Turek, T., 2006. *Prozessintensivierung durch reaktive Extraktion: Untersuchungen zur Hydratisierung von n-Buten*, poster presentation, Katalytikertagung 2006, Weimar, Germany.

Pfeuffer, B., Kunz, U., Hoffmann, U., Hoell, D., Turek, T., 2006. *Modeling of a fixed bed tubular reactor for the direct hydration process of lower olefins over an acid ion exchange resin*, poster presentation, ISCRE 19, Potsdam, Germany.

2007 Pfeuffer, B., Petre, D., Kunz, U., Hoffmann, U., Turek, T., 2007. *Production of sec-butyl alcohol by olefin hydration – a candidate for process intensification?* poster presentation, ECCE 6, Copenhagen, Denmark.

2008 Pfeuffer, B., Kunz, U., Hoffmann, U., Turek, T., Hoell, D., 2008. *Reaktionstechnische Untersuchungen zur Direkthydratisierung niederer Olefine durch Reaktivextraktion*, oral presentation, Jahrestreffen Reaktionstechnik, Würzburg, Germany.

2009 Pfeuffer, B., Kunz, U., Hoffmann, U., Turek, T., Hoell, D., 2009. *Heterogenkatalytische Reaktivextraktion – Ein neuer Prozess zur Herstellung sekundärer C_3- und C_4-Alkohole*, oral presentation, Jahrestreffen Reaktionstechnik, Würzburg, Germany.

Pfeuffer, B., Kunz, U., Hoffmann, U., Turek, T., Hoell, D., 2009. *Heterogeneous reactive extraction for an intensified alcohol production process*, oral presentation, ICOSCAR3, Naples, Italy.

Pfeuffer, B., Kunz, U., Hoffmann, U., Turek, T., 2009. *Multicomponent Mass Transfer Model for Supercritical Extraction: Application to Isopropyl Alcohol Production*, Chem. Eng. Technol. 32, 1384.

Pfeuffer, B., Kunz, U., Hoffmann, U., Turek, T., Hoell, D., 2009. *Heterogeneous reactive extraction for an intensified alcohol production process*, Catal. Today 147S, 357.

2010 Bacher, V., Harting, K., Pfeuffer, B., Kunz, U., Perbandt, C., Schwefer, M., Turek, T., 2010. *Untersuchungen zur Kinetik der NO-Oxidation an Eisen-Zeolith-Katalysatoren*, poster presentation, Katalytikertagung 2010, Weimar, Germany.

Pfeuffer, B., Kunz, U., Hoffmann, U., Turek, T., 2010. *Kinetik der heterogenen mehrphasigen Hydratisierung von Butenen zu 2-Butanol an sauren Ionenaustauscherharzen*, poster presentation, Jahrestreffen Reaktionstechnik, Würzburg, Germany.

Pfeuffer, B., Kunz, U., Hoffmann, U., Turek, T., 2010. *Alternativen zur Reaktivdestillation: Heterogenkatalytische Reaktivextraktion am Beispiel der Isopropanol-Synthese*, oral presentation, Processnet, Aachen, Germany.

Urban, T., Hoell, D., Kohnz, H., Hoffmann, U., Kunz, U., Pfeuffer, B., 2010. *Process for the Production of Lower Alcohols by Olefin Hydration*, EP Pat. 2 208 719 A1.

2011 Pfeuffer, B., Kunz, U., Hoffmann, U., Turek, T., Hoell, D., 2011. *Heterogeneous Reactive Extraction of Secondary Butyl Alcohol Liquid Phase Synthesis: Microkinetics and Equilibria*, Chem. Eng. Sci. 66, 777.